Bis(monoacylglycero)phosphate (BMP), a Novel Macrophage Associated Phospholipid: Implications in Gangliosidoses and Cancer

Author: Zeynep Akgoc

Boston College Electronic Thesis or Dissertation, 2015

Boston College

The Graduate School of Arts and Sciences

Department of Biology

BIS(MONOACYLGLYCERO)PHOSPHATE (BMP), A NOVEL MACROPHAGE ASSOCIATED PHOSPHOLIPID: IMPLICATIONS IN GANGLIOSIDOSES AND CANCER

A dissertation

By

ZEYNEP AKGÖÇ

Submitted in partial fulfillment of the requirements

for the degree of

Doctor of Philosophy

May 2015

ABSTRACT

Bis(monoacylglycero)phosphate (BMP), a Novel Macrophage Associated Phospholipid: Implications in Gangliosidoses and Cancer

Zeynep Akgöç

Thesis Advisor: Thomas N. Seyfried

Bis(monoacylglycero)phosphate, BMP, is a negatively charged glycerol-phospholipid with an unusual sn-1;sn-1' structural configuration. BMP is primarily enriched in endosomal/lysosomal membranes. BMP is thought to play a role in glycosphingolipid degradation and cholesterol transport. It constitutes only about 1-2% of the total phospholipids in most mammalian cells, but is abundant in lung alveolar macrophages where it can comprise up to 16% of the total phospholipids. BMP also accumulates in tissues of humans and animals with lysosomal storage disorders. However, little information is available on BMP levels in gangliosidosis brain tissue.

In this work, I found that total BMP content was significantly greater in cells of macrophage/microglial origin than in cells of macroglial origin (astrocyte, oligodendrocyte progenitor), whether normal or tumorigenic. I also observed that BMP in brain was significantly greater in humans and in animals (mice, cats, American black bears) with either GM1 or GM2 ganglioside storage diseases, than in brains of normal subjects. Since BMP is associated with macrophages, I also analyzed the BMP levels in relation to disease-associated inflammation in

gangliosidoses. I found that BMP levels were increased due to accumulation of primary storage material gangliosides, rather than an outcome of disease-associated inflammation.

In addition, in this thesis I also explored the effect of new ketogenic diet formula from Solace Nutrition (KetoGen) on the growth and metastatic spread of the VM-M3 tumor. Most current drug therapies for cancer are toxic and only marginally effective in providing long-term management. Respiratory insufficiency with compensatory aerobic fermentation (Warburg effect) is the hallmark biochemical phenotype of nearly all neoplastic cells within tumors. Calorie restriction, which lowers blood glucose and elevates ketone bodies, is known to reduce tumor growth to a certain extent, however it does not reduce systemic metastasis. Tumor bearing VM mice were fed either a standard lab chow diet in unrestricted amounts (SD-UR), a standard lab chow restricted to obtain an 18% reduction in body weight (SD-R), or the KetoGen diet restricted (KG-R) to match the body weights of the SD-R group. Tumor size was significantly smaller and organ metastasis was significantly less in the KG-R group than in the SD-UR or SD-R groups. Even though blood glucose was reduced similarly in both the SD-R and KG-R groups, blood ketones were 3-fold higher in the KG-R group than in the SD-R group. These results show that VM-M3 tumor growth and systemic metastasis were managed better with the restricted KetoGen KD than with calorie restriction of a high carbohydrate standard diet. As all human and mouse tumors cells suffer from respiratory insufficiency, my findings suggest that the

restricted KetoGen diet should be an effective non-toxic therapy against tumor growth and systemic metastatic cancer.

DEDICATION

I dedicate this thesis to my parents Hulya Kizilcam and Rahmi Akgoc, for their encouragement, and belief in me throughout my educational career; and also to Alp Artar, for his endless love and support any time that I need.

ACKNOWLEDGEMENTS

First, I would like to thank to my professor Thomas N. Seyfried for making science exciting and explorative for me. He taught me how to think outside the box while standing in the cutting edge of true science. He also educated me everyday not just with scientific facts, but also about history, culture and the world with his excessive knowledge. I want to thank to my committee members Dr. Charlie Hoffman for his endless support during my PhD. I also want to thank Dr. Mary Roberts for fruitful discussions, and also for giving the most interesting class on lipids, which contributed a lot to my work. I also want to thank my other committee members and Dr.Miguel Sena-Esteves and Dr. Junona Moroianu for accepting to be a member of my committee and their help during my education process. In addition I would like to thank to former and current members of Seyfried lab, especially to Laura Shelton and Purna Mukherjee for their endless help and mentoring, and Linh Ta, Kevin Santos, Roberto Flores and Ashley Brown for making the lab environment very fruitful. I also want to thank the hard working and smart undergraduate researchers of the Seyfried lab, especially Sonia Iosim than Xijun Zhu, Catherine Doyle, David Ryan, Wesley Thorne, and Jaimie Chang.

Table of Contents

LIST OF FIGURES

LIST OF TABLES

ABBREVIATIONS

AAV	adeno-associated viral
β-gal	β-galactosidase
β-OHB	β-hydroxybutyrate
BMP	bis(monoacylglycero)phosphate
C8-D30	astrocyte type III clone
CL	cardiolipin
CT-2A	chemically induced mouse astrocytoma
DHA	docosahexaenoic acid
DNA	deoxyribonucleic acid
DMEM	Dulbecco's modified Eagle medium
ER	endoplasmic reticulum
FBS	fetal bovine serum
GA1	asialo GM1
GA2	asialo GM2
GBM	glioblastoma multiforme
Hexβ	β-hexosaminidase
HPTLC	high-performance thin-layer chromatography
HIV	human immunodeficiency virus
i.c.	intracranial
i.p.	intra-peritoneal
ILV	intra-luminal vesicles
KC	KetoCal ketogenic diet
KC-R	KetoCal ketogenic diet restricted
KC-UR	KetoCal ketogenic diet unrestricted
KG	KetoGen ketogenic diet
KG-R	KetoGen ketogenic diet restricted
KG-UR	KetoGen ketogenic diet unrestricted
LBPA	lysobisphosphatidic acid
LSD	lysosomal storage diseases
LPS	lipopolysaccahride
MAFP	methyl arachidonyl fluoro phosphonate
PA	phosphatidic acid
PBS	phosphate buffered saline
PCR	polymerase chain reaction
PG	phosphatidylglycerol
PI	phosphatidylinositol
PS	phosphatidylserine
PM	peritoneal macrophage
RNA	ribonucleic acid
s.c.	subcutaneous

SCID	severe combined immunodeficiency
SD	Sandhoff disease, or Standard chow diet
SD-R	Standard chow diet restricted
SD-UR	Standard chow diet unrestricted
SEM	standard error of the mean
Sulf	sulfatides
VM	VM/Dk mouse strain
VM-M3	spontaneous murine metastatic brain tumor
VM-M3/Fluc	VM-M3 murine metastatic brain tumor expressing firefly luciferase
VM-NM1	spontaneous murine non-metastatic/non-invasive brain tumor
VSV	vesicular stomatitis virus

CHAPTER 1

Introduction

Bis(monoacylglycero)phosphate (BMP), formerly known as lysobisphosphatidic acid (LBPA), is a negatively charged phospholipid, localized to late endosomes and lysosomes [1, 2]. BMP is a structural isomer of phosphatidylglycerol (PG) with an unusual sn-1:sn-1' configuration (Figure 1) [3, 4]. BMP consists of a phosphate bound to two glycerol groups, each with a single acyl chain [3]. Phosphatidylglycerol is considered the biosynthetic precursor of BMP [5]. The synthetic pathway is thought to involve the deacylation of PG by Phospholipase A2 and then transacylation, possibly using two lysoPG molecules to generate BMP (Figure 2) [6]. Substrates for these reactions, such as PG, do not all originate in the lysosome, but are rather obtained by lysosomal interaction with the membranes of other organelles [7]. Degradation of BMP is also unusual, as its rate of degradation is much slower than that of other phospholipids due to its unique sn-1:sn-1' configuration [8]. However, BMP can be degraded by lysosomal phosphodiesterase and lysosomal phospholipase A [9]. The fatty acid composition is oleic acid (C18:1) and docosahexaenoic acid (C22:6n-3) in many cell types such as rat uterine stromal cells, rat adrenal gland PC12 cultured cells, rat and human liver [10-13]. In alveolar macrophages linoleic acid (C18:2) and arachidonic acid (C20:4) is also present in high amounts in BMP. BMP fatty acid

variation might be important for the biochemical function of each particular BMP species [12-15].

BMP can have multiple functions within the endocytic pathway. At low pH, the cone shape of BMP plays a role in membrane asymmetry, resulting in invagination and the formation of internal endosomal vesicles called intraluminal vesicles (ILVs) or multivesicular bodies (MVBs) [16]. As the endosome undergoes maturation, the inner membrane becomes enriched in BMP and the decreasing luminal pH induces ILV formation [17]. These vesicles increase storage capacity, linking BMP to the control of lysosomal cholesterol storage [18]. BMP is also proposed to have a role in the lysosomal degradation of glycosphingolipids through interactions with saposins and hydrolases (Figure 3) [14, 19, 20].

Lysosomal storage diseases (LSD) are a group of inherited disorders that are caused by defective/deficient lysosomal enzymes [21]. Sandhoff disease (SD) and GM1 gangliosidosis are caused by genetic deficiencies of lysosomal β-hexosaminidase (*Hexβ*) and acid β-galactosidase (*β-gal)*, respectively [21-25]. Sandhoff Disease is characterized by the storage of ganglioside GM2 and its asialo derivative GA2, whereas GM1 gangliosidosis involves the storage of ganglioside GM1 and its asialo derivative GA1 [22-25]. Elevated levels of BMP are observed in many lysosomal storage diseases including mucopolysaccharidosis, Niemann-Pick disease type A/B/C, Gaucher and Fabry disease [26-35]. However, this elevation is not present in all LSDs such as the Spielmeyer-Sjogren type of neuronal ceroid-lipofuscinosis [31].

Previous studies showed that BMP was elevated in the brain tissue of a Sandhoff Disease human patient, and in serum obtained from GM2 gangliosidoses patients [31, 36]. However, a detailed study of BMP content in the GM2 and GM1 gangliosidoses brain is lacking [37]. We found that the levels of BMP were significantly higher in humans and animals with either GM1 or GM2 gangliosidoses than in brain tissue from species matched control samples. The data indicated that BMP is a secondary storage material along with gangliosides in the gangliosidosis brain.

Figure 1. Structure of 2, 2' diacyl-sn 1: sn 1' Bis(monoacylglycero)phosphate (BMP) as previously described [38].

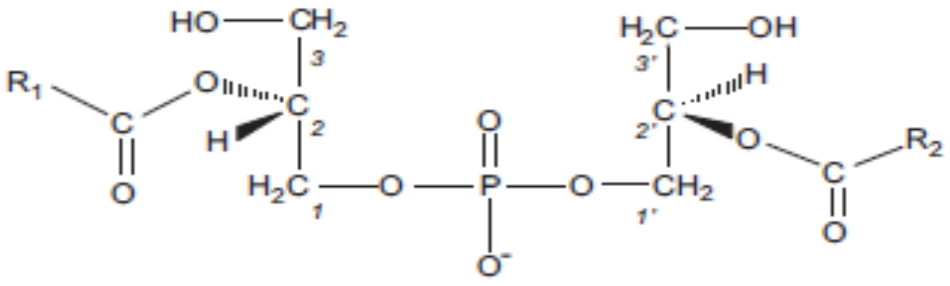
HO
CH2
3
R1
O
C
2
H
C
O
H2C
1
O
P
O
O-
O
CH2
1'
H2C
OH
3'
H
C
2'
O
C
O
R2

Figure 2. **Proposed biosynthesis of BMP suggested by Waite group**: Phosphatidylglycerol (PG) is hydrolyzed by Phospholipase A2 (PLA2) to form 1-acyl-LysoPhosphaditylglycerol (LPG) (step 1). A transacylase (TA) acylate LPG, using a phospholipid (PL) (possibly another PG) as the acyl donor, and forms sn-3:sn-1' BMP (step 2). Sn-3:sn-l'-BMPglycerol backbone is reoriented by an enzymatic activity (ROE), and yields sn-1:sn-1'-LPG by unknown mechanism (step 3). Transacylation of sn-1:sn-1'-LPG yields the final sn-1:sn-1'-BMP (step 4) [39].

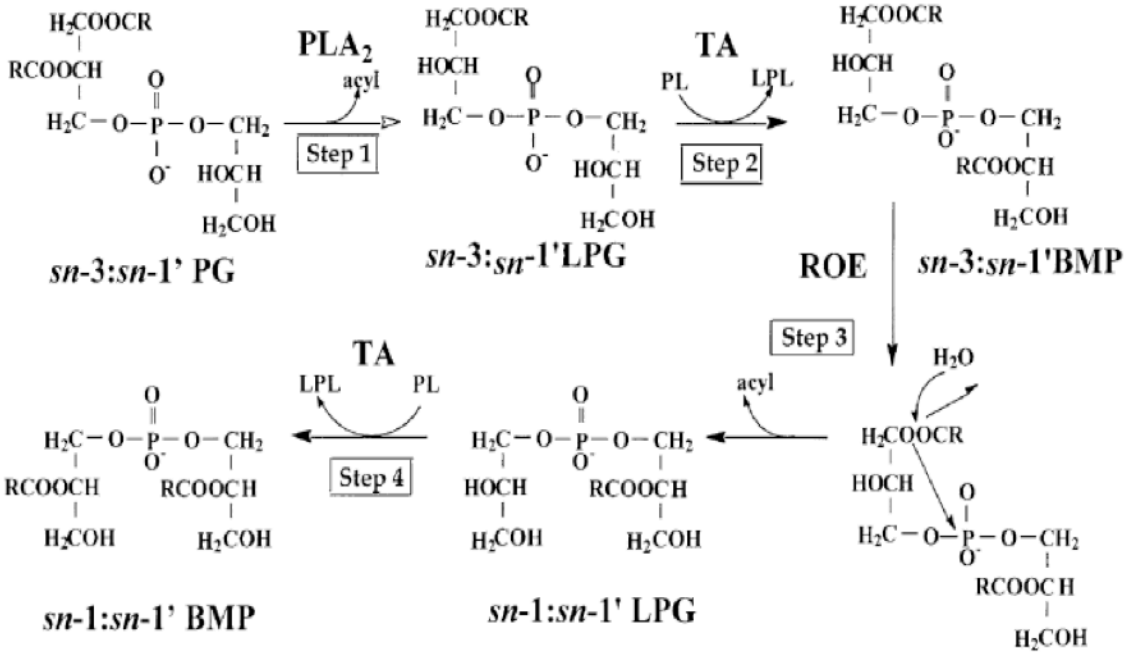
PLA2
acyl
Step 1
TA
PL
LPL
Step 2
ROE
Step 3
H2O
acyl
TA
LPL
PL
Step 4
sn-3:sn-1' PG
sn-3:sn-1'LPG
sn-3:sn-1'BMP
sn-1:sn-1' BMP
sn-1:sn-1' LPG

Figure 3. BMP aids the degradation of glycospingolipids with interacting lysosomal lipid binding proteins in Lysosomes. Cationic lysosomal lipid binding proteins (Saps and GM2-AP) and enzymes such as Acid Ceramidase and Glucocerebrosidase bind BMP containing negatively charged inner membranes. Lysosomal lipid binding proteins present membrane-bound lipids to water-soluble enzymes for degradation [8].

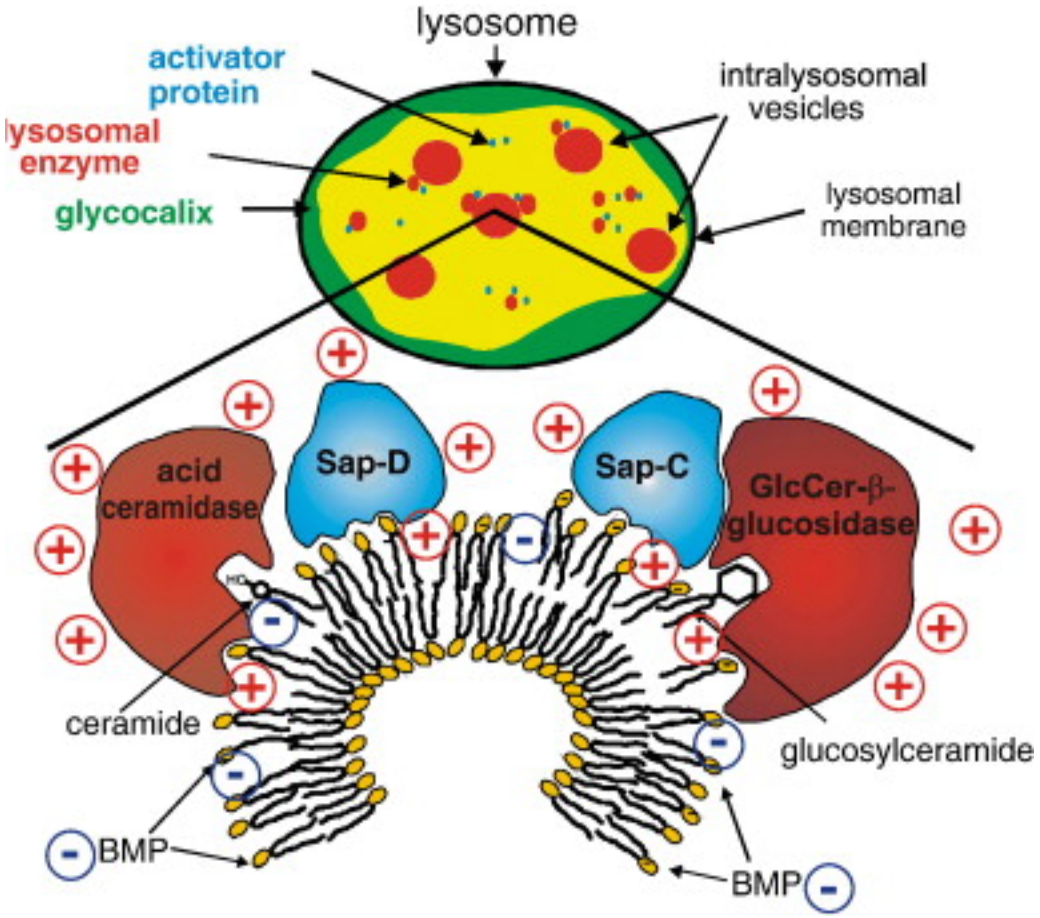
lysosome
activator protein
lysosomal enzyme
glycocalix
intralysosomal vesicles
lysosomal membrane
acid ceramidase
Sap-D
Sap-C
GlcCer-β-glucosidase
ceramide
glucosylceramide
BMP
BMP

Materials and Methods

Mice

VM/Dk mouse strain was obtained from G. Carlson (McLaughlin Research Institute, Great Falls, Montana) and from H. Fraser (University of Edinburgh, Scotland). The SV/129 *Hexβ* (+/−) mice were obtained from Dr. Richard Proia (NIH). β-galactosidase (+/-) mice were derived by homologous recombination and embryonic stem cell technology as previously described [40, 41]. Homozygous (-/-) mouse pups were derived from crossing heterozygous females with heterozygous male mice. Genotypes were determined as described previously [42, 43]. Cortex brain samples were collected at humane end point and stored at -80 °C. Humane end point for *Hexβ* (-/-) mice (Sandhoff Disease) was about 100 days and for β-gal (-/-) (GM1 gangliosidosis) mice was about 180 days. All mice were propagated in the Boston College Animal Care Facility and were housed in plastic cages with filter tops containing Sani-Chip bedding (P. J. Murphy Forest Products Corp.; Montville, NJ). The room was maintained at 22°C on a 12 hour light/12 hour dark cycle. Food (PROLAB R/M/H/3000 Lab Chow; Agway, St. Louis, MO) and water were provided ad libitum. All animal experiments were carried out with ethical committee approval in accordance with the National Institutes of Health Guide for the Care and Use of Laboratory Animals and were approved by the Institutional Animal Care Committee.

Cats

Sandhoff Disease and GM1 cats were obtained from the Baker colony at Auburn University, AL and result from naturally occurring mutations as previously described [44-49]. Sandhoff Disease cats had <3% normal hexosaminidase activity in cerebral cortex [50]. GM1 cats had <10% of β-galactosidase activity. Both feline models showed stereotypical clinical disease progression including corresponding ganglioside storage (GM2 for Sandhoff Disease, and GM1 for GM1 cats). Feline models also showed all brain and peripheral organ pathologies of the ganglioside disease and represented an authentic model to study disease progression [45, 51]. According to the recommendations of the AVMA Panel on Euthanasia, animals were euthanized by pentobarbital overdose, followed by transcardial perfusion with heparinized, cold saline (0.9 % NaCl) until jugular perfusate was clear. Cerebral cortex samples were collected at humane endpoint from gangliosidosis cats (Sandhoff Disease, 4-5 months; GM1, 7-8 months) and from age matched normal cats. Samples were frozen in liquid nitrogen and stored at -80°C. The Auburn University Institutional Animal Care and Use Committee approved all performed animal procedures.

Bears

American black bears with GM1 gangliosidosis were found in Northeast United

States. The bears were in poor clinical condition at 10-14 months in age and humanely euthanized as previously described [52]. The bear brain tissue was obtained as a gift from Joseph Alroy, Tufts University, Boston MA.

Human

Sandhoff Disease human cortex sample and its age-matched control were obtained from the NICHD Brain and Tissue Bank for Developmental Disorders at the University of Maryland, Baltimore.

Lipid isolation, purification, and quantification

Total lipid extraction

Total lipids were extracted from the cortexes of lyophilized whole brain or microsomal fractions with chloroform and methanol 1:1 by volume. Samples were further purified and prepared for column chromatography using previously described procedures [53, 54].

Column Chromatography

DEAE-Sephadex (A-25, Pharmacia Biotech, Uppsala, Sweden) columns were used to separate neutral and acidic lipids [55]. Total lipid extract was applied to

DEAE-Sephadex column that was equilibrated in solvent A (chloroform:methanol:water 30:60:8;v/v/v). Neutral lipids were eluted with solvent A. Acidic lipids, including gangliosides, were eluted with solvent B, comprised of chloroform:methanol: 0.8 M Na acetate (30:60:8 ; v/v/v)

Ganglioside purification

Acidic lipids were dried by rotary evaporation and further separated to acidic lipid and ganglioside fractions by Folch partitioning, as previously described [54, 56]. An aliquot was taken from ganglioside fraction for sialic acid determination and sialic acid was quantified by resorcinol assay. Gangliosides were further purified with base treatment and desalting as previously described [23, 24, 54]. Treatment of gangliosides with mild base is needed to remove contaminating phospholipids and any ganglioside internal esters or salt forms that might arise as artifacts of the lipid isolation procedures [57, 58].

BMP purification

After Folch partitioning, the lower phase including the acidic phospholipid fraction, was dried under nitrogen and resuspended in 10 mL of chloroform: methanol (1:1 by volume). This fraction was composed of bis(monoacylglycero)phosphate, cardiolipin, sulfatides, phosphatidyglycerol, phosphatidylserine, phosphatidylinositol and phosphatidic acid. High-performance thin-layer chromatography (HPTLC) was used to separate and visualize BMP. No BMP was detected in the Folch upper phase indicating that

all BMP partitioned into the lower phase.

High-performance thin-layer chromatography

High-performance thin-layer chromatography (HPTLC) was used to separate and visualize acidic and neutral lipids as previously described [23, 54, 59] Bis(monoacylglycero)phosphate was purchased from Avanti Polar Lipids (Alabaster, AL, USA). Lipid standards were either purchased from Matreya Inc. (Pleasant Gap, PA, USA), Sigma (St. Louis, MO, USA), or were provided by Dr. Robert Yu (Medical College of Georgia, Augusta, GA, USA). For BMP visualization, plates were subjected to a single ascending run with chloroform: methanol: ammonium hydroxide (30% by volume) (65:35:5/v:v:v) for 5 minutes and visualized by charring with 3% cupric acetate in 8% phosphoric acid solution, followed by heating in an oven at 165°C for 7 minutes. A Personal Densitometer SI determined densities of individual bands with ImageQuant software (Molecular Dynamics; Sunnyvale, CA). Concentrations of individual lipids were calculated based on standard curve obtained by standard lanes on HPTLC.

The amount of gangliosides spotted per lane was equivalent to 1.5 μg of sialic acid. Gangliosides were separated by a solution of chloroform:methanol:$CaCl_2$ (0.02%) (55:45:10; v/v/v) and visualized by spraying the dried plates with the resorcinol reagent, followed by heating at 95°C. Following quantification of ganglioside bands, total brain gangliosides were normalized to 100%, and sialic acid values were quantified by percent distribution of each ganglioside band [60].

Sialic acid quantification

Folch upper phase including ganglioside fraction was desalted and amount of sialic acid was measured before and after desalting by the resorcinol assay as previously described. [24, 50]. Three aliquots of each ganglioside sample were dried under vacuum. A resorcinol: dH_2O, 1:1, v/v solution (resorcinol reagent-HCl: 0.2 M resorcinol: dH_2O: 0.1 M $CuSO_4$, 40: 5: 5: 0.125, v/v/v/v) was added to each sample, followed by submersion in a boiling water bath for 17 min. After cooling on ice, the reaction was stopped with butyl acetate-*N*-butanol, 85:15, v/v. Each sample was vortexed and centrifuged at 700 *g* for 2 min. The absorbance of the upper aqueous layer was recorded at 580 nm using a Shimadzu UV-1601 spectrophotometer (Shimadzu; Torrance, CA). Sialic acid values were fit to a standard curve using *N*-acetylneuraminic acid as a standard [61].

Gas chromatography

Preparative HPTLC was used to separate BMP with chloroform: methanol: ammonium hydroxide (30% by volume) (65:35:5/v:v:v). Lipids were detected after spraying HPTLC with acetone:water (80:20) containing 5% primulin. The BMP fraction was scraped from the plate and esterified with acetyl chloride:methanol (1:4 volume/volume), and neutralized with K_2CO_3 (4%) in a sealed borosilicate tube under nitrogen. Separation of fatty acid methyl esters was carried out using gas-liquid chromatography (HP 6890) using a 30m x 0.25mm x 0.25µm Omegawax 250 fused silica capillary column (Supelco). Area

under the curve values used to calculate the percentages of individual fatty acids compared to sum area of all fatty acids.

Mass spectrometry

Preparative HPTLC, using the solvent system chloroform:methanol:ammonia (65:35:5/v:v:v), was used to separate BMP from other phosphoglycerides. Shotgun lipidomics analyses of BMP was performed on a triple-stage quadrupole (QqQ) mass spectrometer (Thermo Scientific, San Jose, CA) equipped with an ionspray ion source as previously described [62].

AAV vector design, preparation and delivery to brain

The following vectors were used in this study: AAV1-CBA-Hexα, and AAV1-CBA-Hexβ. AAV vectors encoding alpha- or beta-subunits of human β-hexosaminidase were constructed by PCR amplification of the respective cDNAs in the Mammalian Gene Collection (MGC) clones 14125 (IMAGE 3353424; Genbank: BC018927), and 1725 (IMAGE: 2967035; Genbank: BC017378) obtained from the American Type Culture Collection (Manassas, VA). The primers used for PCR amplification were:

HexA-1: ATCCACTAGTGGAGCACCATGACAAGTTCCAGGCTTTGGT;

HexA-2: AATTCTCGAGTCAGGTCTGTTCAAACTCCTGCTCAC;

HexB-1: ATCCACTAGTGGAGCACCATGGAGCTGTGCGGGCTGG;

HexB-2: AATTCTCGAGTTACATGTTCTCATGGTTACAATATC.

PCR products were digested with Spe I and Xho I (sequences underlined in the primers above) and cloned into pAAV-CBA-MBG-W [63] in place of the mouse βgal cDNA. All vectors used in this study carry the woodchuck hepatitis virus post-transcriptional regulatory element (WPRE). AAV1 vector stocks were produced as described [63].

Six week-old Sandhoff Disease mice were injected with 2 µl of 1:1 formulation of AAV1-CBA-Hexα + AAV1-CBA-Hex β vectors ($7.2x10^{12}$ gc/ml for each vector in the formulation) stereotaxically into left and right thalamus (n=4) (Coordinates from bregma in mm: AP –2.0, ML ±1.5, DV –2.5) at a rate of 0.2. $\mu l.min^{-1}$ as previously described [64].

Statistical analysis

Statistical significance of data was analyzed by the two-tailed Student's t-Test between the normal and the diseased samples. Interquartile range was approximated between the maximum and minimum elements in the data set divided by 2.

Results

BMP accumulates in brain of mice, cat, bear, and human with GM2 (Sandhoff Disease) or GM1 gangliosidoses

Our objective was to evaluate the content and fatty acid composition of BMP in the brain of mice, cats, bear, and humans with GM2 (Sandhoff Disease) and/or GM1 gangliosidosis. BMP accumulation (up to 32-fold increase) was found in all samples of gangliosidosis brain tissue (Figure 4, Table 1), showing that BMP accumulates as a secondary storage material in the gangliosidosis brain. BMP levels were also higher in juvenile (p15) *β-gal* (-/-) (GM1 gangliosidosis) mouse brains than in age-matched *β-gal* (+/-) (normal) brains (Figure 5).

BMP accumulates in liver of GM2 (Sandhoff Disease) mice but not in liver of GM1 gangliosidosis mice

We also observed BMP was stored in the liver of *Hexβ* (-/-) (Sandhoff Disease mice), but not in the liver of *β-gal* (-/-) GM1 gangliosidosis mice (Figure 6A, Table 1). BMP accumulations were in line with GM2 ganglioside storage seen in Sandhoff Disease mice liver There is no GM1 accumulation in GM1 gangliosidosis mice liver due to absence of GM1 synthesis in liver (Figure 6B) [65].

Effect of LPS injections on BMP content in Sandhoff Disease mice brain.

We analyzed whether further inducing inflammation with LPS could increase BMP levels in Sandhoff Disease mice brain. Sandhoff Disease mice received 4 daily injections of 1mg/kg *i.p* LPS injections to induce microglia inflammation. BMP content was similar in Sandhoff Disease mouse brain injected with LPS or saline (PBS) for 4 consecutive days suggesting increasing inflammation in Sandhoff Disease brain didn't contribute further to already existing BMP levels in Sandhoff Disease mice brain (Figure 7).

BMP separates from its structural isomer PG by HPTLC and Mass Spectrometry

BMP has the same molecular weight with phosphatidylglycerol (PG), therefore it is challenging to separate BMP from PG in mass spectrometry without an initial chromatography procedure. In our solvent system BMP (Rf =0.71), separated from PG (Rf=0.57) clearly. In order to further validate BMP as a separate lipid from PG, we analyzed the isolated BMP from HPTLC plates by a triple-stage quadrupole (QqQ) mass spectrometer. Analysis of commercial standards from Avanti showed BMP to have a distinct peak around m/z 92, while PG standard had two distinct peaks at m/z 171 and m/z 227. The BMP isolated from GM2 gangliosidosis mice brain also showed the distinct peak at m/z 92, while these samples had very low peaks at m/z 171 and m/z 227 (Figure 8). Also the

predominant BMP species in GM2 gangliosidosis mice had molecular weight of 865.5 corresponding to 22:6- 22:6 BMP (Figure 8), which correlates well with the gas chromatography data showing that 22:6 is the predominant BMP fatty acid species in mice with GM2 gangliosidosis.

Fatty acyl species of BMP

We analyzed the fatty acyl species of BMP by gas chromatography. Major fatty acid species in BMP from gangliosidoses brain samples included stearic acid (C18:0), oleic acid (C18:1), arachidonic acid (20:4) and docosahexaenoic acid (22:6) (Table 2). C22:6 was the predominant (57-62%) fatty acid present in brain of GM1 and GM2 gangliosidoses mice and in GM1 gangliosidosis American black bear. These species contained 16-22 % of C18:0 and C18:1. In contrast, C18:0 + C18:1 were the predominant (37-57%) fatty acids in brain of GM1 and GM2 gangliosidosis cats and GM2 gangliosidosis human. These species had lower amounts (17-37%) of C22:6 (Table 2).

AAV-mediated gene therapy reduces storage of brain BMP and ganglioside content

The relationship of BMP storage to ganglioside storage was evaluated in brains of *Hexβ* (+/-) (normal), *Hexβ* (-/-) (Sandhoff Disease) mice that were treated or not treated with AAV gene therapy. Both GM2 and BMP levels were lower in the

AAV-treated Sandhoff Disease mice than in the untreated Sandhoff Disease mice (Table 3). GM2 content was significantly correlated with the BMP content in these 13 brain samples analyzed ($r = 0.9822$, $P < 0.01$). For the correlation analysis, an arbitrary value of 0.5 μg sialic acid/ 100 mg of tissue dry weight was used to represent 0 amounts on the HPTLC plate.

Figure 4. HPTLC analysis of acidic lipids in the brains of mice, cats, humans, and bear with ganglioside storage disease. The normal (N), Sandhoff Disease and GM1 mice represent the *Hexβ* (+/-), *Hexβ* (-/-) and *β-gal* (-/-) mice, respectively. The HPTLC was developed for 5 min with chloroform: methanol: ammonia (30% aqueous solution) (65:35:5; v/v/v). The amount of acidic lipid spotted per lane was equivalent to 200 *μ*g of tissue dry weight. The bands were visualized by charring with 3 % cupric acetate in 8 % phosphoric acid solution. *Std* Standard is a mixture of purified acidic lipids including *BMP* Bis(monoacylglycero)phosphate; *CL* cardiolipin; *PA* phosphatidic acid; *Sulf* sulfatides; *PS* phosphatidylserine and *PI* phosphatidylinositol.

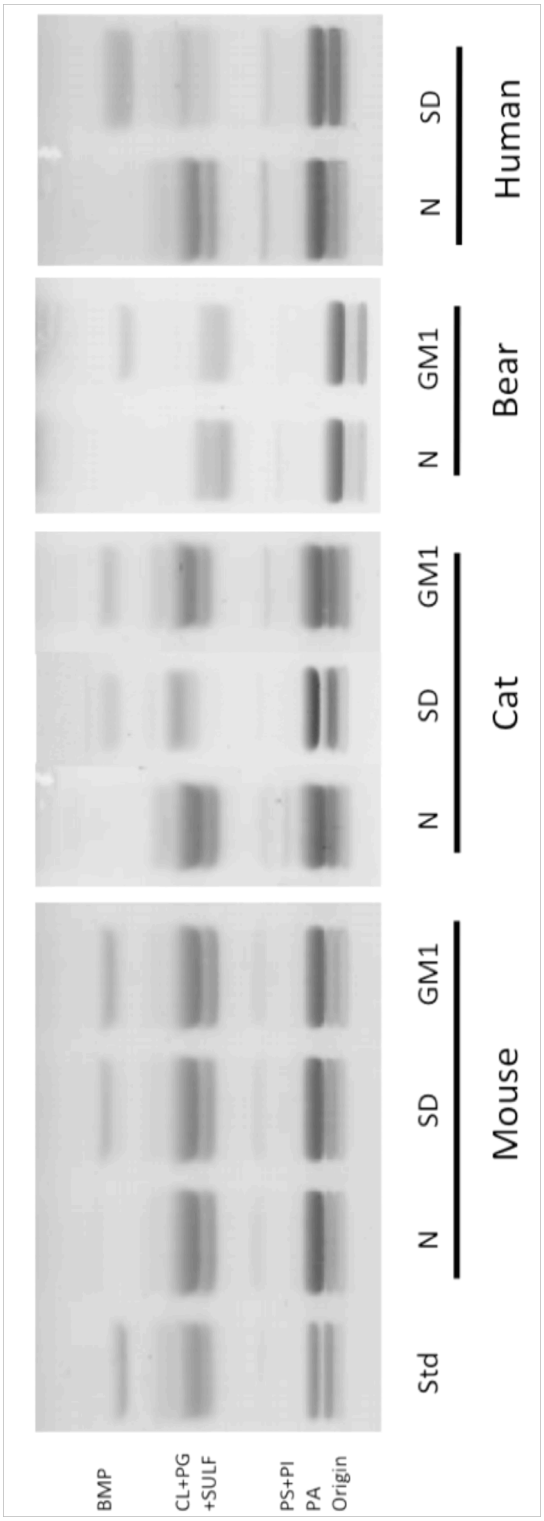
BMP
CL+PG
+SULF
PS+PI
PA
Origin
Std
N
SD
GM1
Mouse
N
SD
GM1
Cat
N
GM1
Bear
N
SD
Human

Figure 5. BMP content in the brains of juvenile (p15) or adult (p100) mice with ganglioside storage disease. The normal (N), GM1 gangliosidosis mice represent the *β-gal* (+/-), *β-gal* (-/-) mice, respectively. The HPTLC was developed for 5 min with chloroform: methanol: ammonia (30% aqueous solution) (65:35:5; v/v/v). The amount of acidic lipid spotted per lane was equivalent to 200 *μ*g of tissue dry weight. The bands were visualized by charring with 3 % cupric acetate in 8 % phosphoric acid solution. BMP accumulation was observed in Juvenile p15 mice as well as adult P100 mice. *Std* Standard is a mixture of purified acidic lipids including *BMP* Bis(monoacylglycero)phosphate; *CL* cardiolipin; *PA* phosphatidic acid; *Sulf* sulfatides; *PS* phosphatidylserine and *PI* phosphatidylinositol.

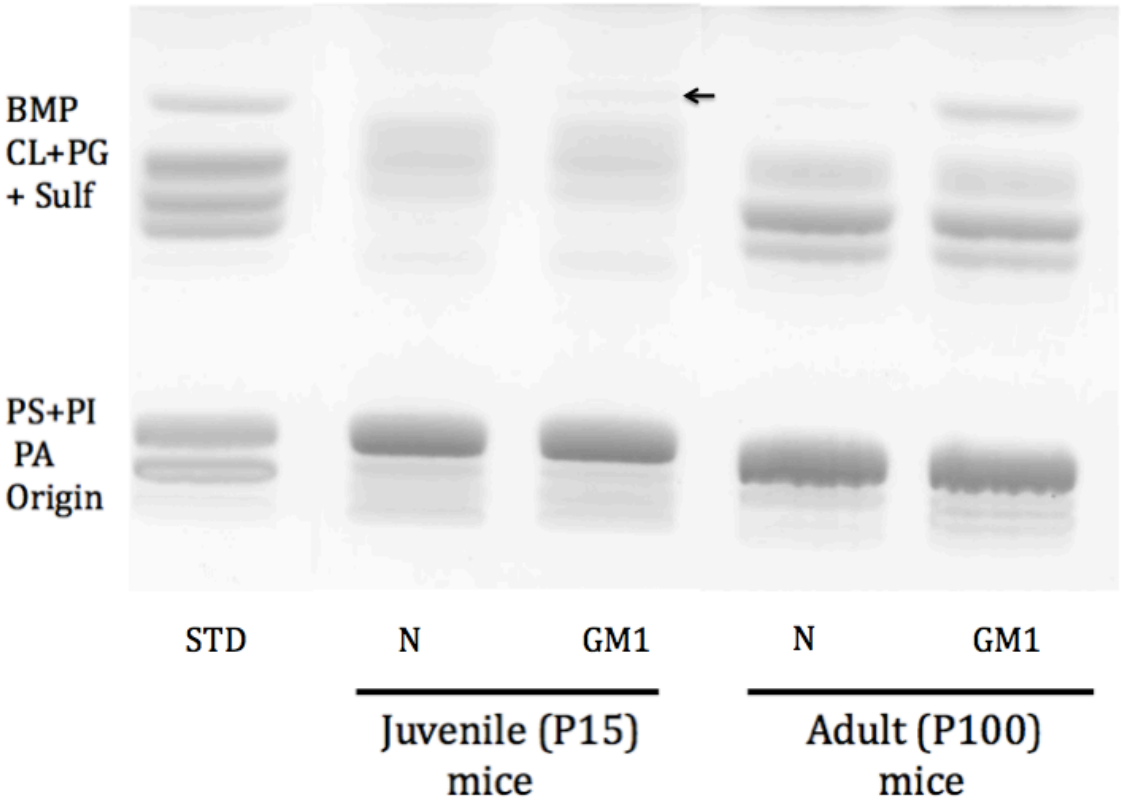
BMP
CL+PG
+ Sulf
PS+PI
PA
Origin
STD
N
GM1
N
GM1
Juvenile (P15)
mice
Adult (P100)
mice

Figure 6. BMP and Ganglioside levels in livers of GM1 Gangliosidosis and Sandhoff Disease mice. (A) HPTLC analysis of acidic lipids in the livers of mice with ganglioside storage disease**.** The normal (N), Sandhoff Disease and GM1 mice represent the 100 days old *Hexβ* (+/-), 100 days old *Hexβ* (-/-) and 180 days old *β-gal* (-/-) mice, respectively. The HPTLC was developed for 5 min with chloroform: methanol: ammonia (30% aqueous solution) (65:35:5; v/v/v). The amount of acidic lipid spotted per lane was equivalent to 200 *μ*g of tissue dry weight. The bands were visualized by charring with 3 % cupric acetate in 8 % phosphoric acid solution. *Std* Standard is a mixture of purified acidic lipids including *BMP* Bis(monoacylglycero)phosphate; *CL* cardiolipin; *PA* phosphatidic acid; *Sulf* sulfatides; *PS* phosphatidylserine and *PI* phosphatidylinositol. **(B)** Ganglioside distribution in the livers of mice with ganglioside storage disease. The amount of ganglioside sialic acid spotted per lane was equivalent to 1.5 μg sialic acid. The plate was developed in a single ascending run (90 min) with chloroform: methanol: water (55:45:10 v/v/v) containing 0.02% calcium chloride. The bands were visualized by spraying with the resorcinol reagent and heating to 95°C.

A

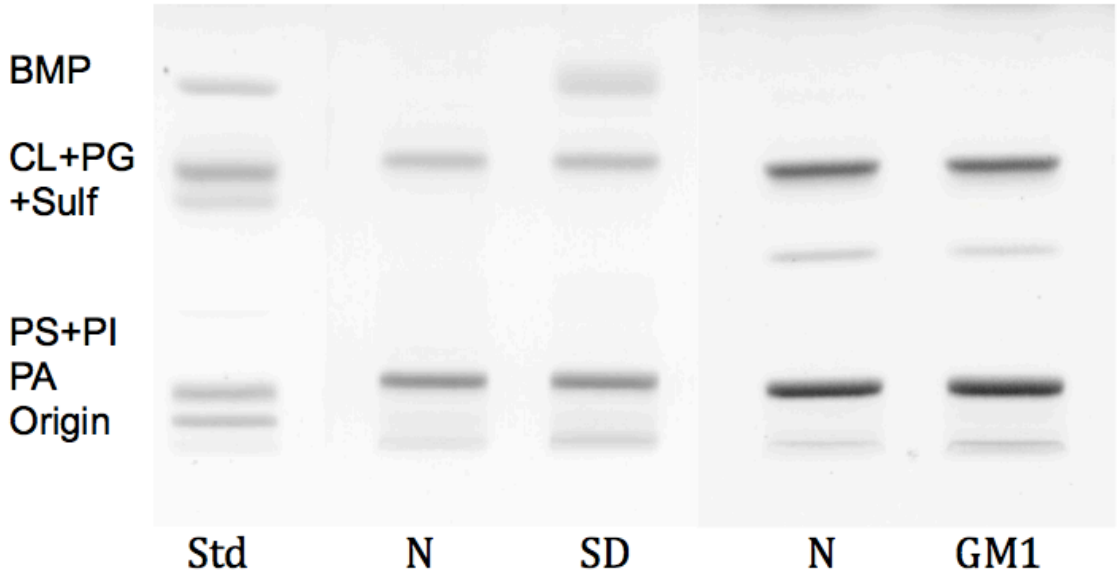
BMP
CL+PG
+Sulf
PS+PI
PA
Origin
Std
N
SD
N
GM1

B

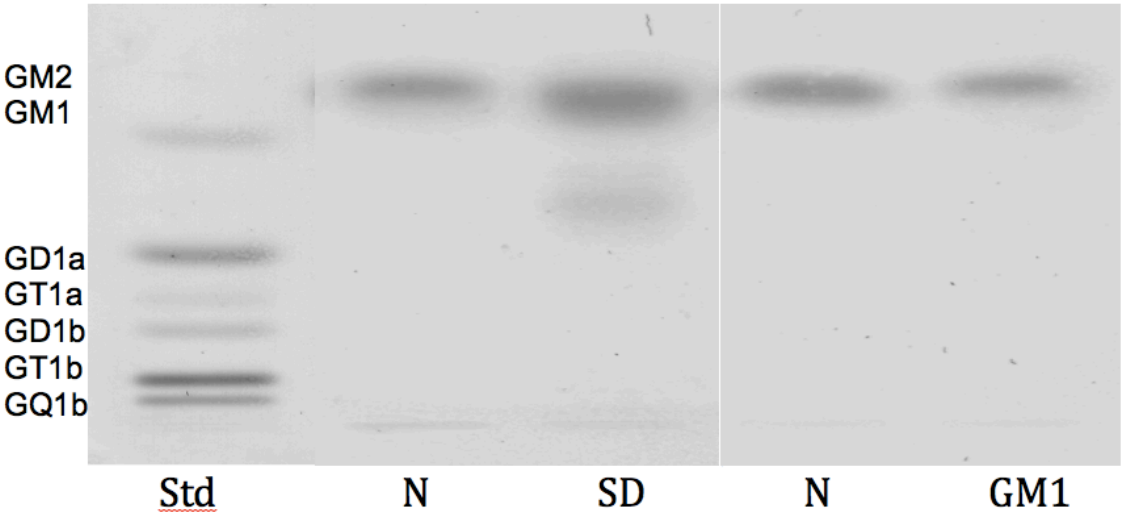
GM2
GM1
GD1a
GT1a
GD1b
GT1b
GQ1b
Std
N
SD
N
GM1

Figure 7. Effect of LPS on BMP content in Sandhoff Disease mouse brain. Sandhoff Disease mice received 4 daily injections of 1mg/kg *i.p* LPS injections. BMP content was analyzed with HPTLC of acidic lipids. The HPTLC was developed for 5 min with chloroform: methanol: ammonia (30% aqueous solution) (65:35:5; v/v/v). The amount of acidic lipid spotted per lane was equivalent to 200 *μ*g of tissue dry weight. The bands were visualized by charring with 3 % cupric acetate in 8 % phosphoric acid solution. BMP content did not increase in Sandhoff Disease mice brain with LPS induced brain inflammation. *Std* Standard is a mixture of purified acidic lipids including *BMP* Bis(monoacylglycero)phosphate; *CL* cardiolipin; *PA* phosphatidic acid; *Sulf* sulfatides; *PS* phosphatidylserine and *PI* phosphatidylinositol.

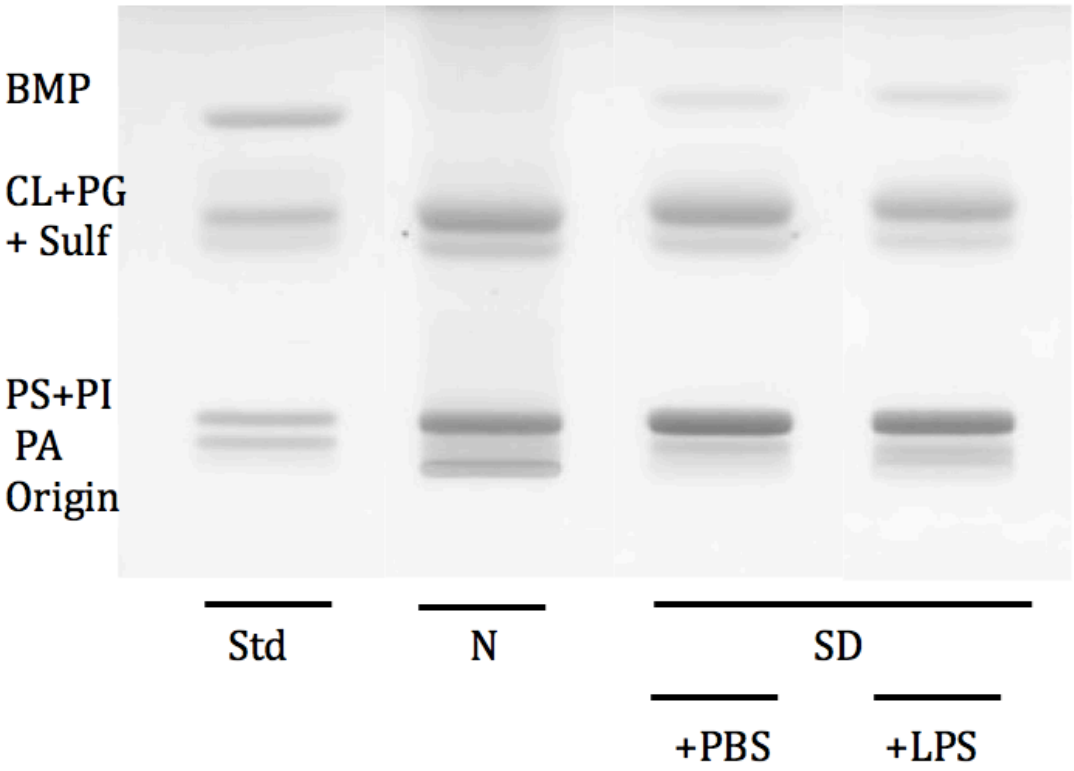
BMP
CL+PG
+ Sulf
PS+PI
PA
Origin
Std
N
SD
+PBS
+LPS

Figure 8. Mass Spectrometry analysis of BMP in Sandhoff disease mouse brain. Triple-stage quadrupole (QqQ) mass spectrometer of (A) C18:1, 18:1 commercial BMP standard, (B) C18:1, C16:0 commercial PG standard and (C) BMP obtained from Sandhoff Disease mouse brain.

A

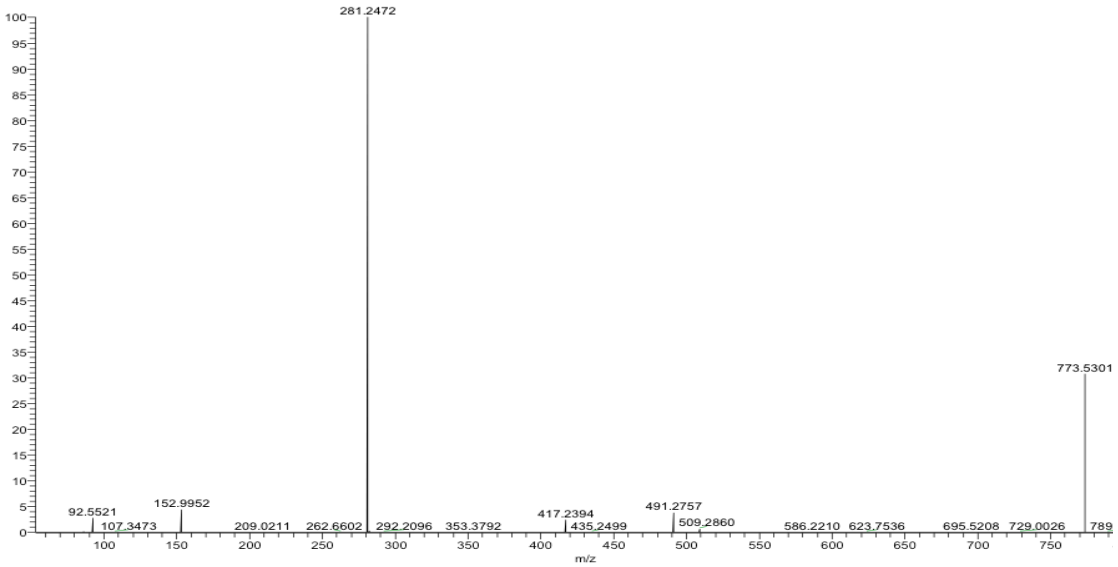
281.2472
773.5301
92.5521
107.3473
152.9952
209.0211
262.6602
292.2096
353.3792
417.2394
435.2499
491.2757
509.2860
586.2210
623.7536
695.5208
729.0026
789
m/z

B

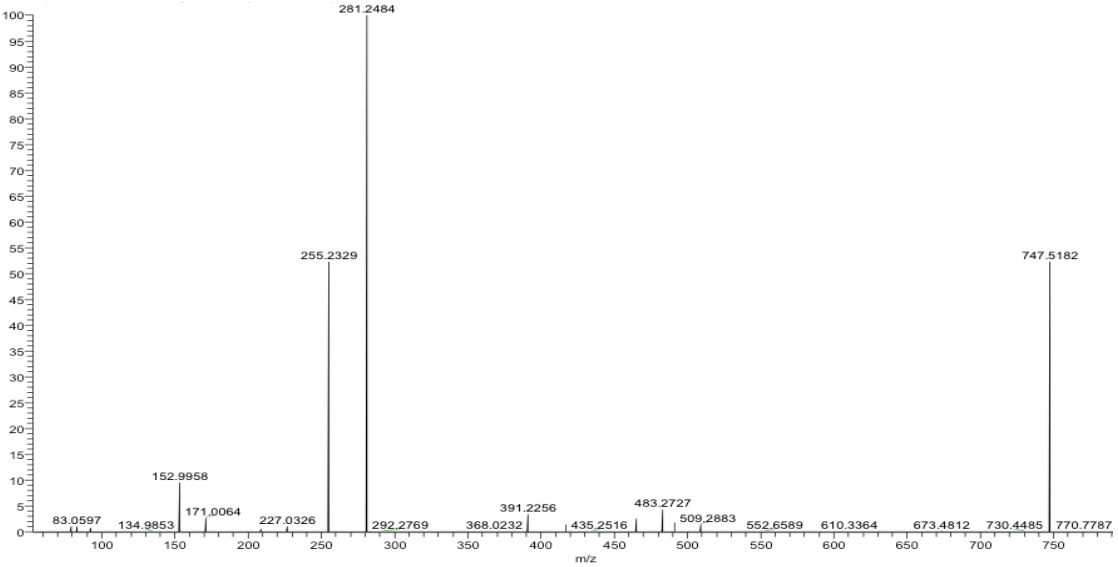
281.2484
255.2329
747.5182
83.0597
134.9853
152.9958
171.0064
227.0326
292.2769
368.0232
391.2256
435.2516
483.2727
509.2883
552.6589
610.3364
673.4812
730.4485
770.7787
m/z

C

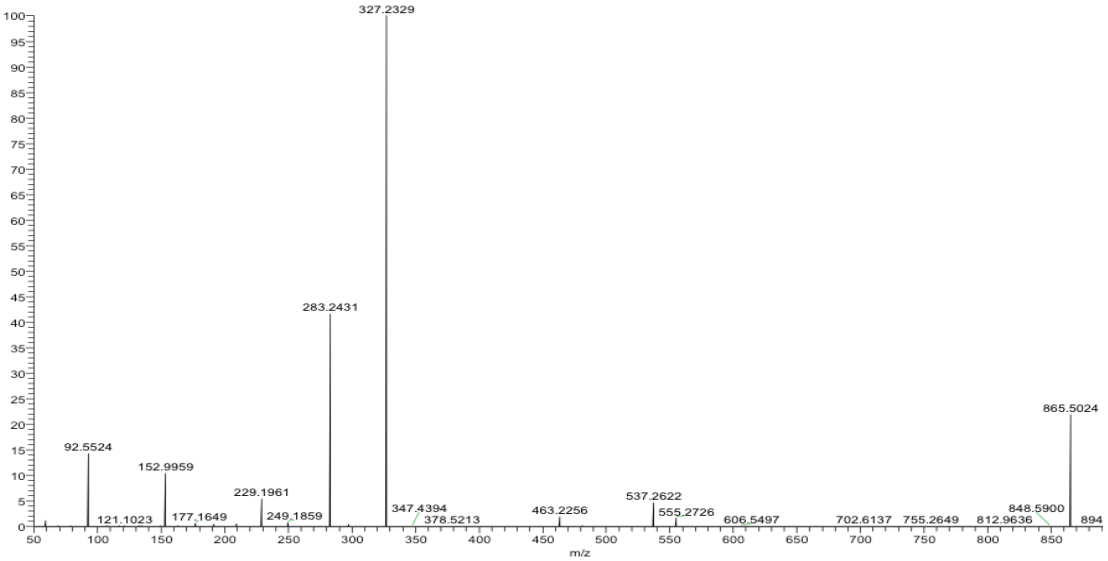
327.2329
283.2431
865.5024
92.5524
121.1023
152.9959
177.1649
229.1961
249.1859
347.4394
378.5213
463.2256
537.2622
555.2726
606.5497
702.6137
755.2649
812.9636
848.5900
894
m/z

Table 1. BMP levels in the brains of mouse, cat, bear, and human with ganglioside storage disease

Species	Age	Phenotype	Tissue	n	BMP [a]	Fold increase
Mouse	Adult	Normal	Brain	6	42.7 ± 11.5	
	Adult	SD	Brain	3	148.6 ± 22.6 [c]	3.4
	Adult	GM1	Brain	3	256.0 ± 11.9 [c]	6.0
	Juvenile [b]	Normal	Brain	3	17.9 ± 2.0	
	Juvenile [b]	SD	Brain	2	109.0 ± 9.4 [c]	6.0
	Adult	Normal	Liver	3	ND	
	Adult	SD	Liver	3	243.9 ± 171.0	>50
Cat	Adult	Normal	Brain	3	12.0 ± 17.3	
	Adult	SD	Brain	3	219.6 ± 16.0 [c]	18.3
	Adult	GM1	Brain	2	370.4 ± 61.1 [c]	30.8
Bear	Adult	Normal	Brain	1	12.2	
	Adult	GM1	Brain	1	184.2	15.0
Human	Adult	Normal	Brain	1	29.5	
	Adult	SD	Brain	1	451.1	15.3

[a] BMP levels are represented as µg/ 100 mg of tissue dry weight. ND=Not Detected

[b] Juvenile mouse brains are analyzed at P15

[c] Significantly different than normal sample in the same group using student t-test ($p<0.05$).

Table 2. Fatty acid distribution of brain BMP from mouse, cat, bear, and human with ganglioside storage disease

Species	Mouse						Cat						Bear	Human
Phenotype	SD			GM1			SD			GM1			GM1	SD
n	3			3			3			2			1	1
Fatty acids														
C16:0	9.0	±	1.8	5.4	±	0.5	5.4	±	1.1	10.9	±	0.6	3.5	4.3
C18:0	10.4	±	1.8	8.7	±	0.8	15.4	±	2.7	24	±	0.9	5.4	33.0
C18:1	11.5	±	1.9	11.7	±	0.6	21.7	±	3.3	22.6	±	0.9	10.7	24.2
C18:2n-6	1.5	±	0.4	1.2	±	0.1	5.2	±	0.4	2.0	±	0.5	3.0	4.9
C20:2	2.0	±	0.6	2.6	±	1.2	0.5	±	0.4	1.6	±	0	0.6	4.2
C20:4n-6	7.2	±	0.4	8.0	±	0.4	6.6	±	0.7	5.9	±	0.2	13.8	5.9
C20:5n-3	ND			4.4	±	1.7	8.5	±	3.0	0.4	±	0.2	0.3	ND
C22:6n-3	58.4	±	4.8	57.9	±	2.4	36.7	±	2.9	32.7	±	1.4	62.6	17.2
C24:0	ND			ND			ND			ND			9.6	6.3

Mouse and cat brain samples are obtained from GM1 and GM2 gangliosidosis(SD) effected animals as described in materials and methods. Bear and human samples are obtained from post-mortem diseased subjects.Values represent mean percentage distribution of fatty acid ± interquartile range of independent samples where n≥2. ND=Not Detected

Table 3. Influence of AAV gene therapy on the content of GM2 and BMP in Sandhoff Disease mouse brain

Sample	Phenotype	Treatment	GM2 [a]	BMP [b]
1	normal	none	ND	66.8
2	normal	none	ND	72.1
3	normal	none	ND	61.9
4	SD	none	357.7	180.0
5	SD	none	376.7	162.5
6	SD	none	347.8	179.3
7	SD	none	391.1	187.5
8	SD	AAV	4.4	74.3
9	SD	AAV	16.4	74.5
10	SD	AAV	34.9	81.8
11	SD	AAV	23.0	81.4
12	SD	AAV	39.1	85.2
13	SD	AAV	4.1	70.2

[a] GM2 values are expressed as µg sialic acid/100 mg of tissue dry weight. ND=Not Detected
[b] BMP values are expressed as µg /100 mg of tissue dry weight

Discussion

Although BMP comprises a small portion of total phospholipids in normal tissues, BMP levels increase in many LSDs such as Niemann-Pick, neuronal ceroid lipofuscinoses, mucopolysaccharidosis (MPS I and II), Fabry disease, and Gaucher disease [27, 28, 30-34, 66, 67]. However, no detailed studies of BMP content and composition have been conducted in the brains of ganglioside storage diseases [37]. We observed a dramatic increase of BMP levels in GM1 and GM2 gangliosidoses brain samples in humans, American black bear, cats, and mice compared to their non-diseased counterparts. LSDs frequently involve a secondary storage material in addition to the primary storage material [37, 68]. Examples include secondary ganglioside storage in Gaucher disease, and MPS, and secondary cholesterol storage in Niemann Pick disease [69].

We found that BMP was stored as a secondary material in the brains of GM1 and GM2 gangliosidoses. An explanation for the secondary storage of BMP in gangliosidosis brain has not been established [38]. Since BMP is localized to endosomal/lysosomal membranes [70], a lysosomal expansion from stored gangliosides could simply increase the amount of a lipid localized in these compartments. However, BMP does not increase proportionally with lysosomal size, and it is not stored as a secondary material in all LSDs [38]. Hence, lysosomal expansion might not be the only mechanism for BMP elevation [31, 38].

It is also unlikely that BMP storage is linked directly to the primary enzyme deficiency in LSDs, as BMP storage was not observed in the liver of GM1 gangliosidosis (*β-gal*(-/-)) mice despite the presence of ganglioside storage in the brain of these mice (data not shown). GM1 is not stored in the liver of *β-gal* (-/-) mice, as GM1 synthesis does not occur in mouse liver [71]. On the other hand, BMP storage was observed in the liver of Sandhoff Disease mice (Table 3), where GM2 and GA2 are also stored [71]. This observation indicates that BMP co-accumulates with ganglioside storage, rather than as a downstream by-product of a non-functional enzyme. We also observed an enrichment of BMP in brain microsomal fractions that were obtained from *β-gal* -/- mice. This observation is consistent with our previous finding of GM1 enrichment in this fraction [61]. These findings support further the co-localization of BMP with the abnormal ganglioside accumulation. Since we did not perform a detailed analysis of BMP accumulation in the microsomal fraction, BMP might co-localize with GM1 in endo-lysosomes, microsomes or mitochondria-associated ER membranes [72]. Further studies needed to resolve this issue.

Kobayashi et al showed that BMP plays a role in the formation, structure, and trafficking of endosomal/lysosomal compartments in cells under normal conditions [2, 70, 73]. Late endosomes/lysosomes form multivesicular bodies under normal conditions, but form multilamellar vesicles in pathological cases such as the gangliosidoses [74, 75]. Both gangliosides and BMP are thought necessary for the formation of these aberrant lamellar bodies. It is possible that

the high BMP levels we observed in the brains from the GM1 and GM2 gangliosidoses contribute to the formation of these multilamellar storage vesicles.

Glycosphingolipids are degraded in lysosomes with the aid of hydrolases and lysosomal lipid binding proteins, e.g. saposins [19, 76]. The lipid composition of lysosomes is thought to be important in this degradation, and anionic phospholipids such as BMP are thought to facilitate the degradation of glycosphingolipids in the limiting membrane of endosomal/lysosomal compartments [77]. BMP facilitates cholesterol transport, and the application of anti-BMP antibodies leads to cholesterol accumulation in lysosomes, mimicking the Niemann Pick phenotype [78]. BMP becomes limiting in Niemann pick disease fibroblasts, and exogenous feeding of BMP decreases excessive cholesterol storage [18]. Also Hein et al show that selective decrease of BMP, reduces the storage material glucosylceramide in THP-1 Gaucher macrophages [26] Further studies will be needed to determine if modulation of BMP levels can decrease ganglioside storage in the GM1 and GM2 gangliosidoses.

Inflammation is a hallmark of the gangliosidoses [79]. Microglial infiltration is observed with the onset of behavioral symptoms (about 2.5 months) in Sandhoff Disease (*Hexβ* (-/-)) mice and GM1 gangliosidosis (*β-gal* -/-) mice [79, 80]. Since BMP is a major lipid in alveolar macrophages, it is possible that microglial/macrophage infiltration could contribute in part to the increased BMP levels observed in the brains of the gangliosidoses. To address this possibility,

we analyzed BMP levels in young *Hexβ* (-/-) mice at postnatal day 15 (p15), well before the onset of behavioral symptoms and inflammation. However, GM2 gangliosides storage is observable in the p15 *Hexβ* (-/-) mice [71]. We found that brain levels of BMP were higher in the p15 *Hexβ* (-/-) mice than in the normal age matched controls. Also In order to test a possible disease associated-microglia infiltration contribution to BMP levels, we induced microglia proliferation with *i.p* injections of LPS. However, BMP levels were similar in Sandhoff Disease mouse brain injected with LPS or saline (PBS). These findings suggest that BMP storage is not likely associated with inflammation, but is associated with ganglioside storage.

Adeno-associated viral (AAV) gene therapy has been successfully used to treat GM1 and GM2 gangliosidosis in both mice and cats [63, 64, 81-83]. Vectors expressing the deficient enzymes needed for corresponding ganglioside degradation are delivered intracranially. AAV treatments can successfully restore the deficient enzymatic activity and eliminate most of the corresponding ganglioside storage [63, 64, 81-83]. We observed that AAV treatment also eliminated secondary storage of BMP in Sandhoff Disease mouse brains. A significant positive correlation was observed between BMP storage and GM2 storage in the AAV-treated and untreated mice. These results show that AAV therapy that targets the primary storage successfully clears the secondary BMP storage as well.

Another property of BMP is its unique fatty acid composition. C18:1 is a major BMP fatty acid in many cell types [11-13, 15, 84, 85]. In alveolar macrophages, BMP predominantly contains n-6 fatty acids such as linoleic acid (18:2) and arachidonic acid (20:4) [10, 86]. Interestingly, docosahexaenoic acid (DHA, C22:6, n-3) comprises a significant portion of BMP fatty acids in many cell types, in drug-induced phospholipidosis, and also in many LSDs [12, 13, 15, 33, 84, 87-92]. We also found that DHA was a major fatty acid species in BMP from the brains of mouse, cat, and bear with gangliosidosis. This predominance was most dramatic in mouse and bear samples where DHA comprised 57-62% of the BMP fatty acids. The reason for this high DHA percentage is unclear. Polyunsaturated fatty acids can influence membrane fluidity, which might be important for control of endosomal sorting and membrane fusion. Bouvier et al showed that 22:6/22:6 BMP can be oxidized in the presence of oxygen radicals [15], thus protecting cholesterol from oxidation. However, the specific function of 22:6 in LSDs remains unclear [38].

Here we analyzed the content and fatty acid composition of BMP in humans and in animals (mice, cats, American black bears) with either GM1 or GM2 ganglioside storage disease. Our results showed that BMP was a significant secondary storage material in the gangliosidoses. BMP storage might be linked to lysosomal size, or might have a functional role in clearing excess storage material. Further studies will be needed to address these issues.

CHAPTER 2

Introduction

Macrophages are the major phagocytes of the immune system, digesting intra-cellular material by autophagy, or extracellular material engulfed by endocytosis. Engulfed materials are either recycled to the plasma membrane or are directed to the lysosomes by endosomal transport. Early endosomes mature into late endosomes and then lysosomes, while forming intraluminal vesicles for efficient sorting and degradation of the cargo [93]. BMP is enriched in intraluminal vesicles, representing up to 70% of the phospholipids [73]. While the diameter of lysosomes is around 1.0 micron in most cell types, the diameter in macrophages can reach up to several microns [94].

In most mammalian cells, BMP levels are low, comprising only about 1-2 % of total phospholipids. However, BMP constitutes 16% of the total phospholipids in lung alveolar macrophages [10]. In this work, we show that BMP comprises a significant portion of phospholipids in various mouse cells of macrophage origin compared to cell lines of macroglial origin, such as oligodendrocyte progenitors and astrocytes. BMP, with its unique properties in lysosomal function and storage, could be an important lipid for macrophage biology and function.

Materials and Methods

Origin of the VM-M3, VM-M2 and CT-2A tumor cells

Spontaneous VM-M3 and VM-M2 tumors were identified in the cerebrum of VM/Dk inbred mice that showed cranial swelling and lethargy during routine examination. Tumors were passaged in brain and maintained *in vivo* as previously described [95]. The CT-2A was produced with intracranial chemical carcinogen implantation into C57BL/6J mouse brain as previously described [96]. CT2A is an NG2-rich stem cell-like murine glioma [97-99]

Cell lines and culture conditions

VM-M3, VM-M2 and CT-2A clonal cell lines were generated from the primary tumors by tissue disassociation and cell culture seeding. The macrophage RAW 264.7, BV2 and the mouse astrocyte C8-D30 (Astrocyte type III clone) cell lines were purchased from American Type Culture Collection (Manassas, VA). The cell lines were grown in high glucose (25 mM) Dulbecco's modified Eagle medium (DMEM, Sigma, St. Louis, MO) supplemented with 10% fetal bovine serum (FBS, Sigma) and 50 lg/ml penicillin– streptomycin (Sigma). The cells were maintained in 95% air and 5%CO2 at 37°C in a CO2 incubator.

Peritoneal macrophage isolation

Peritoneal macrophages were isolated as previously described [100]. Briefly, adult VM mice (3-4 months old) received 1.0 ml intraperitoneal injection of Brewer's thioglycollate broth. The mice were euthanized with CO2 four days after the injection, and the peritoneal area was cleaned with 70% ethanol. Ice-cold PBS (10 ml) was injected intraperitoneally and cells were collected with an 18-gauge needle, and immediately transferred to a 50 ml conical tube on ice. Elutes that had blood contamination were discarded. Cells were spun at 400 x g for 10 min and re-suspended in high glucose (25 mM) Dulbecco's modified Eagle medium supplemented with 10% fetal bovine serum and 50 Ulg/ml penicillin–streptomycin. Cells were washed with PBS 3-4 hours after initial seeding and were cultured in DMEM for 24 hours before collection.

Lipid isolation, purification, and quantification

See Chapter 1 Materials & Methods for details.

Gas chromatography

See Chapter 1 Materials & Methods for details.

Statistical analysis

See Chapter 1 Materials & Methods for details.

Results

BMP levels in cells with macroglial and microglial/macrophage origin

Our goal was to determine if the amount of BMP differed between normal cells and tumor cells classified as microglia/macrophages (VM-M3, VM-M2, BV2, and peritoneal macrophages), and the cells classified as macroglia (murine astrocytes and CT-2A). BMP levels were significantly greater in cells of microglial/macrophage origin than in cells of macroglial origin (Figure 9, Table 4). BMP represented only about 1.8 - 3.7% of total phospholipids in the CT-2A tumor cells and astrocytes, whereas it represented 7.1 - 10.4% in the microglia/macrophage cells.

Fatty acid distribution of BMP from cells with macrophage/microglia origin

C18:1 was the predominant fatty acid species in BMP obtained from the cultured macrophage/microglia cell lines (VM-M3, VM-M3, RAW and BV2), comprising 49.8 - 66.9% of the total fatty acids (Table 5). BMP from these cell lines also expressed C16:0, C16:1, C18:0, C20:1, C20:4, C20:5 and C22:6 in variable percentages. However, C16:0 was the predominant fatty acid (21.5%), followed by C18:1 (19.7%), in thioglycollate-elicited peritoneal macrophages. The percentage of C22:6 was highest in BMP from thioglycollate-elicited peritoneal macrophages (18.0%) with a lower percentage in the cultured BV2 microglial cells (8.2%).

Figure 9. HPTLC of acidic phospholipids from cell lines with macroglial (CT2A, astrocyte) and macrophage/microglial origin (VM-M3, VM-M2, RAW 264.7, BV2, peritoneal macrophages (PM)). The amount of acidic lipid spotted per lane was equivalent to 300 *μ*g of dry cell pellet weight. The bands were visualized by charring with 3 % cupric acetate in 8 % phosphoric acid solution. *Std* Standard is a mixture of purified acidic lipids including *BMP* Bis(monoacylglycero)phosphate; *CL* cardiolipin; *PA* phosphatidic acid; *PG* phosphatidylglycerol; *PS* phosphatidylserine and *PI* phosphatidylinositol.

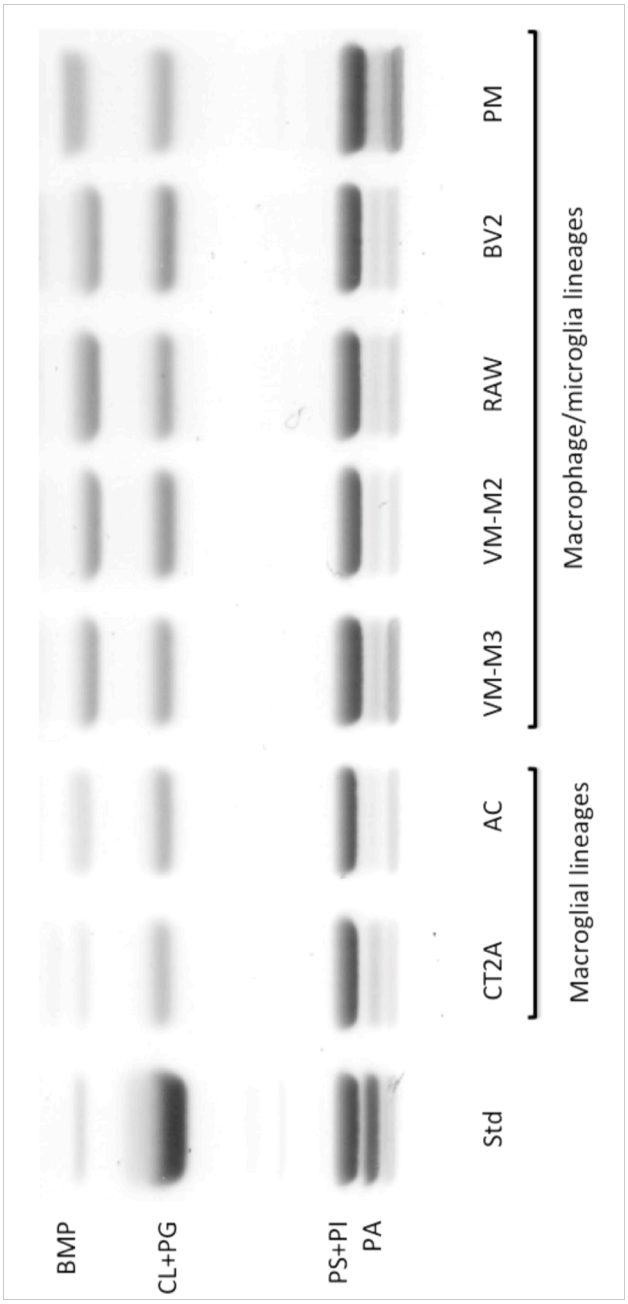
BMP
CL+PG
PS+PI
PA
Std
CT2A
AC
VM-M3
VM-M2
RAW
BV2
PM
Macroglial lineages
Macrophage/microglia lineages

Table 4. BMP levels in cells with macroglial and macrophage/microglial origin

Cell Line	Origin	BMP concentration [a]	BMP % of total phospholipids[b]
CT2A	Oligodendrocyte progenitor	47.9 ± 1.8	1.8 ± 0.1
C8-D30	Astrocyte	122.8 ± 7.8	3.7 ± 0.1
VM-M3	Macrophage/ Microglia	202.3 ± 3.9[c]	7.2 ± 0.2
VM-M2	Macrophage/ Microglia	215.5 ± 4.0[c]	7.1 ± 0.2
RAW	Macrophage	294.3 ± 7.5[c]	10.4 ± 0.1
BV2	Microglia	214.0 ± 5.3[c]	7.1 ± 0.1
PM[d]	Macrophage	226.6 ± 15.9[c]	8.1 ± 0.5

[a] BMP levels are represented as µg/ 100 mg of cell pellet dry weight
[b] BMP % phospholipid values are calculated by amount of BMP divided by amount of total phospholipids
[c] Significantly different than non-macrophage lineage cell lines (CT2A and astrocyte) ($p<0.01$).
[d] Peritoneal Macrophages.

Table 5. Fatty acid distribution of BMP from cells with macrophage/microglia origin

	VM-M3	VM-M2	RAW 264.7	BV2	PM
Fatty acids					
C16:0	15.4 ± 4.6	12.6 ± 5.6	3.6 ± 0.8	4.2 ± 2	21.5 ± 4.8
C16:1	5.9 ± 0.3	9.7 ± 0.7	4.8 ± 0.2	1.9 ± 1	2.6 ± 0.8
C18:0	3.5 ± 1.6	6.1 ± 0.1	2.9 ± 0	12.3 ± 0.9	9.8 ± 1.7
C18:1	49.8 ± 11.4	66.9 ± 4	65.6 ± 1.8	65 ± 0.6	19.7 ± 4.2
C18:2n-6		ND	3.8 ± 2.2	ND	5.5 ± 0.6
C20:0	ND	ND	2.5 ± 0.1	1.7 ± 0.4	ND
C20:1	ND	ND	6.6 ± 0.2	ND	1.7 ± 1.4
C20:2	9.9 ± 3.3	ND	2.6 ± 0.2	ND	ND
C20:3	5.2 ± 2.5	ND	ND	ND	ND
C20:4n-6	11.3 ± 4.9	ND	1.3 ± 0.2	ND	3.2 ± 0.7
C20:5n-3	2 ± 0.7	ND	2.6 ± 0.4	6.7 ± 1.6	14.8 ± 2.7
C22:6n-3	0.8 ± 0.1	1.7 ± 1.1	2.5 ± 0.2	8.2 ± 2.3	18.0 ± 2.6
C24:0	ND	ND	0.5 ± 0	ND	ND
C24:1	ND	ND	ND	ND	3.8 ± 1.2

Values represent mean percentage distribution of fatty acid ± standard deviation of 3 samples, except peritoneal macrophages (PM) where n=6.
ND= Not Detected

Discussion

BMP represents 1-2% of all the phospholipids in many cell types, except in alveolar macrophages, where it represents 16% of phospholipids [10]. Here, we confirmed that cells with macrophage/microglia origin had significantly higher BMP content compared to non-macrophage cell lines. BMP enrichment in macrophages could be linked to the increased size of their endo-lysosomal capacity [94]. In this study, we evaluated BMP content in both tumorigenic (VM-M3, VM-M3, CT2A, RAW) and non-tumorigenic (BV2, Peritoneal macrophages, astrocytes) cell types. BMP levels were not correlated with the tumor forming capacity of these cells, making it unlikely that BMP levels are linked with tumorigenic potential. Recent work from Sandhoff and co-workers showed that BMP aids the degradation of glycosphingolipids by interacting with glycosphingolipid degradative enzymes and saposins in the lysosomes [14, 19, 20]. Also, exogenous BMP decreased excess cholesterol storage in Nieman Pick fibroblasts [18, 101]. These observations suggest BMP might also have a functional role in macrophages.

Pathological conditions involving macrophages might provide information regarding possible roles of BMP in macrophage biology. The selective decrease of BMP can reduce glucosylceramide storage in Gaucher disease macrophages [26]. BMP might also have a role in macrophages associated with atherogenesis, and foam cell formation involving the cellular uptake of oxidized LDL (oxLDL) and enzymatically modified LDL (eLDL) particles. Scavenger receptors and receptor-

mediated endocytosis can internalize oxLDL particles. Increased BMP levels are associated with storage of partially degraded oxLDL particles in acidic compartments of macrophages. However, BMP levels are not increased in macrophages following uptake of eLDL particles that are stored in non-endolysosomal lipid droplets and enriched in cholesterol and free fatty acids [102] . Further studies are needed to determine if alterations in BMP content can influence oxLDL particle uptake by macrophages or oxLDL-mediated apoptosis.

Vesicular Stomatitis Virus (VSV) and Human Immunodeficiency Virus (HIV) exploit the endosomal pathway for their release through the plasma membrane [103, 104]. Chapuy-Regaud recently showed that progesterone, the cationic amphiphile U18666A, and a phospholipase inhibitor (Methyl Arachidonyl Fluoro Phosphonate, MAFP) could increase BMP levels, and inhibit viral production in human monocytes and macrophages [104]. These observations suggest a critical role for BMP in macrophages, especially in certain diseases that involve the endo-lysosomal system.

Although the highest levels of BMP were found in cells of macrophage/microglial origin, BMP comprised about 3.7% of total phospholipids in normal mouse astrocytes. This percentage was slightly higher than that found in the CT2A oligodendrocyte progenitor tumor stem cells (1.8%). Astrocytes release glutamate, D-serine, and ATP through Ca^{2+}-dependent exocytosis [105]. While neurons use synaptic vesicles for neurotransmitter release, astrocytes use small vesicles and lysosomes, which are stained positively for endo-lysosomal markers

such as CD63/LAMP3, and VAMP7, for gliotransmitter release [106]. The slight elevations of BMP observed in astrocytes might be linked to these endo-lysosomal associated vesicular compartments. This observation suggests that BMP might be enriched in other cell types that use the endo-lysosomal system for their specific cellular functions, but additional studies are needed to support this hypothesis.

We observed fatty acid heterogeneity in BMP isolated from different macrophage cell types. The levels of C:18-1 were higher in the cultured macrophage/microglia cell lines (49-66%) than in the peritoneal macrophages (19%). In contrast, the distribution of C16:0 and polyunsaturated fatty acids (C20:5n-3 and the C22:6n-3) were significantly higher in the peritoneal macrophages than in the cultured macrophage/microglia cell lines. As discussed in Chapter I, C22:6 was present in BMP in high percentages from gangliosidosis brain. These findings suggest that the culture environment might cause differences in the BMP fatty acid profile of macrophages and cells might synthesize longer and more diverse fatty acids in their natural *in vivo* environment. We previously showed that the cell culture environment inhibited fatty acid remodeling of cardiolipin in normal mouse astrocytes leading to elevated levels of saturated and monounsaturated fatty acids and reduced levels of polyunsaturated fatty acids [107]. We suggested that this phenomenon resulted from the suppression of oxidative phosphorylation through the Crabtree effect, as high lactate levels indicative of fermentation metabolism were seen in

the cultured astrocytes. Further studies will be needed to determine if the BMP fatty acid differences observed between the macrophages grown in vitro and those grown *in vivo* result from differences in growth environment.

BMP enrichment in macrophages could be due simply to the increased lysosomal size observed in this type of cell. However, BMP has functional roles in endosomes and lysosomes such as controlling endosomal sorting and aiding the degradation of glycosphingolipids [19, 20, 70, 78, 101]. BMP might also have a critical role in macrophages under certain pathological conditions described above. Hence modulating BMP levels in macrophages might provide therapeutic insights in diseases involving the endo-lysosomal system such as atherogenesis, lipid storage diseases, and viral infections.

CHAPTER 3

Introduction

Glioblastoma Multiforme (GBM)

GBM is the most common brain cancer type in adults [108]. It has the worst prognosis among brain cancers, and the survival period is generally less than 12 months [109]. GBM has an invasive nature, spreading to many regions of the brain (with sub-pial, sub-ventricular, perivascular, perineuronal, intra-fesicular invasion) forming the “Secondary Structures of Scherer” [110]. It also invades the contralateral hemisphere. Therefore, it is almost impossible to surgically remove all tumor tissue in GBM patients, which is also another cause of the poor prognosis GBM is not considered a metastatic tumor due to low frequency of distant tissue or organ metastasis [111]. However, recent research shows that, if it reaches extraneural sites, it can metastasize to other tissues [112-115]. From our perspective, a highly invasive cancer type is expected to be metastatic, since these phenomena are generally linked to each other [116, 117]. GBM is most commonly considered to have an astrocyte-like origin. However, it has a widely mixed population of cells with different morphology, and expresses different cell origin markers seen in astrocytes, neurons and mesenchymal cells [118-121] We hypothesize that neoplastic macrophage/microglia present in GBM and contributes to highly invasive nature of GBM[122] .

VM mouse as a GBM and metastatic tumor model

The VM mouse strain has a high rate (1.5%) of spontaneous brain tumor development. Three brain tumors from these mice have been obtained in our laboratory [95, 123]. Two of them (VM-M2 and VM-M3) are highly invasive when injected orthotropic to brain, and are highly metastatic to distant organs such as lung, liver and spleen when injected to non-brain regions as flank (Figure 10) [95]. These two metastatic tumors have macrophage-like characteristics defined by morphology and gene expression [95]. The other tumor, VM-NM1 has a neural stem cell like origin and was not invasive in the brain or metastatic when implanted in flank [95]. VM-M3 tumor also manifests all the infiltrative patterns of "Structures of Scherer" seen in Glioblastoma Multiforme when injected intra-cranially [124]. These phenomena are not observed in most of the GBM models, except in the chemically induced CNS-1 rat glioma model [125, 126]. Numerous *in vivo* mouse tumor models require an inducement of a chemical for the tumor formation, which is not the case for most spontaneously occurring human tumors [127].

Figure 10. VM-M3/fluc metastatic tumor model (A) Dorsal and ventral images VM-M3/fluc subcutaneous tumor bearing VM mouse **(B)** Representative images of liver and lung metastasis **(C)** *Ex vivo* quantification of distant organ metastasis by photon count [95].

in vivo VM-M3 model of systemic metastasis

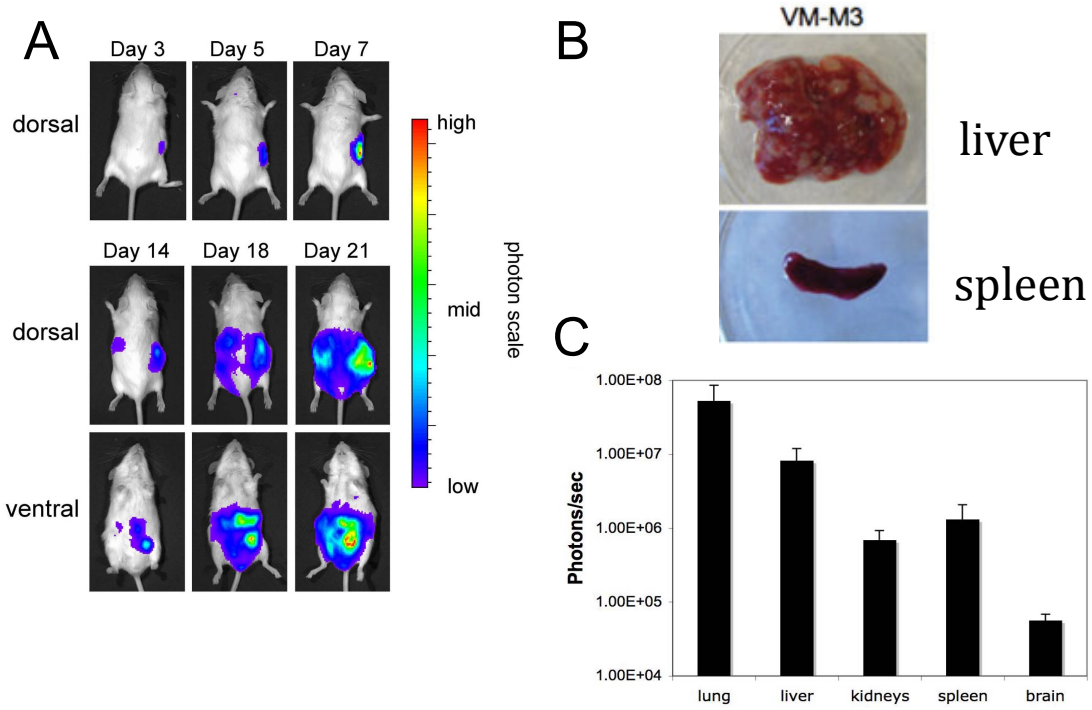

Xenograft mouse models, in which the human tumors are injected into immune compromised mouse models, are often used for *in vivo* tumor analyses [128]. Unfortunately, due to the absence of mouse immune system, tumor cells do not experience the natural tumor environment factors such as inflammation, which also contributes to the growth and metastasis of the tumor cells [129] [130]. Xenograft grown human tumor cells uptake murine carbohydrates and lipids, causing the generation of mouse-human hybrid cells [131]. Also basal metabolic rate of a mouse cell is 8-10 times higher than human cells [132]. Considering all these artifacts, it is very unlikely that Xenograft tumor models can recapitulate the natural tumor growth behavior and assess the effect of potential therapies [133] [134]. Most naturally invasive tumors (such as GBM) do not invade when grown as Xenografts [127]. In order to observe a distant site metastasis, tumor cells are generally injected intravenously, which already bypasses the first steps of metastasis [133, 135]. VM-M3 cells show all characteristics of metastatic tumor cells including local invasion, intravasation, immune system survival and extravasation [95, 136]. The inability to study cancer in its natural environment, or in its original background is one of the rate limiting steps in cancer biology [136]. These issues illustrate the importance of the VM-mouse model system for studying the metastatic behavior of tumor cells.

Abnormal metabolism of tumors

Cancer cells alter their metabolism through a high glycolytic phenotype rather

than oxidative phosphorylation [137]. In normal cells, under aerobic conditions, pyruvate generated from glucose enters to mitochondria and generates NADPH in TCA cycle, which is then used for ATP generation through electron transport chain in mitochondria [138]. However, under anaerobic conditions, such as oxygen limitation resulting from excessive exercise, pyruvate is fermented to lactate in the cytosol instead of entering into mitochondria [138]. Otto Warburg discovered that cancer cells generate most of their ATP through glucose fermentation in the presence of oxygen [139]. This discovery was later named as "Warburg Effect". Otto Warburg stated that insufficient respiration causes cancer initiation, and glycolysis compensates for the insufficient respiration [140, 141]. After this discovery, many findings suggested that there were mitochondrial abnormalities in cancer cells [142-147]. Cardiolipin (CL) is a phospholipid found in the inner mitochondrial membrane and it maintains coupled respiration and mitochondrial functionality. Kiebish et al found that CL content was lower, and CL molecular species were altered in tumor tissues, suggesting major defects in CL synthesis and remodeling. The tumor tissues also had lower electron transport chain activities compared to normal tissues. As Pederson states, tumor mitochondria are markedly different in morphology, lipid and protein profile compared to normal mitochondria [148]. Tumor mitochondria also have many defects in electron transport chain, calcium shuttle and anion membrane transport; thus pyruvate cannot be properly oxidized for ATP generation [148]. Therefore, cancer cells need to compensate their insufficient respiration through upregulation of fermentation for ATP generation [134, 141]. Most tumor cells do

not obtain enough oxygen in necrotic and poorly vascularized tumor core. This hypoxic environment causes Hypoxia Induced Factor 1 (HIF1) upregulation, which causes an upregulation in glycolytic pathways [149]. HIF1a also can be upregulated due to defective mitochondria, which further links this hypoxia-initiated glycolytic phenotype to mitochondrial abnormalities [150]. Therefore, high uptake of glucose and upregulation of glycolytic pathways are obligatory in cancer cells with respiratory defects [141, 151].

Reactive oxygen species (ROS) can form from electron leakage during oxidation reactions in mitochondria [152]. These reactive oxygen molecules can attack proteins, DNA, and lipids, eventually leading to cell death [153]. They can cause membrane damage because of lipid peroxidation of polyunsaturated fatty acids, which results in changes in the membrane fluidity, permeability, and inactivation of membrane proteins [154]. There is a substantial amount of research indicating a significant increase in intracellular O_2 and H_2O_2 in cancer cells relative to normal cells [155]. Cardiolipin deficiencies and higher proton leak observed in tumor mitochondria might explain the reason for high ROS levels in tumor cells [148]. High glycolysis, and glycolytic regulators such as PKM2, causes a flux through the pentose phosphate pathway (PPP), and upregulate antioxidant systems through NADPH generation. NADPH generated through PPP also supplies the high macromolecule demand of cancer cells [156]. Therefore, cancer cells are highly dependent on glucose utilization for anti-oxidant mechanisms in order to cope with their high ROS levels [157].

Calorie restriction

Glucose dependency of cancer cells has been exploited by tumor detection with (^{18}F) fluorodeoxyglucose positron emission tomography (FDG–PET) imaging [158]. However, cancer therapies exploiting cancer abnormal metabolism are very limited and not widely used in standard practice [151]. If all cancer cells suffer from respiratory insufficiency, treatments that target glycolysis should be very effective in managing cancer [134]. Inhibition of glycolysis can be obtained by drugs that target glycolytic pathways, such as dichloroacetate, 2-deoxyglucose and 3-Bromopyruvate [159-163]. However, restriction of calorie intake is a more natural way of targeting glycolysis, which decreases blood glucose levels in natural ways [164]. Calorie restriction (CR) has been shown to reduce growth of many human and mouse tumors types [165-168]. CR reduces the growth of tumor cells in many ways such as restricting the availability of glucose as a fuel to cancer cells, targeting nutrient sensing and growth signaling pathways such as PI3K/Akt/HIF1α/IGF1, and controlling tumor environment that contribute to tumor pathogenesis by reducing angiogenesis and inflammation [168-172]. Glucose withdrawal and the conversion to lipid metabolism *increases* oxidative stress, leading to apoptosis in cancer cells [173]. Restriction of glucose can also selectively target cancer cells that rely on glucose for ROS detoxification [174].

Ketogenic diet

Glucose deficiency in the blood causes the liver to oxidize fatty acids into ketone bodies (KB), which later on get exported to other tissues, where they are used as an energy source [175]. In order to drive cellular respiration, these ketones, the majority of which are acetoacetate and β-hydroxybutyrate, are then converted into acetyl-CoA [176]. Ketones can be elevated in blood by either fasting, with long-term calorie restriction or by high fat (ketogenic) diets [177-179]. With these methods, due to a limited carbohydrate intake, body's stored glycogen is depleted and there is a transition to the fat dependency for energy, which is termed as the state of ketosis [179]. Ketogenic diets, with high fat: protein + carbohydrate ratios are alternative ways to reduce blood glucose levels and increase high ketone levels, and these diets are safely used as treatments in some pathological conditions such as epilepsy [180, 181]. Ketogenic diets might be an alternative way to reach the therapeutic effects of calorie restriction, which can also provide additional therapeutic benefits. Ketones are directly converted to acetyl-CoA, therefore they can be used for ATP generation only in mitochondria for oxidative phosphorylation in normal cells [182]. Considering mitochondrial defects and apparent respiratory insufficiency, ketones might not be metabolized in cancer cells efficiently. Therefore ketogenic diets can be a very useful treatment strategy, to selectively kill tumor cells [182, 183]. Ketogenic diets are shown to be effective in reducing the tumor growth in animal models of glioma, non-small lung cancer, colon cancer, gastric cancer and prostate cancer

in animal tumor models [163, 184-187]. Ketogenic diets have also been shown to increase the therapeutic effects of conventional cancer therapies, such as chemotherapy and radiation [188, 189].

Ketogenic diets may have additional therapeutic benefits due to their correlation with reactive oxygen species (ROS) production in cells. In normal cells, β-hydroxybutyrate metabolism increases reduction of NAD^+ and increases oxidation of coenzyme-Q; thus resulting in lower semiquinone levels, which decreases superoxide production [190]. Through this mechanism, ketones could lower ROS in normal cells and therefore protect cells from oxidative damage [190]. However, ketones force cells to use oxidative phosphorylation and this might result in increased O_2 leak from the mitochondria in cancer cells due to their defective mitochondria. Ketones are shown to increase reactive oxygen species in cancer cells, yet contrary results are also presented in literature [191, 192]. Recently Poff et al. showed that, a combination of ketogenic diet and hyperbaric oxygen therapy resulted in a decreased tumor growth rate and increased mean survival time in VM-M3 tumor model system [191]. These findings suggest that ketones might further increase the ROS levels in cancer cells beyond the levels that they can not cope with in the absence of glucose. Therefore ketogenic diets, which lower the blood glucose and increase ketones, can be an alternative and non-toxic therapy for the management of tumor growth, invasion and metastasis [134].

In this chapter of my thesis, I examined the effects of different diets on VM-M3

tumor growth and metastasis. I observed that restricted KetoGen ketogenic diet (KG-R) reduced VM-M3 tumor growth and distant organ metastasis, and increased the survival of VM-M3 tumor bearing mice significantly. KG-R was able to reduce blood glucose and increase β-hydroxybutyrate levels significantly compared to control (SD-UR) groups. These results suggest that restricted KetoGen ketogenic diet might be an alternative non-toxic therapy for managing metastatic cancers.

Materials and Methods

Mice

VM/Dk (VM) strain mice were obtained as gifts from H. Fraser (University of Edinburgh, Scotland) and from G. Carlson (McLaughlin Research Institute, Great Falls, Montana). Housing and breeding of all mice used for this study were done in the Boston College Animal Care Facility, utilizing husbandry condition as described elsewhere [193]. All animal procedures used for this study were approved by the Institutional Animal Care Committee and were in strict accordance with the National Institute of Health Guide for the Care and Use of Laboratory Animals.

Origin of VM tumors

As previously described [95], VM-M3 tumor arose spontaneously in the cerebrum of adult VM mice. With a routine examination of the VM mouse colony over several years, the VM-M3 tumor was detected (between 1993-2000). The tumors in the cerebrum were poorly defined masses with volumes about 3 x 1 x 1 mm, which are similar to previous spontaneous tumor descriptions in the VM mouse brain [123, 194]. Preservation of *in vivo* viability was established by immediately resecting and implanting each tumor intracerebrally (*i.c.*) into the host VM mice. This procedure is described below in detail. Tumors were passaged into several host VM vice right after cranial dome appearance. Three *i.c.* passages were required before the tumors were grown subcutaneously and cell lines were prepared from each tumor. Environmental variability was reduced by culturing all

cell lines under identical conditions.

Intracranial implants

Tumor implantation was performed as previously described [193]. Briefly, mice were anaesthetized with Avertin (0.1mL/10g). Ethanol was used to disinfect the top of the heads, followed by a small incision made in the mouse's scalp over the midline. A $3mm^3$ burr hole was made in the skull lateral to the sagital suture and over the right parietal region behind the coronal suture.

A small (about $1mm^3$) tumor fragment was implanted into the burr hole in the skull by using a trocar. Colloidon was used to immediately closing the flaps of skin. All mice reached morbidity at around 12 to 15 days period. All methods resulted in the 1.5 to 2 mm deep implantation of tumor fragments into the cortical region as described elsewhere [195]. Mice were housed in a warm room of 37°C temperature until they recovered fully.

Subcutaneous implants

VM mice were anaesthetized with Isoflurane (obtained from Halocarbon, River Edge, NJ) for *s.c.* implantation, and the tumor implantation was carried by a *s.c.* injection of 0.1 ml of tumor pieces suspended in 0.2 ml PBS, by the utilization of a 1 cc tuberculin syringe attached to an 18- gauges needle into the right flank. After all mice recovered from the surgical procedure, they were returned to their cages once they became fully active.

Bioluminescent imaging

Bioluminescent signal from the luciferase labeled tumors were recorded with the Xenogen IVIS system (obtained from Xenogen, Hopkington, MA), as described elsewhere [95]. An intraperitoneal injection of D-Luciferin (50mg/kg, Xenogen) and Avertin (0.1 mL/10g) were given to mice for *in vivo* imaging. Depending based on the time point, imaging times changed from 30 seconds to 15 minutes. Organs were removed entirely and rinsed in PBS for *ex vivo* imaging. Organ imaging was performed in 300 µg/ml D-luciferin in PBS for 2 minutes after 2 minutes of incubation. Brains were removed and split down through the midline for *i.c.* studies. Each hemisphere imaging was performed separately in 300 µg/ml D-luciferin in PBS for 2 minutes. Imaging of the right and left hemispheres was performed separately.

Diets

Standard high carbohydrate mouse chow diet (SD) is a nutritionally complete diet and was purchased from PROLAB chow (Agway Inc., NY). SD nutritional ingredients carbohydrate, fat, protein, and fiber comprised 62g, 6g, 27g of 100g of the total diet, respectively. KetoGen ketogenic diet (KG) and Vitamin and mineral mix (NanoVM 1-3 years) was a gift of Nancy Moore (Solace Nutrition, Pawcatuck, CT). KG is composed of 2.54g, 74g, 15.17g of carbohydrate, fat, protein for 100g of the total diet, respectively (information provided with personal communication). 9g of NanoVM added for 91g of KetoGen powder to make the complete formula. KetoCal® ketogenic diet was purchased from Nutricia North

America (Rockville, MD, formally SHS International, Inc.). KetoCal® is a nutritionally complete ketogenic formula and, according to the manufacturers specification, carbohydrate, fat, protein comprised 8.8g, 69.1g, 14.4 g of 100g the total diet, respectively. There are also minor differences between the two diets for the content (g/kg of diet) of amino acids, vitamins, minerals and trace elements. The KetoGen and KetoCal® diet was fed to the mice in paste form (water: KetoCal®; 1:2) within the cage. A comparison of the nutritional composition of the SD, KetoGen and the KetoCal® diet is presented in Table 7.

Dietary feeding regimens, body weight, and food intake measurements

Approximately 1 to 2 days before the tumor implantation, adult female and male VM mice (each mouse 60 to 120 days old) were separated into different housings. Each mouse was kept in plastic cages with Sani-Chip bedding (P.J. Murphy Products Corp., Montville, NJ) and with filter tops. SD food was provided *ad libitum*, food intake and body weight measurements were performed and recorded daily. Tumor fragment implantation took place on day zero. After confirming the presence of a tumor by imaging on the Xenogen Imaging System, mice were separated into groups matched for body weights 2-3 days after implantation. Mice were fasted 18 hours before diet (SD, KG, or KC) initiation. Mice on calorie restriction, received 40-60% of their food intake at around 10 AM (60% CR), in order to reach 18-20% body weight reduction compared to their initial weight, for the total duration of the study. Unrestricted (UR) mice received food *ad libitum* of their corresponding diet. Daily body weight measurements for

all mice were performed prior to food administration.

Measurement of plasma glucose, β-hydroxybutyrate and calculation of Glucose Ketone Index

Blood collection from mice was performed on the last day of the study, before sacrifice and tumor resection. Before the blood collection, all mice were fasted for 2 hours, in order to stabilize blood glucose levels. Mice were anesthetized with isoflourane (obtained from Halocarbon, NJ) and blood collected with submandibular bleeding in heparinized tubes. Collected blood was centrifuged at 1,500 Å~ g for 10 minutes, after that the plasma was collected and stored at 80°C until assayed. StanBio® Enzymatic Glucose Assay (1075-102) (obtained from StanBio Laboratory, Boerne, TX) and a modification of the Williamson et al., enzymatic procedure [196] was used to spectrophotometrically measure plasma glucose and β-hydroxybutyrate concentrations, respectively. For blood ketone body analysis, only β-hydroxybutyrate levels were measured since it is the major blood ketone body in plasma [175, 197]. Glucose Ketone Index is calculated by dividing mM glucose values to mM β-hydroxybutyrate levels [198].

Statistical analysis

For calculating significance of organ metastasis with photons/sec values, non-parametric Whitney Mann U Test was performed. All other statistical analysis were performed using Student T-Test.

Results

Influence of diet on subcutaneous growth and distant organ metastasis of VM-M3/Fluc tumor

In this experiment we analyzed whether feeding of VM mice with restricted standard diet, unrestricted ketogenic diet or restricted ketogenic diet has any effect on VM-M3 tumor growth and metastasis. VM mice were implanted *s.c* with the VM-M3/Fluc tumor on Day 0. Mice were fasted for 18 hours on Day 3 and diet was initiated at Day 4. When control (SD-UR) groups showed signs of morbidity, such as lethargy and sudden body weight loss, all mice were terminated (Figure 11). Restricted mice received 40-60% less food compared to unrestricted groups, and reached 18% of their initial body weights 2-3 days after diet initiation. Unrestricted groups returned to their initial body weight 2-3 days after diet initiation (Figure 12A). Restriction of Standard Diet (SD-R) and KetoGen Diet (KG-R) equally decreased blood glucose significantly compared to their unrestricted counterparts (SD-UR, KG-UR) at $p<0.05$ (Figure 12B). SD-R, KG-UR and KG-R groups had significantly higher β-hydroxybutyrate levels compared to control SD-UR group at $p<0.05$. Also KG-R group had significantly higher β-hydroxybutyrate values compared to SD-R and KG-UR groups at $p<0.01$ (Figure 12C). Glucose ketone index (GKI) was calculated as described in materials and methods. KG-R group had significantly lower GKI compared to all other groups at $p<0.01$ (Figure 12D).

Primary tumor growth was significantly lower in SD-R, KG-UR and KG-R compared to control (SD-UR) group at $p<0.01$. Also KG-R group had significantly lower primary tumor weight compared to SD-R and KG-UR groups at $p<0.05$ (Figure 13, 14). KG-R group had significantly lower metastasis to liver, lung, spleen and kidney compared to SD-UR and SD-R groups at $p<0.05$. However, SD-R or KG-UR groups did not reduce the metastasis to organs compared to control SD-UR mice (Figure 15). KG-R group also had significantly lower metastasis to brain compared to SD-UR group at $p<0.05$ (Figure 16).

Figure 11. Experimental design for the analysis of diet influence on VM-M3/Fluc flank tumor growth and metastasis. VM mice were implanted *s.c.* with the VM-M3/Fluc tumor as explained in Materials and Methods. Mice were fasted for 18 hours on Day 3 before the initiation of the diet on Day 4. Mice were fed either with unrestricted Standard Diet (SD-UR), restricted Standard Diet (SD-R), unrestricted KetoGen diet (KG-UR) or restricted KetoGen diet (KG-R). All mice were imaged *in vivo*, organs and tumors collected and imaged *ex vivo* at the time of termination.

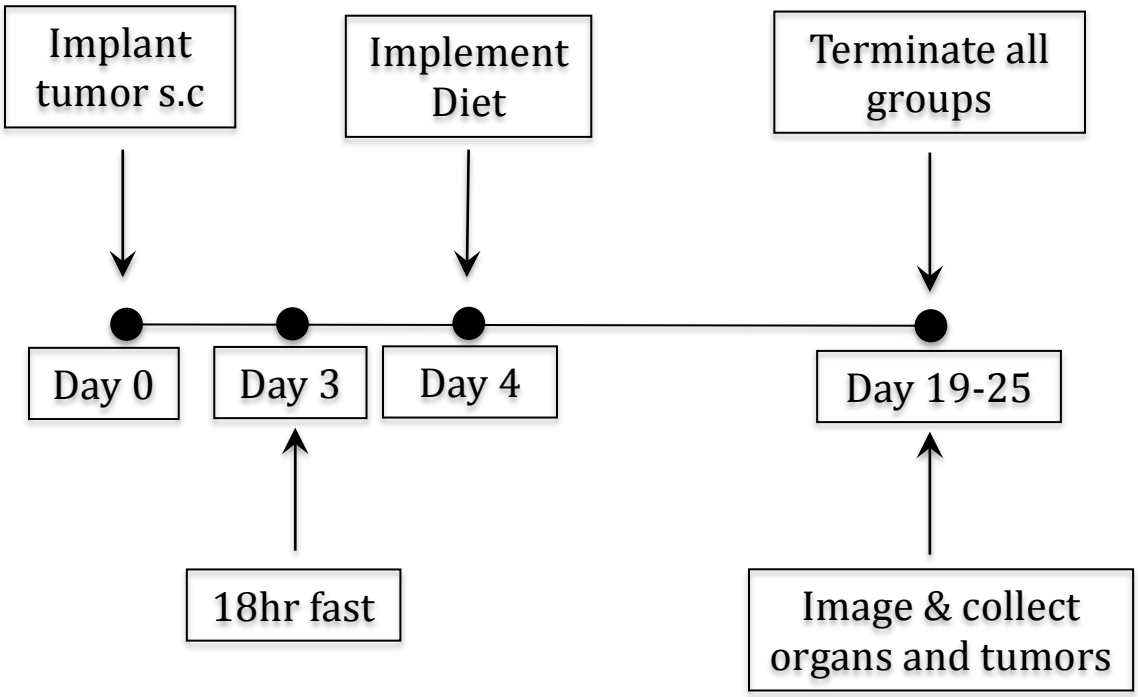

Experimental Groups (N = 8 / all groups):
Standard Diet Unrestricted (SD-UR)
Standard Diet Restricted (SD-R) (18% body weight reduction)
KetoGen Unrestricted (KG-UR)
KetoGen Restricted (KG-R) (18% body weight reduction)

Figure 12. Influence of diet on body weight, blood glucose and β-hydroxybutyrate levels of VM-M3/fluc subcutaneous tumor bearing mice. Mice were fed either with unrestricted Standard Diet (SD-UR), restricted Standard Diet (SD-R), unrestricted KetoGen diet (KG-UR) or restricted KetoGen diet (KG-R). **(A)** Restricted groups received 40-60% less food in order to reach 18% body weight reduction. Body weights were monitored daily. Prior to treatment, the body weights of all mice were averaged for a single value. Values represent the average ± standard error of the mean (SEM). Mice were sacrificed 20–25 days post-implantation and blood was collected for the analysis of **(B)** glucose and **(C)** β-hydroxybutyrate **(D)** Glucose Ketone Index levels, as explained in Materials and Methods. All data is represented as mean ± standard error of the mean (SEM). Single asterisk indicates that values are significantly different compared to control (SD-UR) group at $p < 0.05$. Double asterisk indicates that KG-R values are significantly different than SD-UR, SD-R and KG-UR values at $p < 0.01$.

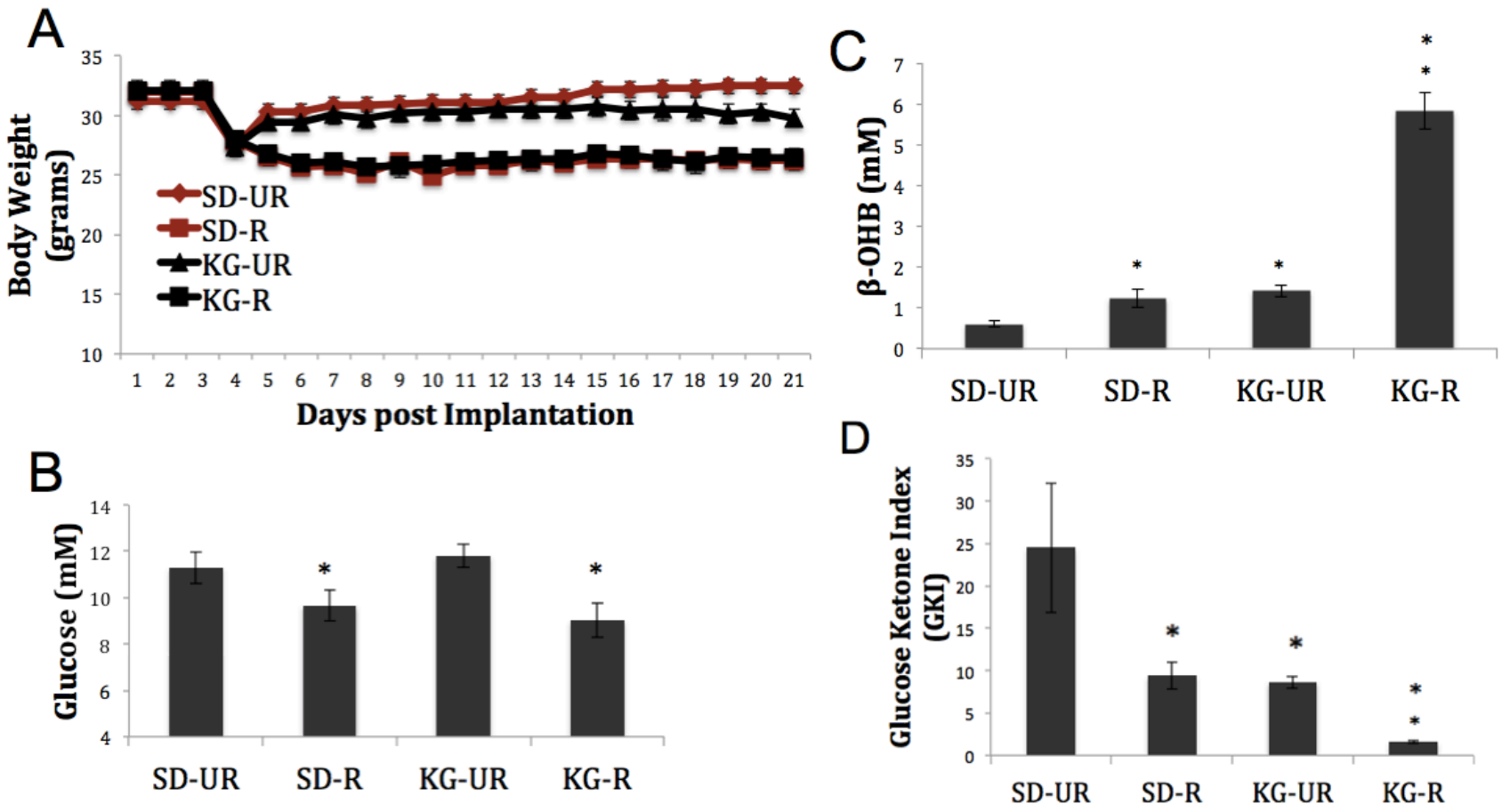
A
Body Weight (grams)
35
30
25
20
15
10
SD-UR
SD-R
KG-UR
KG-R
1 2 3 4 5 6 7 8 9 10 11 12 13 14 15 16 17 18 19 20 21
Days post Implantation
B
Glucose (mM)
14
12
10
8
6
4
SD-UR
SD-R
KG-UR
KG-R
C
β-OHB (mM)
7
6
5
4
3
2
1
0
SD-UR
SD-R
KG-UR
KG-R
D
Glucose Ketone Index (GKI)
35
30
25
20
15
10
5
0
SD-UR
SD-R
KG-UR
KG-R

Figure 13. Influence of restricted ketogenic diet on subcutaneous growth of VM-M3/Fluc tumor. Representative images of tumor bearing mice either fed with unrestricted standard diet (SD-UR) or restricted KetoGen Diet (KG-R). VM mice implanted *s.c.* with VM-M3/Fluc tumor. Pictures were taken 25 days after implantation.

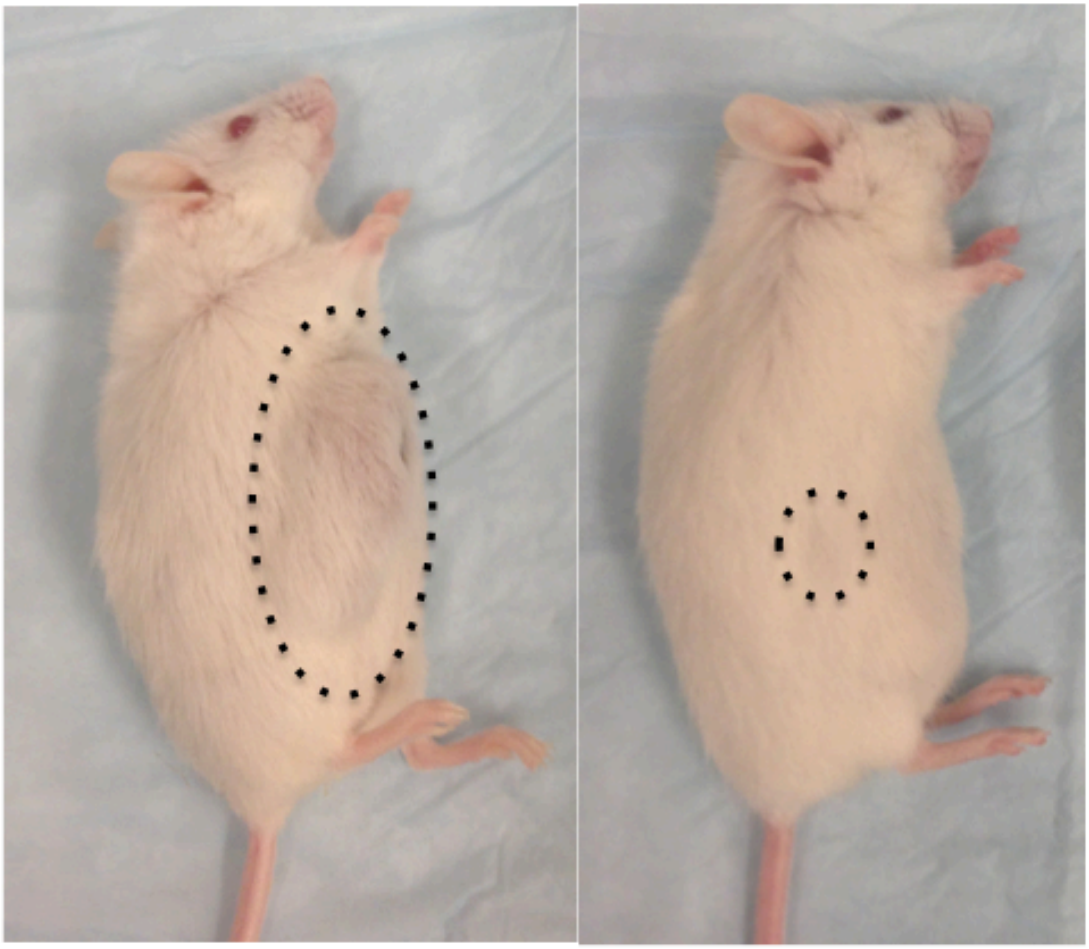

SD-UR KG-R

N=8 /all groups

Figure 14. Influence of diet on primary tumor weight of VM-M3/Fluc subcutaneous tumor. VM mice were either fed with unrestricted Standard Diet (SD-UR), restricted Standard Diet (SD-R), unrestricted KetoGen diet (KG-UR) or restricted KetoGen diet (KG-R). All values are represented as mean ± SEM. Single asterisk indicates that values are significantly different than the control (SD-UR) group at $p<0.01$. Double Asterisk indicates that KG-R values are significantly different than SD-UR, SD-R and KG-UR groups at $p<0.05$.

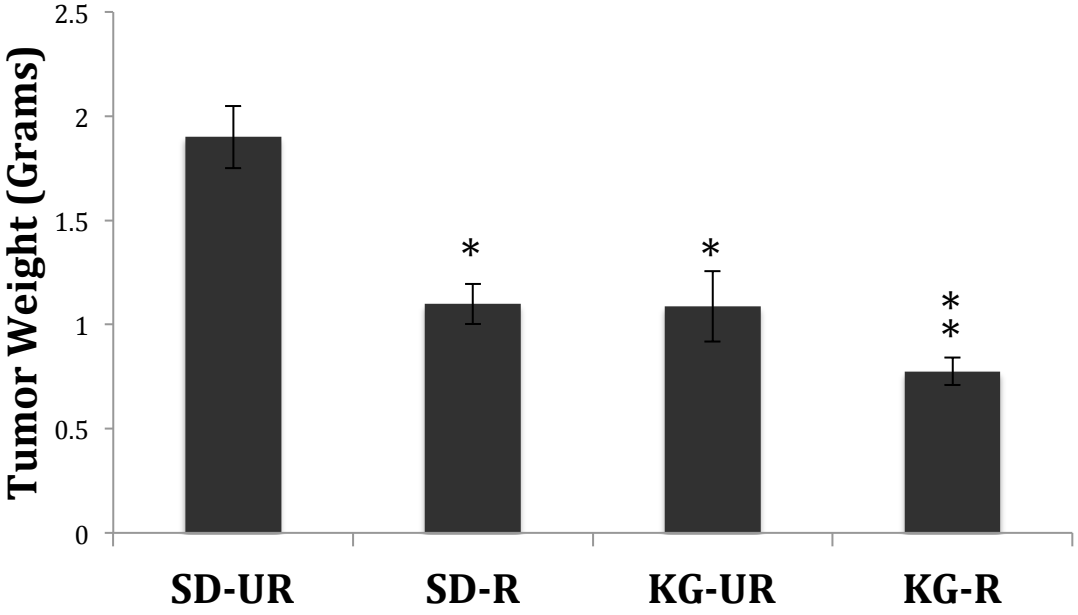

N=8 /all groups

Figure 15. Influence of diet on distant organ metastasis of VM-M3/fluc tumor. VM mice were fed either with unrestricted Standard Diet (SD-UR), restricted Standard Diet (SD-R), unrestricted KetoGen diet (KG-UR) or restricted KetoGen diet (KG-R). At the time of sacrifice, the organs were removed and imaged ex vivo. Bioluminescence values were plotted on a log scale. All values represent the average ± SEM. Asterisk indicates that KG-R values are significantly different than SD-UR and SD-R groups at $p<0.05$.

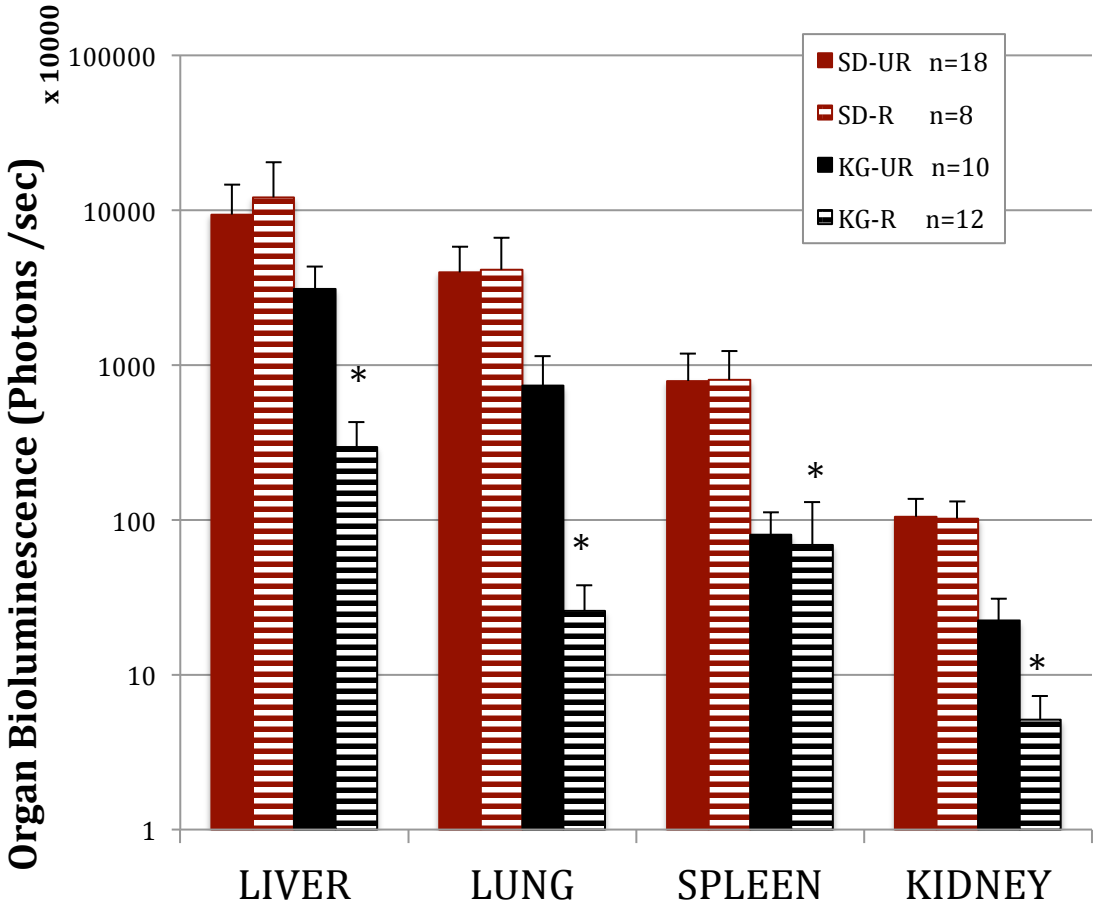
x 10000
Organ Bioluminescence (Photons /sec)
100000
10000
1000
100
10
1
SD-UR n=18
SD-R n=8
KG-UR n=10
KG-R n=12
*
*
*
*
LIVER
LUNG
SPLEEN
KIDNEY

Figure 16. Influence of diet on brain metastasis of VM-M3/fluc tumor. VM mice were fed either with unrestricted Standard Diet (SD-UR), or restricted KetoGen diet (KG-R). **(A)** Representative images of VM-M3 tumor brain metastasis with SD-UR and KG-R feeding. Images were taken in vivo 10 minutes after *i.p* luciferin injection. Whole body was covered with black masking paper to prevent the bioluminescence contribution from primary tumor. **(B)** At the time of sacrifice, the brains were removed and imaged *ex vivo*. All values represent the average ± SEM. Asterisk indicates that KG-R values are significantly different than SD-UR group at $p<0.05$.

A

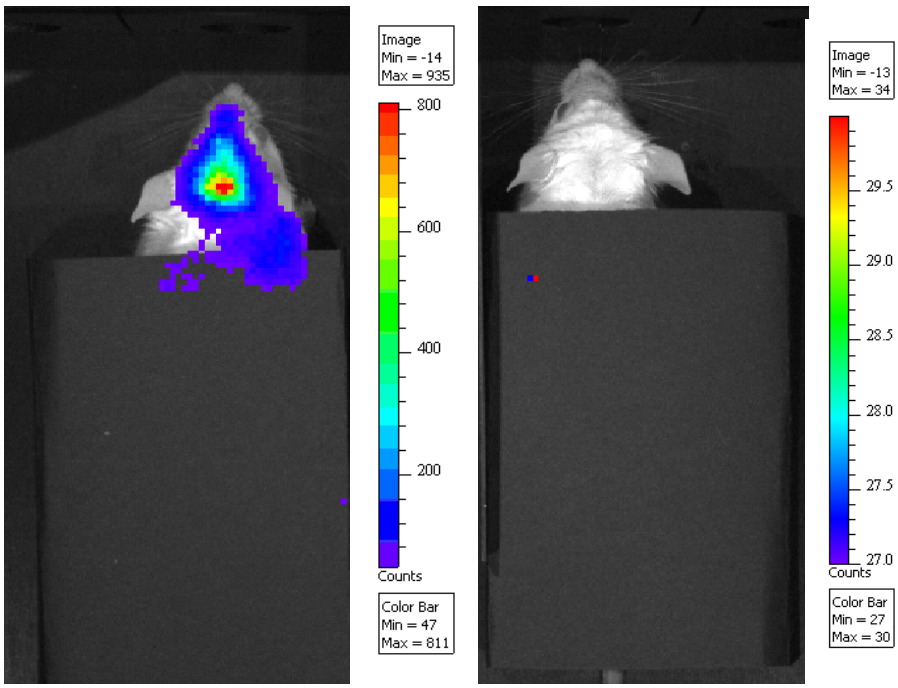
Image
Min = -14
Max = 935
800
600
400
200
Counts
Color Bar
Min = 47
Max = 811
Image
Min = -13
Max = 34
29.5
29.0
28.5
28.0
27.5
27.0
Counts
Color Bar
Min = 27
Max = 30

SD-UR KG-R

B

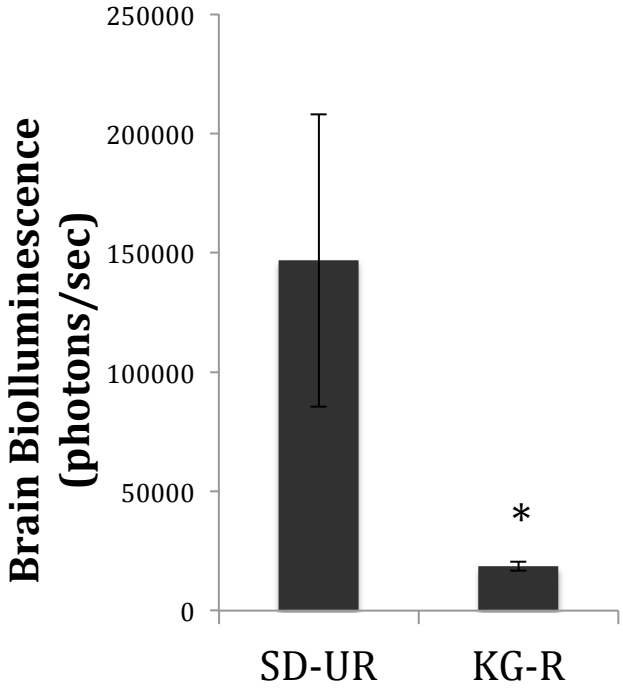
Brain Biollumineescence (photons/sec)
250000
200000
150000
100000
50000
0
*
SD-UR
KG-R

Influence of diet on survival of VM-M3/Fluc subcutaneous tumor bearing mouse

In this experiment we analyzed whether calorie restriction and/or ketogenic diet can increase VM-M3 tumor bearing mouse survival. VM mice were implanted *s.c* with the VM-M3/Fluc tumor on Day 0. Mice were fasted for 18 hours on Day 3 and diet (SD-UR, SD-R, KG-UR or KG-R) was initiated at Day 4. Mice were euthanized individually when they showed signs of morbidity, such as lethargy and sudden body weight loss (Figure 17). Restricted groups (SD-R, KG-R) reached 18% of their initial body weights (Figure 18A, 18B) and had significantly lower blood glucose compared to unrestricted groups (SD-UR, KG-UR) at $p<0.05$. KG-R group had significantly higher ketone values compared to all other groups, and had lowest GKI values at $p<0.01$ (Figure 18C, 18D). Primary tumor volume was significantly lower in SD-R, KG-UR and KG-R compared to control (SD-UR) group at $p<0.05$. Also KG-R group had significantly lower primary tumor volume compared to SD-R and KG-UR groups at $p<0.05$ (Figure 19)

All control group (SD-UR) mice reached morbidity 17-22 days post implantation. KG-R group survived longer compared to SD-R and KG-UR groups at $p<0.05$ (Figure 20).

Figure 17. Experimental Design for the diet influence on survival of VM-M3/Fluc subcutaneous tumor bearing mouse

VM mice were implanted *s.c.* with the VM-M3/Fluc tumor as explained in Materials and Methods. Mice were fasted for 18 hours on Day 3 before the initiation of the diet on Day 4. Mice were fed either with unrestricted Standard Diet (SD-UR), restricted Standard Diet (SD-R), unrestricted KetoGen diet (KG-UR) or restricted KetoGen diet (KG-R). Tumor volumes were measured with Caliper on Day 14. Mice with clear signs of morbidity such as lethargy and heavy breathing were euthanized throughout the study. Study terminated with the euthanization of last mice on Day 37.

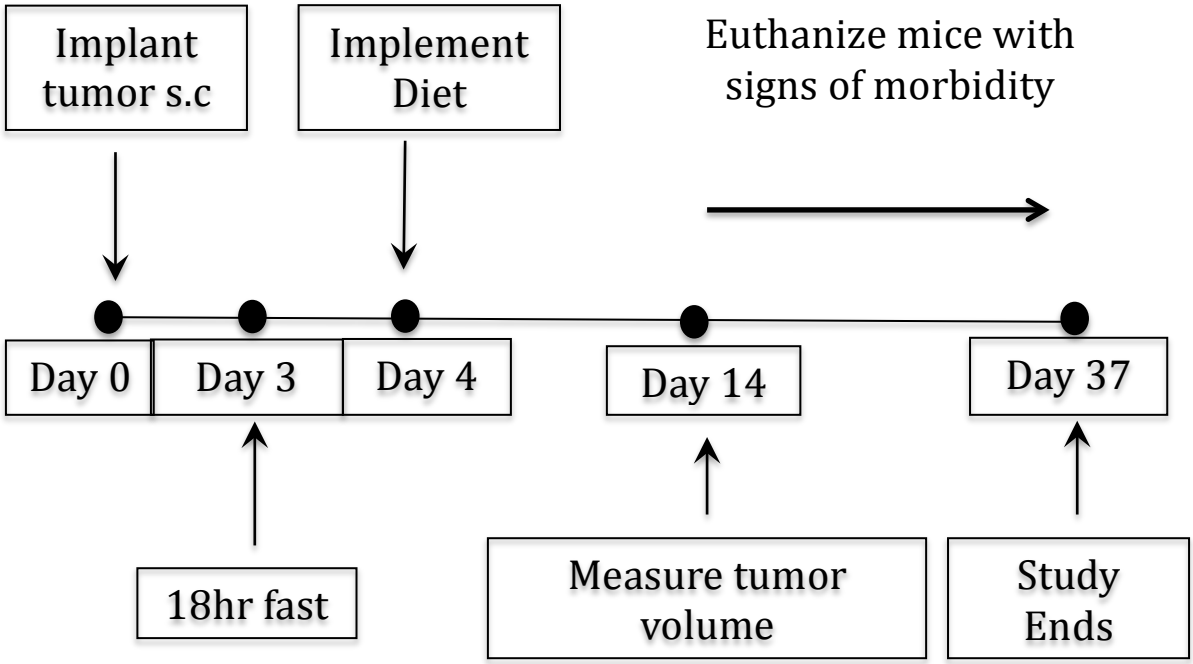

Experimental Groups (N = 8 / all groups):
Standard Diet Unrestricted (SD-UR)
Standard Diet Restricted (SD-R) (18% body weight reduction)
KetoGen Unrestricted (KG-UR)
KetoGen Restricted (KG-R) (18% body weight reduction)

Figure 18. Influence of diet on body weight, blood glucose and β-hydroxybutyrate levels of VM-M3/fluc tumor bearing mice (A) Mice were fed either with unrestricted Standard Diet (SD-UR), restricted Standard Diet (SD-R), unrestricted KetoGen diet (KG-UR) or restricted KetoGen diet (KG-R). Restricted groups received 40-60% less food in order to reach 18% body weight reduction. Body weights were monitored daily. Prior to treatment, the body weights of all mice were averaged for a single value. Values represent the average ± standard error of the mean (SEM). Body weights are not plotted after day 22, due to the decrease in number of animals. Blood was collected for the analysis of **(B)** glucose and **(C)** β-hydroxybutyrate **(D)** Glucose Ketone Index levels as explained in Materials and Methods. All data is represented as mean ± standard error of the mean (SEM). Single asterisk indicates that values are significantly different compared to control (SD-UR) group at $p < 0.05$. Double asterisk indicates that KG-R values are significantly different than SD-UR, SD-R and KG-UR values at $p < 0.01$.

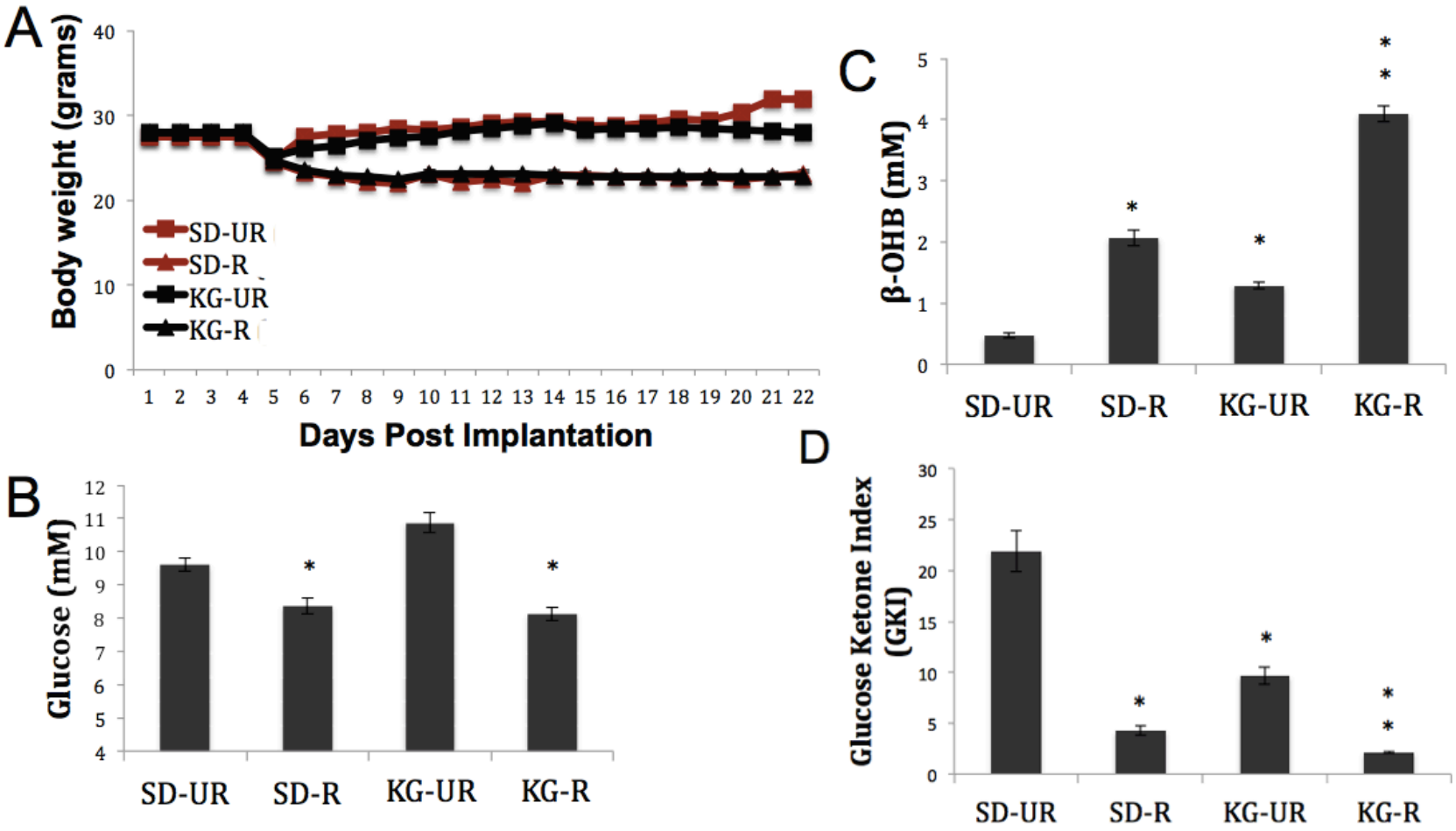
A
Body weight (grams)
40
30
20
10
0
SD-UR
SD-R
KG-UR
KG-R
1 2 3 4 5 6 7 8 9 10 11 12 13 14 15 16 17 18 19 20 21 22
Days Post Implantation
B
Glucose (mM)
12
11
10
9
8
7
6
5
4
SD-UR
SD-R
KG-UR
KG-R
C
β-OHB (mM)
5
4
3
2
1
0
SD-UR
SD-R
KG-UR
KG-R
D
Glucose Ketone Index (GKI)
30
25
20
15
10
5
0
SD-UR
SD-R
KG-UR
KG-R

Figure 19. Influence of diet on primary tumor volume of subcutaneous VM-M3/Fluc tumor growth. VM mice were fed either with unrestricted Standard Diet (SD-UR), restricted Standard Diet (SD-R), unrestricted KetoGen diet (KG-UR) or restricted KetoGen diet (KG-R). Tumor volumes were measured with digital caliper and volumes calculated as $V = (\text{length} \times \text{Width}^2)/2$. All values are represented as mean ± SEM. The asterisk indicates that values are significantly different than the control (SD-UR) group at $p < 0.05$. Double Asterisk indicates that KG-R values are significantly different than SD-UR, SD-R and KG-UR groups at $p < 0.05$.

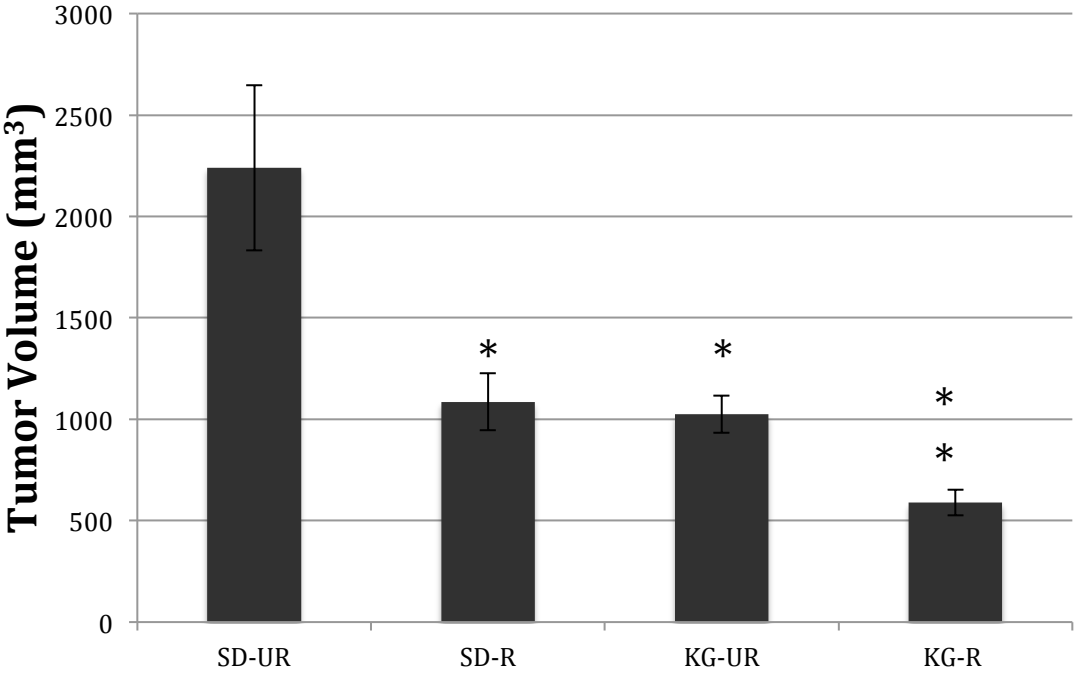

N=8 /all groups

Figure 20. Influence of diet on the survival of VM-M3/fluc tumor bearing mice. VM mice were fed either with unrestricted Standard Diet (SD-UR), restricted Standard Diet (SD-R), unrestricted KetoGen diet (KG-UR) or restricted KetoGen diet (KG-R). VM mice were implanted with the VM-M3/Fluc tumor as described in Materials and Methods.17-25 days after tumor implantation, SD-UR (control) groups mice reached morbidity. Asterisk indicates that KG-R grouped survived significantly longer than SD-UR, SD-R and KG-UR groups at $p<0.05$.

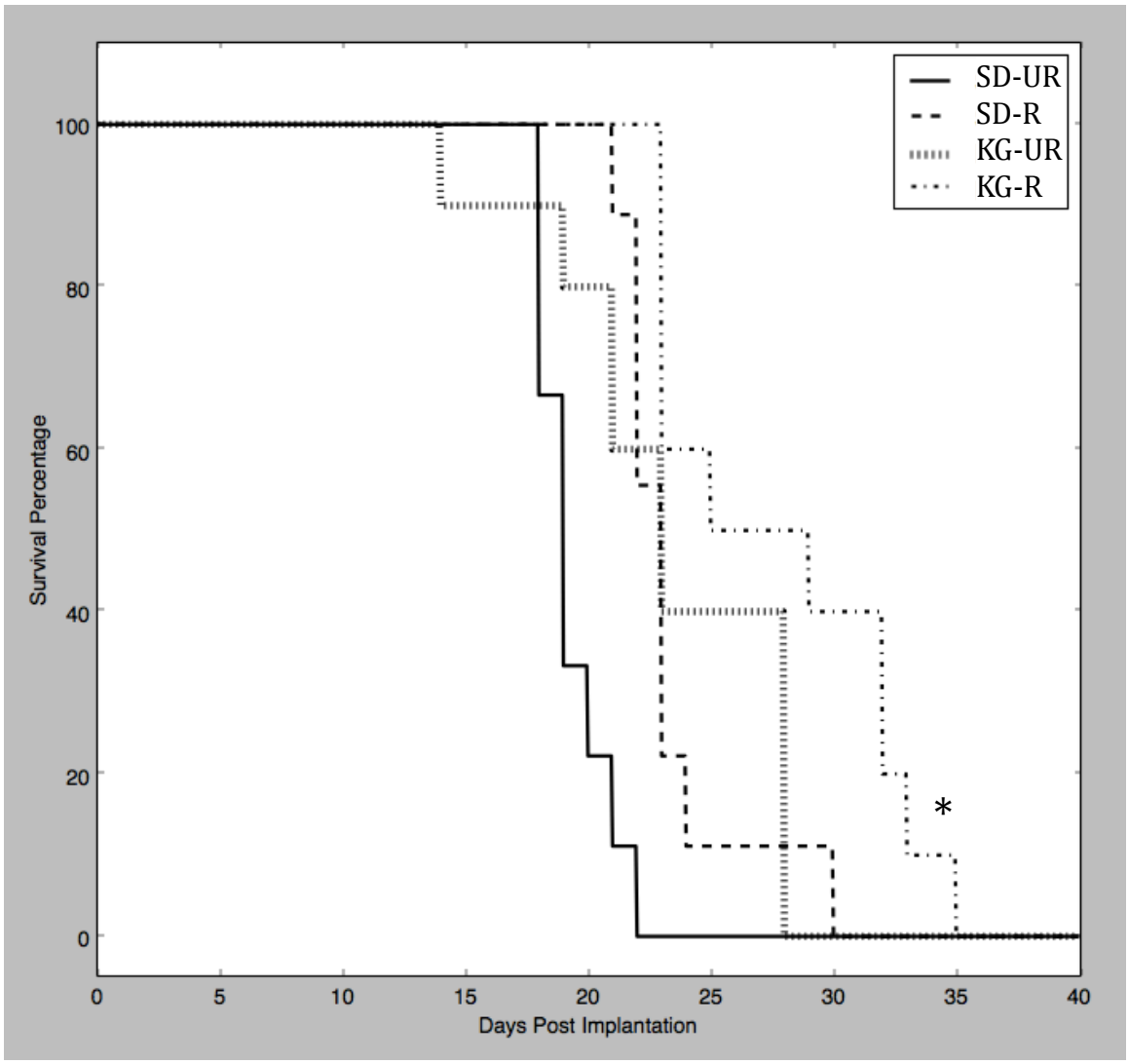

N=8 /all groups

Influence of diet on intracranial growth and contra-lateral invasion of VM-M3/Fluc brain tumor

VM-M3 tumor was originally identified in the brain and shows all the characteristics of glioblastoma multiforme including invasion to the contralateral side of the brain. Therefore we analyzed the effect of diet on VM-M3 tumor growth in brain and contralateral invasion. 1 mm^3 of VM-M3/Fluc tumor tissue pieces were implanted into right hemisphere of VM mice on Day 0. Mice were fasted for 18 hours on Day 3 and diet (SD-UR, SD-R, KG-UR or KG-R) was initiated at Day 4 (Figure 21). In correlation with previous experiments, KG-R delivered the lowest GKI values with significantly higher ketone values at $p<0.05$ (Figure 22). At Day 15, removed brains were dissected into ipsi-lateral and contra-lateral hemispheres and imaged ex-vivo as represented in Figure 23. Whole brain bioluminescence represents sum of ipsi-lateral and contra-lateral hemispheres. KG-R group had significantly lower whole brain bioluminescence compared to SD-UR and SD-R groups at $p<0.05$ (Figure 24A). Contra-lateral invasion was measured by the bioluminescence light coming from contra-lateral brain hemisphere. KG-R had significantly lower contra-lateral invasion compared to all the other groups at $p<0.05$ (Figure 24B).

Figure 21. Experimental design for the analysis of diet influence on intracranial growth and contra-lateral invasion of VM-M3/Fluc brain tumor. VM mice were implanted *i.c* with the VM-M3/Fluc tumor as explained in Materials and Methods. Mice were fasted for 18 hours on Day 3 before the initiation of the diet on Day 4. Mice were fed either with unrestricted Standard Diet (SD-UR), restricted Standard Diet (SD-R), unrestricted KetoGen diet (KG-UR) or restricted KetoGen diet (KG-R). All mice are imaged *in vivo*, brains collected and imaged *ex vivo* at time of termination.

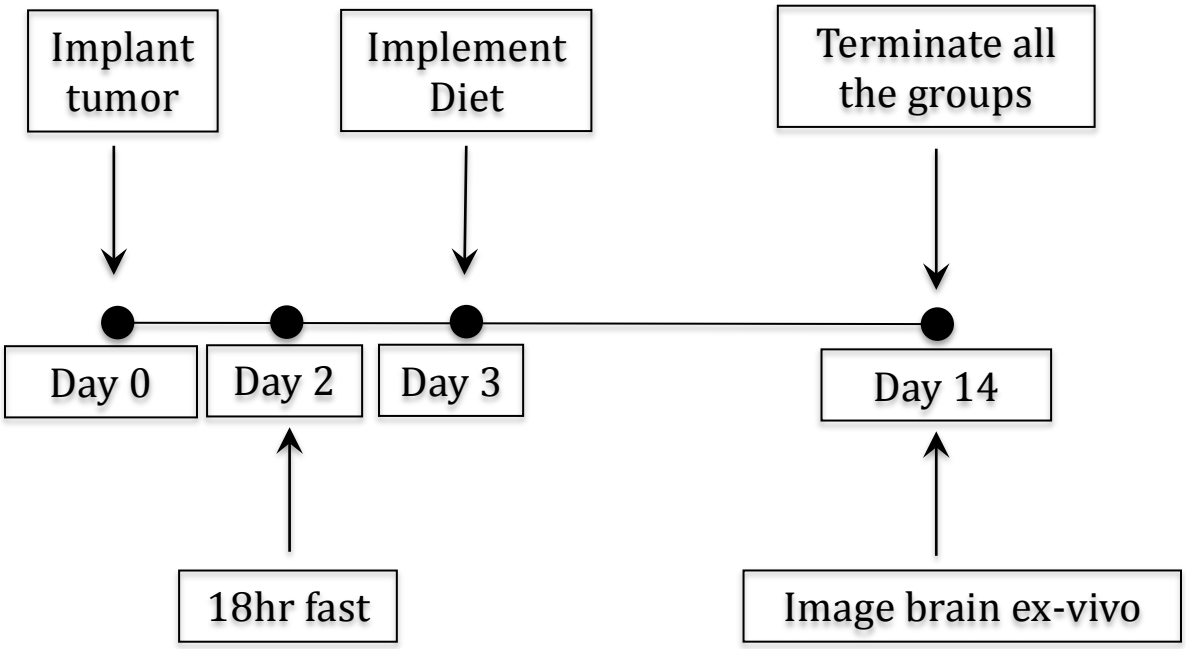

Experimental Groups (N = 12 / all groups):
Standard Diet Unrestricted (SD-UR)
Standard Diet Restricted (SD-R) (18% body weight reduction)
KetoGen Unrestricted (KG-UR)
KetoGen Restricted (KG-R) (18% body weight reduction)

Figure 22. Influence of diet on body weight, blood glucose and β-hydroxybutyrate levels of VM-M3/fluc brain tumor bearing mice. (A) Mice were fed either with unrestricted Standard Diet (SD-UR), restricted Standard Diet (SD-R), unrestricted KetoGen diet (KG-UR) or restricted KetoGen diet (KG-R). Restricted groups received 40-60% less food in order to reach 18% body weight reduction. Body weights were monitored daily. Prior to treatment, the body weights of all mice were averaged for a single value. Values represent the average ± standard error of the mean (SEM). Mice were sacrificed 14 days post-implantation and blood was collected for the analysis of **(B)** glucose and **(C)** β-hydroxybutyrate **(D)** Glucose Ketone Index levels as explained in Materials and Methods. All data is represented as mean ± standard error of the mean (SEM). Single asterisk indicates that values are significantly different compared to control (SD-UR) group at $p < 0.05$. Double asterisk indicates that KG-R values are significantly different than SD-UR, SD-R and KG-UR values at $p < 0.05$.

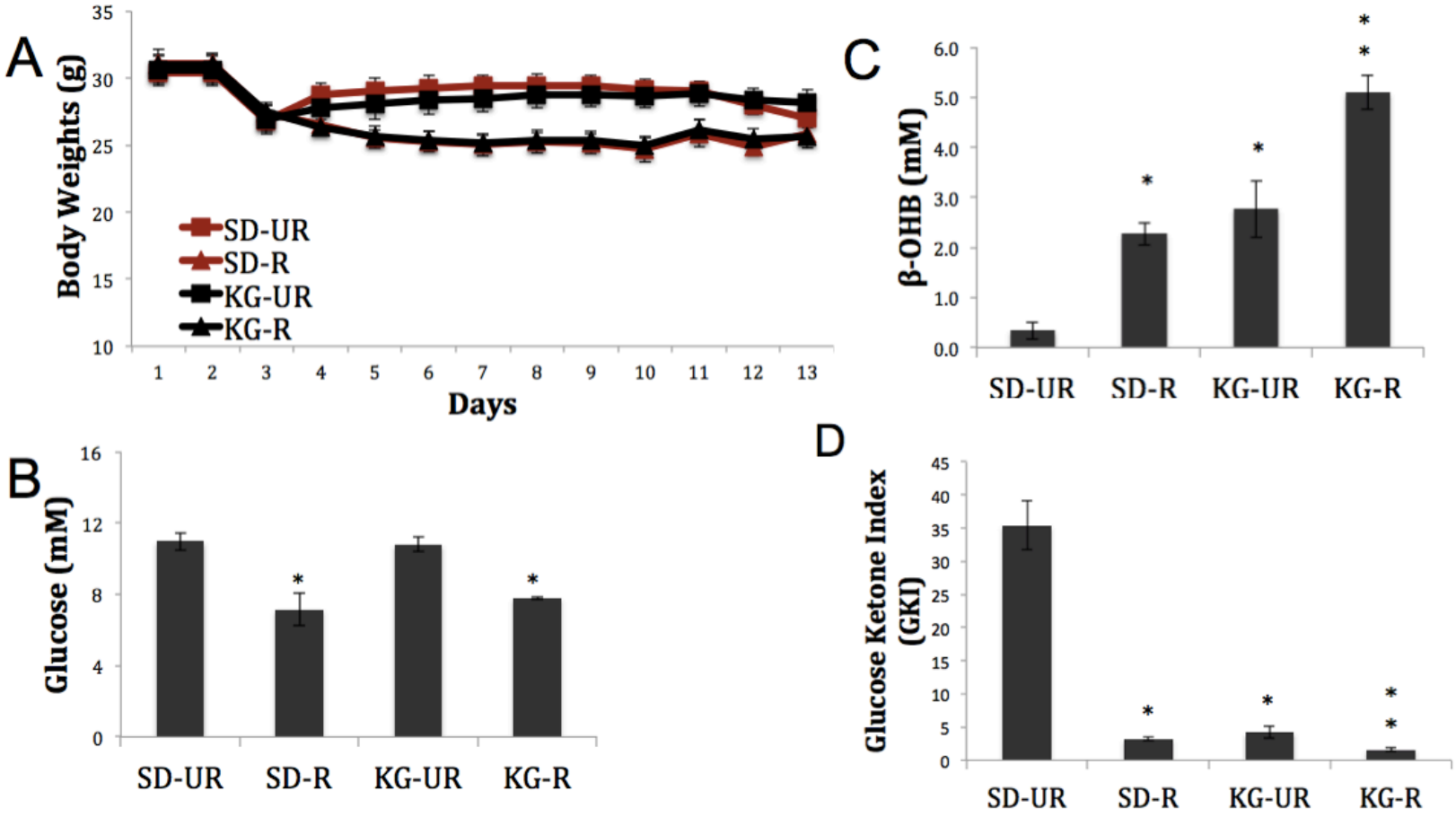
A
Body Weights (g)
35
30
25
20
15
10
1
2
3
4
5
6
7
8
9
10
11
12
13
Days
SD-UR
SD-R
KG-UR
KG-R
B
Glucose (mM)
16
12
8
4
0
SD-UR
SD-R
KG-UR
KG-R
C
β-OHB (mM)
6.0
5.0
4.0
3.0
2.0
1.0
0.0
SD-UR
SD-R
KG-UR
KG-R
D
Glucose Ketone Index (GKI)
45
40
35
30
25
20
15
10
5
0
SD-UR
SD-R
KG-UR
KG-R

Figure 23. Bioluminescent imaging of VM-M3/Fluc tumor growth in VM mouse brain. (A) 1 mm^3 of VM-M3/Fluc tumor tissue pieces were implanted into right hemisphere of VM mice. At Day 15, Removed brains were dissected into ipsi-lateral and contra-lateral hemispheres. **(B)** Bioluminescence images were taken with Xenogen Imaging system. Representative images are shown.

A

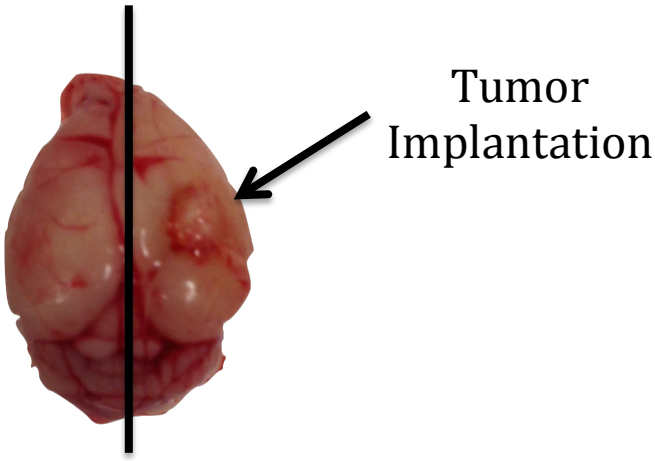

B

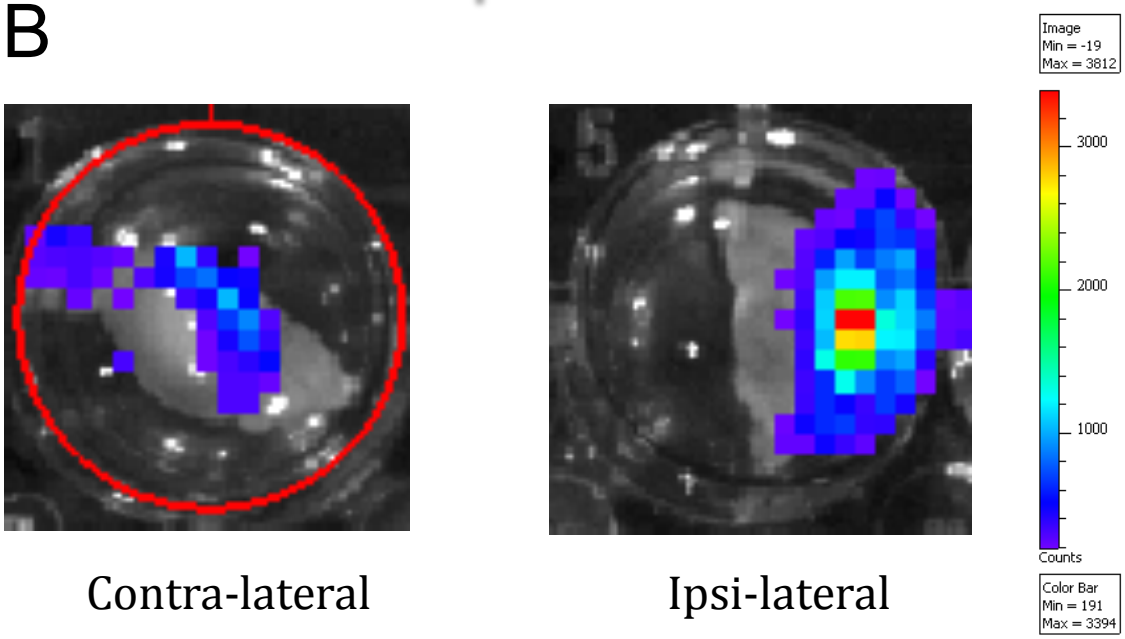

Contra-lateral

Ipsi-lateral

Figure 24. Influence of diet on intracranial growth and contra-lateral invasion of VM-M3/Fluc brain tumor. VM mice were fed with either unrestricted Standard Diet (SD-UR), restricted Standard Diet (SD-R), unrestricted KetoGen diet (KG-UR) or restricted KetoGen diet (KG-R). Brains were removed 14 days after tumor implantation and were dissected to ipsi-lateral and contra-lateral hemispheres. Bioluminescence images were taken with Xenogen Imaging system. (A) Whole brain bioluminescence (sum of ipsi-lateral and contra-lateral hemispheres) (B) Contra-lateral hemisphere bioluminescence. Values are expressed as mean ± standard error of the mean (SEM). Asterisk indicates that values are significantly different compared to control (SD-UR) group at $p < 0.05$

A

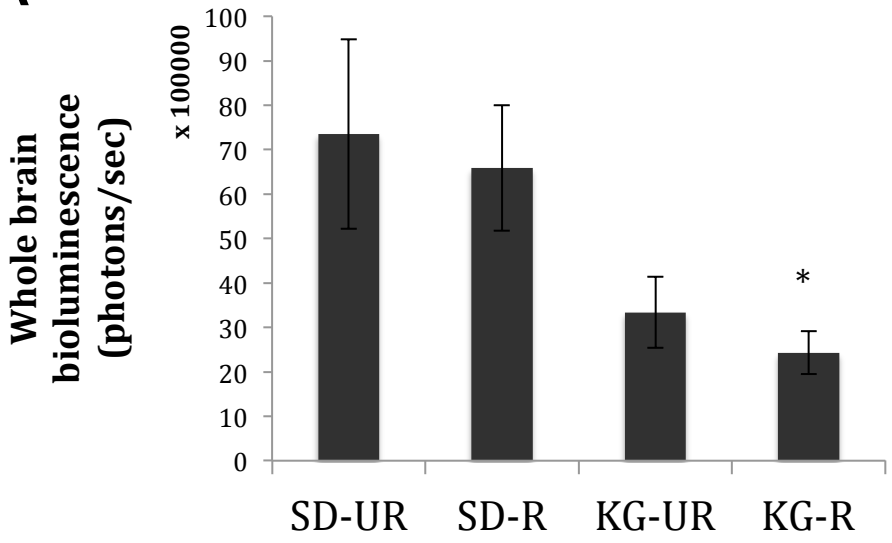

B

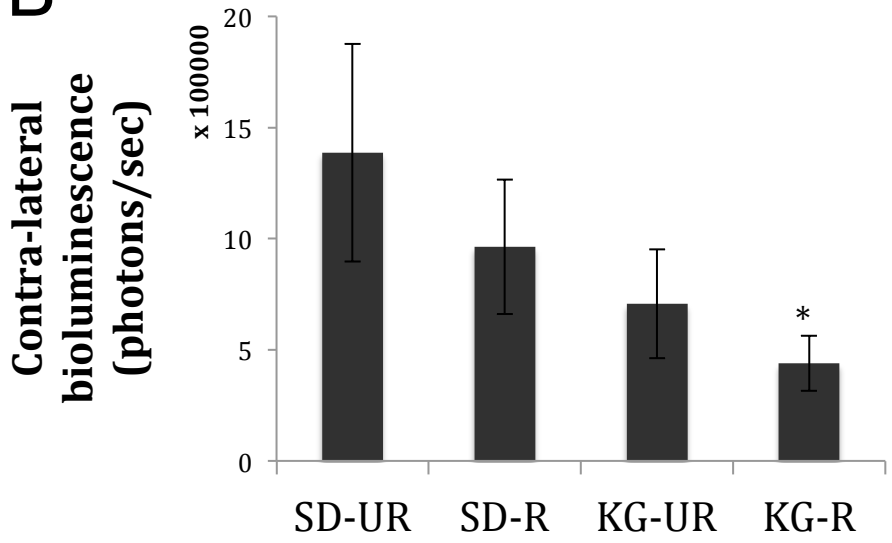

N = 12 / all groups

Influence of KetoGen ketogenic diet vs KetoCal ketogenic diet on growth and metastatic spread of VM-M3/fluc subcutaneous tumor

In this experiment we analyzed whether restricted feeding of different brand ketogenic diets would have similar effect on VM-M3 tumor growth and metastasis. VM mice were implanted *s.c* with the VM-M3/Fluc tumor on Day 0. Mice were fasted for 18 hours on Day 3 before diet initiation at Day 4 (Figure 25). The mice were fed either with KetoCal ketogenic diet (Nutricia LLC) or KetoGen ketogenic diet (Solace Nutrition LLC) in restricted amounts, in order to reach 18% body weight reduction. Body weights of KC-R and KG-R mice were similar throughout the study (Figure 26A). However, in KG-R group, blood glucose levels were significantly lower and β-hydroxybutyrate levels were significantly higher compared to KC-R group at $p < 0.05$ (Figure 26B, 26C). Therefore KG-R groups had significantly lower GKI values compared to KC-R group (Figure 26D).

Restricted feeding of KetoGen ketogenic diet (KG-R) significantly lowered primary VM-M3 tumor growth compared to restricted feeding of KetoCal ketogenic diet (KC-R) at $p<0.01$ (Figure 27). KG-R also significantly lowered VM-M3 tumor metastasis to liver, lung, spleen and kidney compared to KC-R at $p<0.05$ (Figure 28).

Figure 25. Experimental design for the analysis of KetoGen and KetoCal ketogenic diet influence on VM-M3/Fluc growth and metastasis. . VM mice were implanted *s.c.* with the VM-M3/Fluc tumor as explained in Materials and Methods. Mice were fasted for 18 hours on Day 3 before the initiation of the diet on Day 4. VM mice were fed either with restricted KetoGen diet (KetoGen-R) or restricted KetoCal (KetoCal-R). All mice were imaged *in vivo*, organs and tumors collected and imaged *ex vivo* at time of termination.

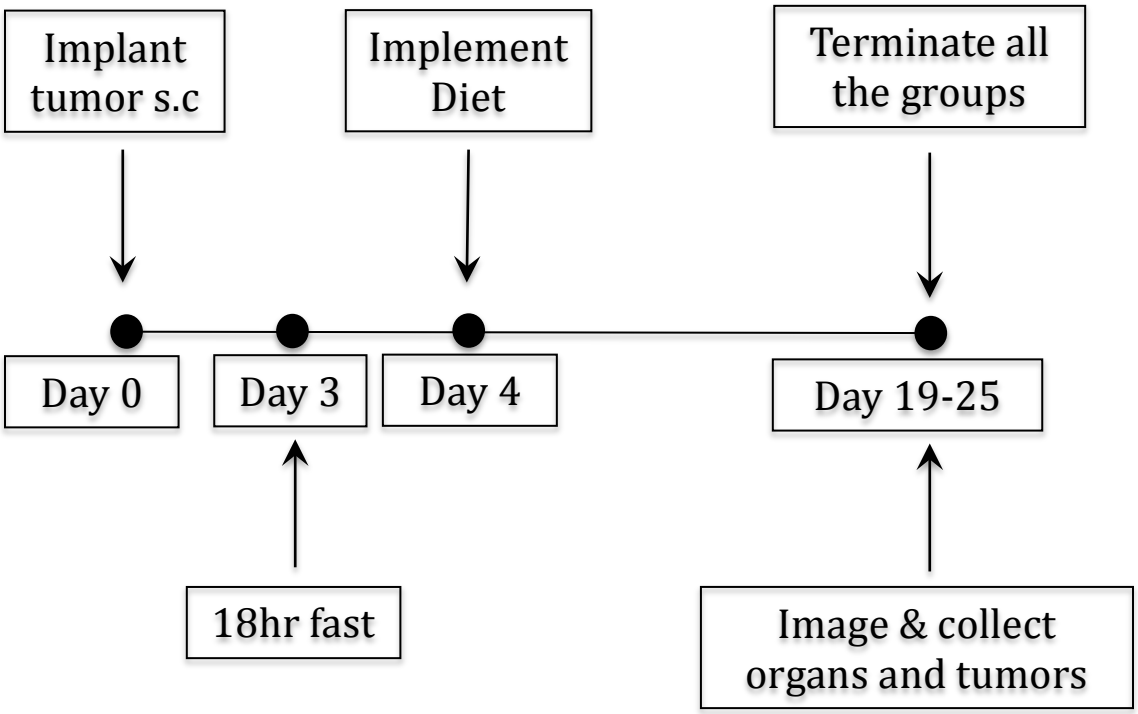

Experimental Groups (N=6 / all groups):
KetoGen Restricted (KG-R) (18% Body weight reduction)
KetoCal Restricted (KC-R) (18% Body weight reduction)

Figure 26. Influence of restricted KetoGen and KetoCal ketogenic diet on body weight, blood glucose and β-hydroxybutyrate levels of VM-M3/Fluc subcutaneous tumor bearing VM mice. **(A)** VM mice were fed either with restricted KetoGen diet (KetoGen-R) or restricted KetoCal (KetoCal-R). Restricted groups received 40-60% of daily food intake in order to reach 18% body weight reduction. Body weights were monitored daily. Prior to treatment, the body weights of all mice were averaged for a single value. Values represent the average ± standard error of the mean (SEM). Mice were sacrificed 20–25 days post-implantation and blood was collected for the analysis of **(B)** glucose and **(C)** β-hydroxybutyrate **(D)** Glucose Ketone Index levels, as explained in materials and methods. All data is represented as mean ± standard error of the mean (SEM). Asterisk indicates KetoGen feeding significantly reduced blood glucose levels and increased β-hydroxybutyrate level compared to restricted KetoCal feeding that at $p < 0.05$.

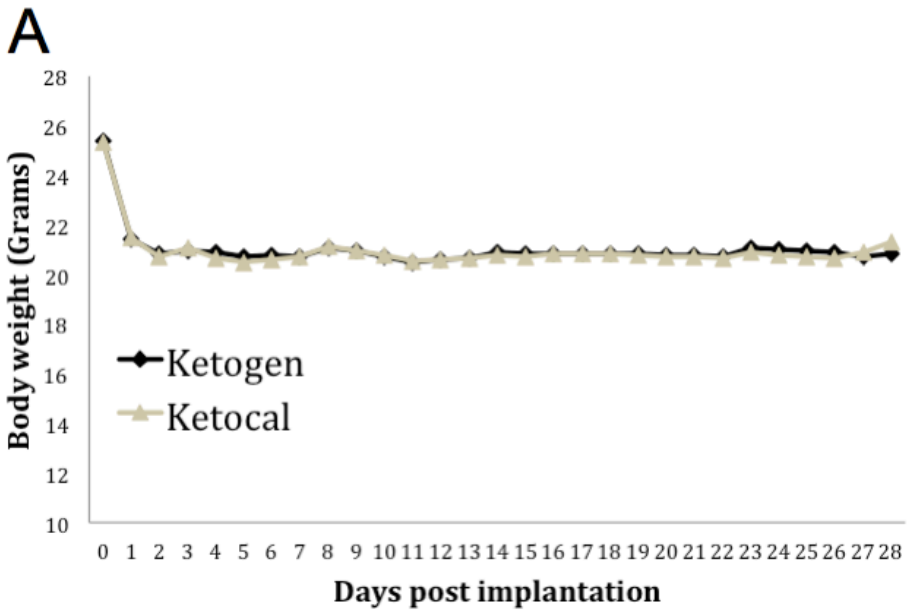
A
Body weight (Grams)
Days post implantation
Ketogen
Ketocal

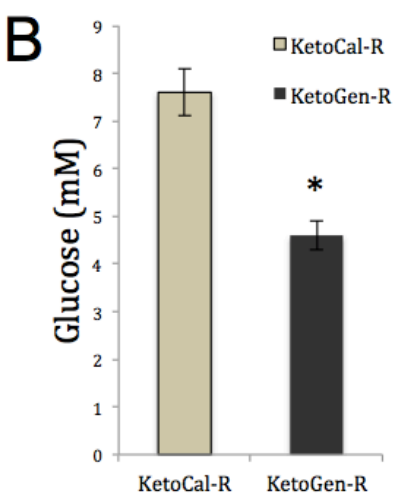
B
Glucose (mM)
KetoCal-R
KetoGen-R
*

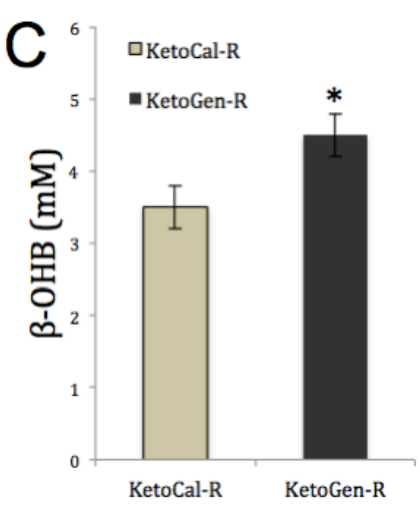
C
β-OHB (mM)
KetoCal-R
KetoGen-R
*

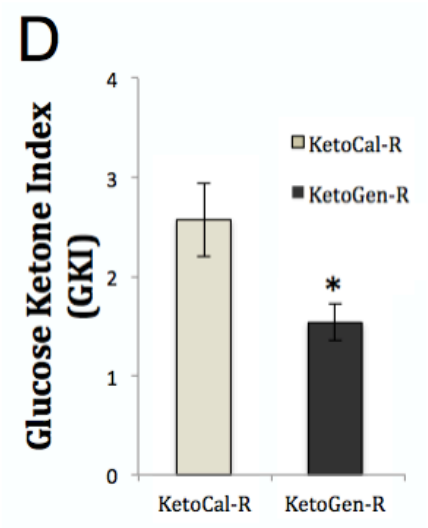
D
Glucose Ketone Index (GKI)
KetoCal-R
KetoGen-R
*

Figure 27. Influence of restricted KetoGen and KetoCal diet on primary VM-M3 tumor growth. VM mice were fed either with restricted KetoGen diet (KetoGen-R) or restricted KetoCal (KetoCal-R). All values are represented as mean ± SEM. The asterisk indicates that restricted KetoGen feeding reduced VM-M3/Fluc tumor growth significantly at $p<0.01$ compared to restricted KetoCal feeding.

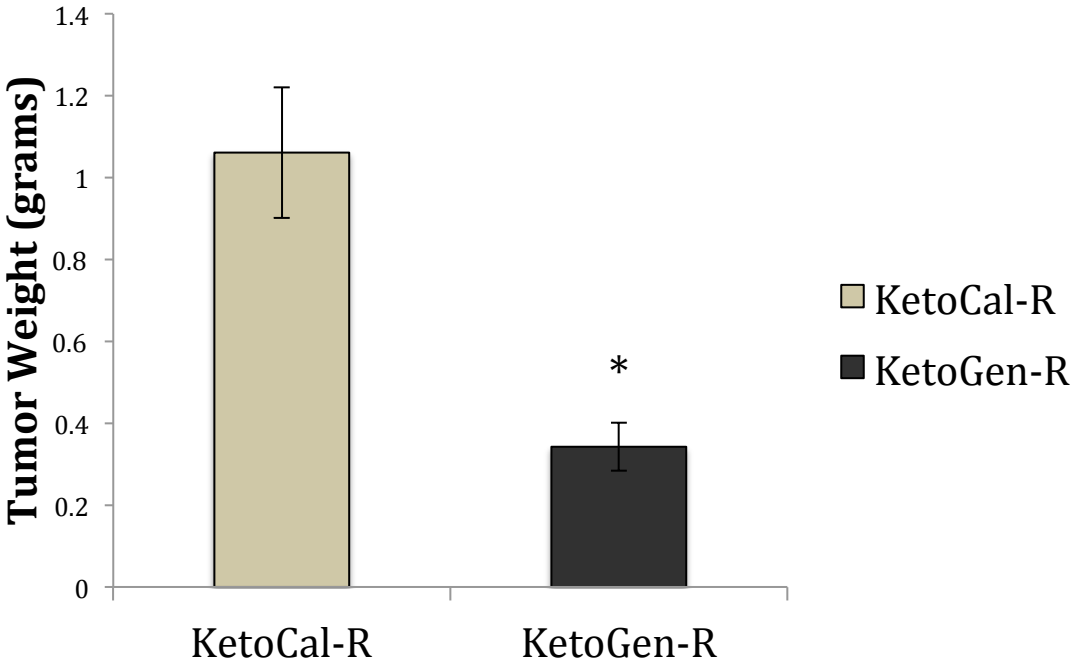
Tumor Weight (grams)
1.4
1.2
1
0.8
0.6
0.4
0.2
0
*
KetoCal-R
KetoGen-R
KetoCal-R
KetoGen-R

Figure 28. Influence of restricted KetoGen and KetoCal diet on distant organ metastasis of VM-M3/Fluc tumor. VM mice were fed either with restricted KetoGen diet (KetoGen-R) or restricted KetoCal (KetoCal-R). All values are represented as mean ± SEM. The asterisk indicates that restricted KetoGen feeding reduced VM-M3/Fluc tumor growth significantly compared to restricted KetoCal feeding. At the time of sacrifice, the organs were removed and imaged ex vivo. Bioluminescence values were plotted on a log scale. All values represent the average ± SEM. The asterisk indicates that restricted KetoGen feeding reduced organ metastasis significantly at $p<0.05$ compared to restricted KetoCal feeding.

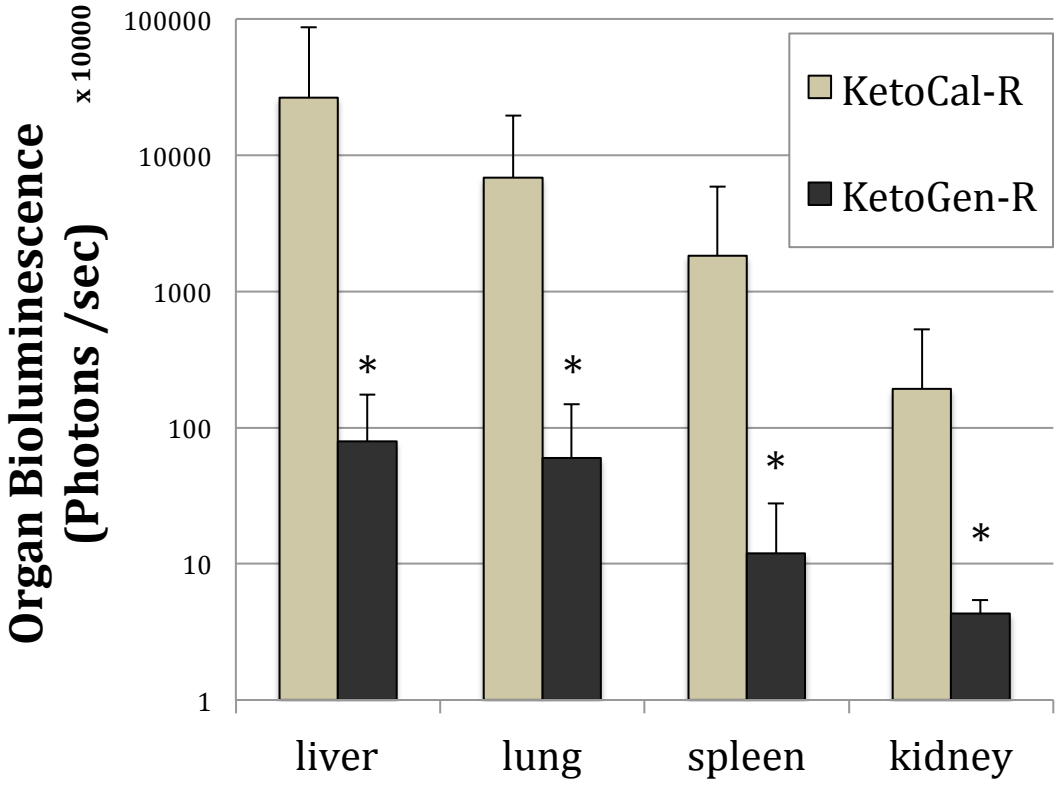

N = 6 / all groups

Influence of diet on CL, BMP and PG amount of VM-M3 tumor tissues

It has been shown that BMP increases in starved cells, due to increased autophagy. CL is an essential component for respiration in mitocohondria and CL abnormalities found in many tumor cell types. Therefore we were interested in BMP and CL, and their precursor PG levels in VM-M3 tumor cells under different diet conditions. Acidic lipids were analyzed from VM-M3 tumor tissues fed with unrestricted Standard Diet (SD-UR), restricted Standard Diet (SD-R), unrestricted KetoGen diet (KG-UR) or restricted KetoGen diet (KG-R). CL, BMP and PG were significantly higher in KetoGen fed animals (KG-UR, KG-R) compared to control animals (SD-UR) at $p < 0.05$ (Figure 29, Table 6).

Figure 29. Influence of diets on acidic lipids of VM-M3 subcutaneous tumor. Mice were fed either with unrestricted Standard Diet (SD-UR), restricted Standard Diet (SD-R), unrestricted KetoGen diet (KG-UR) and restricted KetoGen diet (KG-R). Tumors were collected at the end of study and lipids were isolated as described in Materials and Methods in Chapter 1. Plate was developed to a height of 6.0 cm with chloroform: methanol: acetic acid: formic acid: water (70:30:12:4:2 by volume), and developed to the top with hexanes: diisopropyl ether: acetic acid (65:35:2 by volume). The amount of acidic lipids spotted on the HPTLC for each cell line was equivalent to 600 μg of cell dry weight, FFA, free fatty acid; IS, internal standard; CL, cardiolipin; PA, phosphatidic acid; PG, PhosphatidylGlycerol; PS, phosphatidylserine; and PI, phosphatidylinositol.

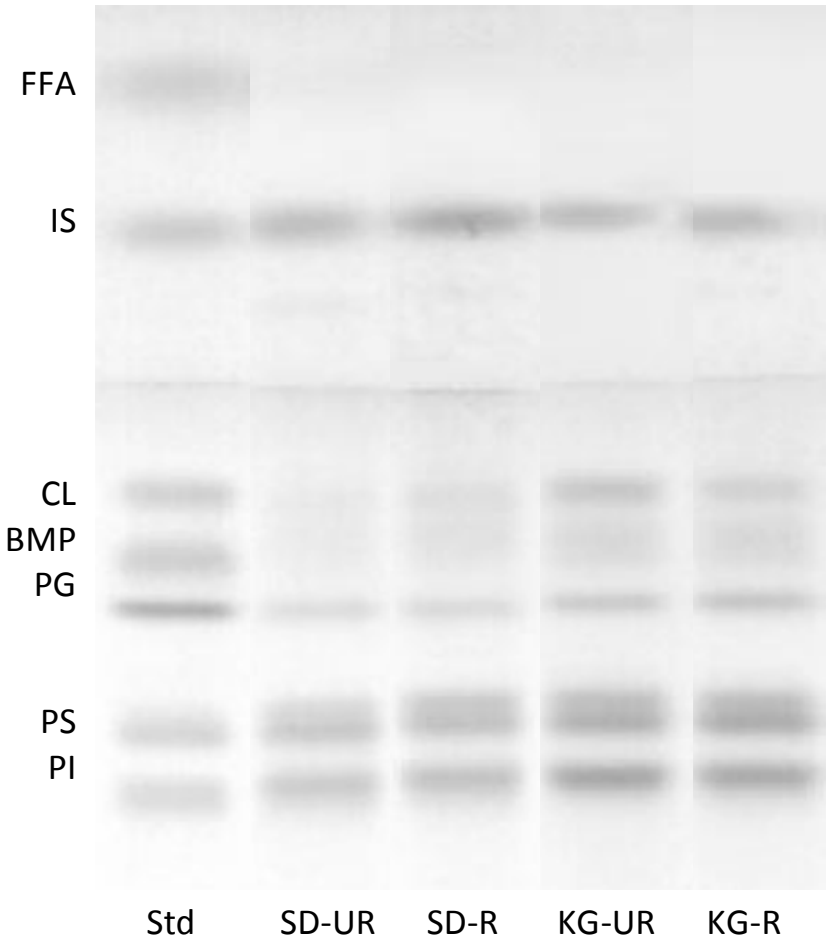
FFA
IS
CL
BMP
PG
PS
PI
Std
SD-UR
SD-R
KG-UR
KG-R

Table 6: Influence of diet on acidic lipids of VM-M3 tumor tissue

Acidic Lipids	SD-UR	SD-R	KG-UR	KG-R
CL	127.2 ± 6.9	142.9 ± 10.2	192.4 ± 3.3*	165.2 ± 5.6*
BMP	99.9 ± 7.2	125.6 ± 8.1	162.1 ± 8.3*	165.9 ± 7*
PG	113.5 ± 8.1	118.6 ± 9.3	155.0 ± 11.1*	153.6 ± 9.1*
PS	264.0 ± 21.3	287.8 ± 17.0	283.6 ± 4.8	262.9 ± 20.6
PI	246.8 ± 16.5	266.3 ± 21.5	260.8 ± 19.5	235.5 ± 16.5

* Significantly different than SD-UR and SD-R values at $p < 0.05$

Composition of Standard Diet and KetoGen ketogenic diet (KG) and KetoCal® ketogenic diet (KC)

As seen in Table 7, standard diet includes higher carbohydrate amounts (62 g) compared to KetoGen (2.54g) and KetoCal (8.8g) ketogenic diets for every 100g of the complete formula. Standard diet has lower fat amounts (6g) compared to KetoGen (74g) and KetoCal (69.1g) ketogenic diets. Also, KetoGen ketogenic diet has lower carbohydrate (2.54g vs 8.8g) and higher fat amounts (74g vs 69.1g) compared to KetoCal ketogenic diet.

Table 7: Composition of Standard Diet and KetoGen ketogenic diet and KetoCal® ketogenic diet

Components	Standard Diet (SD)	KetoGen (KG)	KetoCal Diet (KC)
Carbohydrate *	62	2.54	8.8
Fat *	6	74	69.1
Protein *	27	15.17	14.4
Energy (Kcal/gr)	4	6.9	7.2
Fat/(Protein+Carbohydrate)	0.07	4.17	3

*Values are presented as g/100g diet

Discussion

Cancer is the second leading cause of death in United States after heart disease and cancer kills more people than heart disease in every age group other than 65+ according to National Center for Health statistics report on 2013. Despite years of extensive research, little accomplishment has been achieved on cancer treatments [199]. Most conventional therapies, such as radiation and chemotherapy, are extremely toxic and these therapies do not target tumor cells specifically, which also causes damage to normal cells and tissues [200]. Since all cancers suffer from an abnormal metabolism, therapeutic strategies that focus on cancer metabolism promise effectiveness with reduced adverse effects on normal cells and tissues [201].

Cancer cells generate ATP mainly through glucose fermentation due to their mitochondrial abnormalities [141]. Non-toxic metabolic therapies can exploit the cancer cell mitochondria defects, while protecting normal cells [151, 202]. Calorie restriction or ketogenic diets can reduce the glucose available to cancer cells, while providing ketones as an alternative fuel that can only be metabolized efficiently by normal cells [184]. Low carbohydrate, high fat ketogenic diets are previously used safely and successfully in humans, for treatment of epilepsy and also cancer [203-206]. Seyfried and his colleagues showed that KetoCal ketogenic diet reduced primary tumor growth of mouse CT2A glioma in B6 mouse as well as U87 human tumor growth in SCID mouse [207]. However, in

these studies, restricted KetoCal ketogenic feeding did not reduce tumors compared to calorie matched restricted standard diet counterparts [207]. In other words, restriction was the primary reason of therapeutics, but not the type of diet. In these studies, calorie restriction decreased blood glucose and increased ketone levels compared to unrestricted feeding, and tumor growth directly correlated with reduced blood glucose levels. Authors also observed a slight increase in body weight and blood glucose in animals fed with unrestricted KetoCal ketogenic diet. Therefore, Seyfried et al overemphasized the importance of calorie restriction for tumor management, since feeding with unrestricted KetoCal ketogenic diet can increase blood glucose levels and can cause insulin insensitivity [151, 208]. Reduced availability of glucose as the primary fuel for cancer cells cause an energy restriction to tumor cells, and reduce their proliferative capabilities. However, therapeutic effect of calorie restriction on primary tumors does not only result from the decreased metabolite availability, but it is also a result of the down regulation of growth pathways such as PI3K/Akt, decrease in inflammation and angiogenesis in the tumor environment [168-172].

In this work, I analyzed the growth and metastasis of VM-M3 cells under Standard diet or KetoGen ketogenic diet (Solace Nutrition LLC) feeding, in unrestricted or restricted conditions. Calorie restriction of a standard diet (SD-R) group significantly decreased VM-M3/Fluc primary tumor growth when compared to unrestricted SD-UR control group as previously shown by Shelton et al (Figure

14) [209]. SD-R group had significantly lower blood glucose levels and higher ketone values compared to SD-UR group (Figure 12). However, calorie restriction did not decrease metastasis to organs liver, lungs, spleen and kidneys (Figure 15). On the other hand, it significantly increased the survival rate of VM-M3 tumor bearing animals [209]. Positive effects of calorie restriction on tumor bearing mice survival might result from other health benefits obtained from calorie restrictions, such as reduction of systemic inflammation [210]. Also In SD-UR fed tumor bearing animals, tumors reach to considerable sizes (2-3 grams) towards the end of study (Figure 14). Tumor cells need high amounts of fuel to maintain their viability and cause systemic protein breakdown, known as cancer cachexia. Therefore, high tumor burden in SD-UR group, might also be contributing to the worse prognosis seen in this group.

Restricted KetoGen feeding (KG-R) decreased the tumor growth significantly when compared to SD-UR, SD-R and KG-UR groups (Figure 14). KG-R had similar blood glucose levels to SD-R group suggesting that blood glucose might not be the only predictor for primary tumor growth (Figure 12). In fact, ketones were significantly higher (up to 3 fold) in KG-R group compared to SD-UR, SD-R and KG-UR groups, supporting the tumor reducing capabilities of ketones (Figure 12). KG-R delivered lowest GKI values and suggests that Glucose Ketone Index (GKI) values could be efficiently used to assess the efficacy of metabolic therapies on primary tumor growth (Figure 12). KG-R group had also significantly lower metastasis to liver, lungs, spleen and kidneys compared to SD-UR and SD-

R groups (Figure 15). KG-R group also survived significantly longer compared to SD-UR, SD-R and KG-UR groups (Figure 20). These results showed that restricted feeding of KetoGen ketogenic diet (KG-R) delivered better therapeutic effect compared to restricted feeding of standard diet (SD-R). Since KG-R group had lower GKI values compared all other groups in these studies, GKI values possibly can be used to assess the effect of metabolic treatments on metastasis and overall survival (Figure 18D).

Animals fed with unrestricted ketogenic diet (KG-UR) had similar body weights when compared to animals fed with unrestricted standard diet (SD-UR) (Figure 12A,18A). However, in some occasions, slight body weight reductions were observed with KG-UR feeding if initial mouse body weight was higher than 30g (Figure 18A). KG-UR feeding did not decrease blood glucose levels when compared to unrestricted feeding of standard diet (SD-UR) (Figure 12B,18B), but it increased β-hydroxybutyrate levels compared to SD-UR group (Figure 12C,18C). Therefore KG-UR had lower GKI levels compared to SD-UR group (Figure 12D,18D). These results further suggests that blood glucose is not the only predictor of tumor growth, but lower GKI values can predict the therapeutic potential of dietary treatments.

I also evaluated the effect of diet on growth of VM-M3 tumor in brain of VM mice, and also on contra-lateral invasion. Shelton et al demonstrated that VM-M3 brain tumor shows all characteristics of the Glioblastoma Multiforme (GBM) and it can

be used to evaluate rapid therapeutic strategies for this invasive and deadly tumor type[110]. Restricted KetoGen diet effectively reduced the overall VM-M3/Fluc tumor growth in brain of VM mice compared to SD-UR and SD-R groups (Figure 24A). VM-M3 tumor cells also showed lower invasion to contra-lateral site of the brain in KG-R group suggesting this diet was also effective against highly invasive VM-M3 brain tumor (Figure 24B).

Previously it has ben shown that unrestricted KetoCal ketogenic diet did not have tumor reducing effect on on CT2A and U87 brain tumors [207]. In addition, unrestricted feeding of KetoCal ketogenic diet increased body weight of VM mouse, increased VM-M3 tumor growth and metastasis (unpublished observation by Shelton LM). However in these studies we found that unrestricted KetoGen ketogenic diet (KG-UR) reduced both flank and brain VM-M3 tumor growth and significantly prolonged survival compared to SD-UR group (Figure 14,20,24). Therefore, I compared the effect of different brand ketogenic diets, KetoGen and KetoCal, on VM-M3 tumor growth and metastasis. In order to eliminate possible body weight differences with unrestricted feeding, both diets were given in restricted amounts in order to reach 18% body weight reduction (Figure 26A). Ketogen restricted (KG-R) group had significantly lower tumor growth and metastasis compared to KetoCal-restricted (KC-R) group (Figure 27,28). These results suggested that all ketogenic diets might not deliver the same therapeutic effect on tumor growth and metastasis. KG-R fed animals also had significantly lower glucose levels, higher ketone levels and lower GKI ratio compared to KC-R

animals (Figure 26B,C,D). These observations suggest that effective metabolic therapy for the treatment of tumor growth and metastasis results from both increased ketones and decreased glucose levels.

Ketones, mainly β-hydroxybutyrate, can only generate ATP through oxidative phosphorylation, and cannot be metabolized efficiently in cancer cells with abnormal metabolism [211]. Also enzymes that are needed for ketone utilization, such as β-hydroxybutyrate dehydrogenase (β -OHBDH), and succinyl-CoA: 3-ketoacid CoA transfer (SCOT) expressions are altered in many types of cancer cells [184, 186, 212-214]. However, our results suggest that ketones also have anti-tumor effects rather than simple absence of utilization, since elevation of ketones reduces tumor growth and metastasis. Recently, Poff et al showed that ketones inhibit the growth of VM-M3 cells *in vitro*, and ketone supplementation inhibited VM-M3 organ metastasis, suggesting a direct therapeutic effect of ketones on tumor growth and metastasis [215].

Cardiolipin content and structure is crucial for mitochondrial function and its efficient respiration. Kiebish et al observed cardiolipin content and fatty acid profile is altered in tumor tissues compared to normal tissues [107]. We observed that cardiolipin content was higher in tumor cells in ketogenic diet groups (KG-UR, KG-R) compared to control (SD-UR) group (Figure 29,Table 6). Ketones get converted to Acetyl-Coa and enter mitochondria directly, and cannot be metabolized to lactate as glucose [175]. Ketones might force cancer cells to

oxidative phosphorylation and might be cause an increase in cardiolipin content and/or remodeling of the CL fatty acid species, *i.e.* mitochondrial biogenesis. It needs to be further investigated however, if this mitochondrial biogenesis can rescue the cancer phenotype, and revert uncontrolled proliferation of tumor cells. Warburg stated that respiratory insufficiency in cancer cells becomes eventually irreversible [141]. If respiration damage in cancer cells is irreversible, forcing cancer cells to use oxidative phosphorylation might cause an increased electron leak, and more ROS formation, and eventually death of the cancer cells. Bonnet et al showed that Dichloroacetate (DCA), shifts metabolism from glycolysis to glucose oxidation, increases mitochondrial ROS and eventually causes cancer cell death [216]. This mechanism might explain why ketogenic diet increased the efficacy of ROS generating cancer therapies such as radiation and hyperbaric oxygen therapies[188, 189, 191]. Cancer cells cannot cope with excessive ROS levels beyond their capacity, and detrimental oxidative stress can lead to cell death. Reduced glucose can limit the anti-oxidant capabilities of tumor cells due to decreased NADPH generation by down regulation of pentose phosphate pathway and additional ROS generation can cause cancer cell death [157].

BMP content is increased in serum-starved cells as a result of nutrient stress and autophagy, the process where cells degrade its own materials [5, 217]. I observed that BMP increased in tumor tissues with restricted feeding of standard diet (SD-R) compared to control (SD-UR) group (Figure 29, Table 6). Also, BMP was even further increased in tumor tissues from ketogenic diet groups (KG-UR

and KG-R) and this increase was significant compared to control (SD-UR) tumors. These results might suggest that ketogenic diet feeding might cause further nutrient stress and autophagy in tumor cells.

Damaged mitochondria is recycled in lysosomal machinery by a different autophagy mechanism, called mitophagy. A successful mitophagy is necessary for clearing the defective mitochondria and an efficient respiration. CL level increase observed in VM-M3 tumor cells with ketogenic diet might be resulted from increased CL synthesis with mitocohondria utilization increase with ketones, or an increased clearance of defective mitochondria. Degradation of CL can be the result to an increase PG, which is the precursor for BMP. It has been previously shown that CL is not the precursor for BMP synthesis. However, elevation of CL, PG and BMP in VM-M3 tumor cells with ketogenic diet feeding brings a question whether there is a crosstalk between these lipids. Even though CL might not be a precursor for BMP in de novo synthesis, in certain situations such as CL degradation in lysosomes with mitophagy, PG can be abundant in lysosomes and can be directly used for BMP synthesis. These questions need further research to be answered.

CONCLUSIONS

In this thesis work, First I observed a dramatic increase of BMP levels in GM1 and GM2 gangliosidoses brain samples in humans, American black bear, cats, and mice compared to their non-diseased counterparts. BMP have functional roles in endo-lysosomal system such as formation, structure, and trafficking of endosomal/lysosomal compartments. BMP facilitates the degradation of glycosphingolipids in the limiting membrane of endosomal and lysosomal compartments. BMP also plays roles in many pathological conditions such as atherogenesis, viral infection and lysosomal storage diseases and modulating BMP levels can alleviate the pathologies observed in these diseases. Lysosomal storage diseases also involve inflammation. Within the discovery of BMP as a macrophage associated lipid, it was very important to evaluate the reason for BMP storage in gangliosidosis in relation to inflammation. In this regard, I found evidence suggesting BMP stored in gangliosidoses as a consequence of the primary stored gangliosides rather than being an inflammation associated phenomena. We hope that the information presented in this thesis could be helpful in future studies that evaluate BMP synthesis and function.

I also found that macrophage/microglia originated cells with different tissue of origins had significantly higher BMP content compared to non-macrophage cell lines. Macrophages are important players of immune response and they play

either a direct role in pathology of many diseases such as atheroschlerosis, HIV infection and cancer. Therefore this discovery is of utmost importance for understanding the role of BMP, and its possible contributions to disease pathology.

In this thesis work, I also found that restricted KetoGen ketogenic feeding (KG-R) decreased the VM-M3 tumor growth, metastasis to liver, lungs, spleen and kidneys when compared to control (SD-UR) group. VM-M3 tumor bearing mice survived significantly longer in KG-R group compared to SD-UR, SD-R and KG-UR groups. Shelton et al showed that VM-M3 tumor is a pre-clinical model for GBM since it shows all the characteristics of growth and invasive spread when injected orthotropic to brain. VM-M3 tumors are also highly metastatic to distant organs such as liver, lung and spleen when injected to non-brain regions. It is known that the metastatic cancer is the major cause of mortality and morbidity in humans. Therefore, therapies that have significantly positive effects on VM-M3 tumor, are high potential candidates for translating to human cancer therapies, especially for GMB and other metastatic cancer types. KetoGen ketogenic diet is a non-toxic alternative therapy for VM-M3 tumor growth, invasion and metastasis. These results might bring valuable insights for the treatment of highly invasive and metastatic cancer types in humans with alternative non-toxic metabolic therapies.

APPENDIX

Figure 30. Influence of vitamin and mineral supplementation on growth of VM-M3 subcutaneous tumor. VM mice were fed either with unrestricted Standard Diet (SD-UR), restricted Standard Diet (SD-R), unrestricted KetoGen diet without vitamins and minerals (KG-UR), unrestricted KetoGen diet with vitamins and minerals(KG-UR + V/M), restricted KetoGen diet without vitamins and minerals (KG-R) and restricted KetoGen diet with vitamins and minerals (KG-R+ V/M) . Tumor volumes were measured with digital caliper at Day 12 and Day 22 and volumes calculated as V= (length × $Width^2$)/2. SD-UR and SD-R Day 22 values are not presented due to lack of enough alive mice. All values are represented as mean ± SEM. Tumor volumes were slightly higher in restricted KetoGen + vitamins and minerals group (KG-R + v/m) than in KetoGen restricted no vitamins and minerals group (KG-R) in measurements taken in Day 12 and Day 22. This increase was not statistically significant.

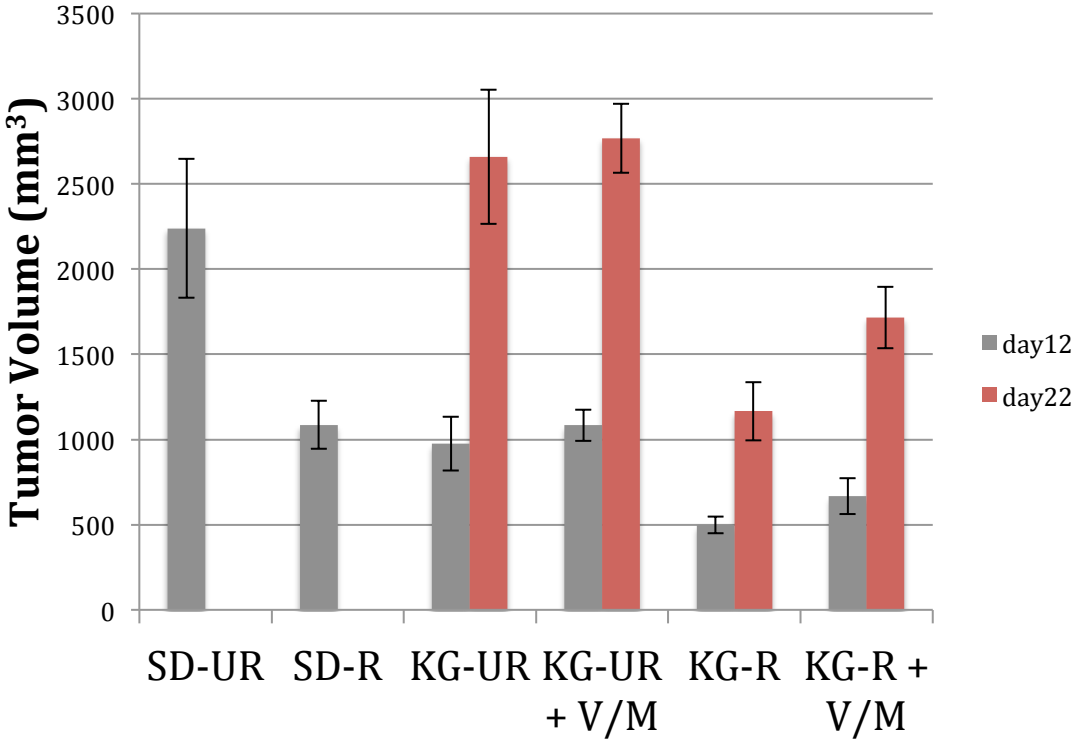
Tumor Volume (mm3)
3500
3000
2500
2000
1500
1000
500
0
SD-UR
SD-R
KG-UR
KG-UR + V/M
KG-R
KG-R + V/M
day12
day22

References

1. Brotherus, J. and O. Renkonen, *Subcellular distributions of lipids in cultured BHK cells: evidence for the enrichment of lysobisphosphatidic acid and neutral lipids in lysosomes.* J Lipid Res, 1977. **18**(2): p. 191-202.
2. Kobayashi, T., et al., *Localization of lysobisphosphatidic acid-rich membrane domains in late endosomes.* Biol Chem, 2001. **382**(3): p. 483-5.
3. Brotherus, J., et al., *Novel stereoconfiguration in lyso-bis-phosphatidic acid of cultured BHK-cells.* Chemistry and physics of lipids, 1974. **13**(2): p. 178-82.
4. Tan, H.H., et al., *Spectroscopic evidence for the unusual stereochemical configuration of an endosome-specific lipid.* Angewandte Chemie, 2012. **51**(2): p. 533-5.
5. Hullin-Matsuda, F., et al., *De novo biosynthesis of the late endosome lipid, bis(monoacylglycero)phosphate.* J Lipid Res, 2007. **48**(9): p. 1997-2008.
6. Heravi, J. and M. Waite, *Transacylase formation of bis(monoacylglycerol)phosphate.* Biochim Biophys Acta, 1999. **1437**(3): p. 277-86.
7. Poorthuis, B.J. and K.Y. Hostetler, *Conversion of diphosphatidylglycerol to bis(monoacylglyceryl)phosphate by lysosomes.* J Lipid Res, 1978. **19**(3): p. 309-15.
8. Schulze, H., T. Kolter, and K. Sandhoff, *Principles of lysosomal membrane degradation: Cellular topology and biochemistry of lysosomal lipid degradation.* Biochim Biophys Acta, 2009. **1793**(4): p. 674-83.
9. Matsuzawa, Y. and K.Y. Hostetler, *Degradation of bis(monoacylglycero)phosphate by an acid phosphodiesterase in rat liver lysosomes.* J Biol Chem, 1979. **254**(13): p. 5997-6001.
10. Mason, R.J., T.P. Stossel, and M. Vaughan, *Lipids of alveolar macrophages, polymorphonuclear leukocytes, and their phagocytic vesicles.* The Journal of clinical investigation, 1972. **51**(9): p. 2399-407.
11. Wherrett, J.R. and S. Huterer, *Bis-(monoacylglyceryl)-phosphate of rat and human liver: fatty acid composition and NMR spectroscopy.* Lipids, 1973. **8**(9): p. 531-3.
12. Luquain, C., et al., *Bis(monoacylglycerol) phosphate in rat uterine stromal cells: structural characterization and specific esterification of docosahexaenoic acid.* Biochem J, 2000. **351 Pt 3**: p. 795-804.
13. Besson, N., et al., *Selective incorporation of docosahexaenoic acid into lysobisphosphatidic acid in cultured THP-1 macrophages.* Lipids, 2006. **41**(2): p. 189-96.
14. Gallala, H.D. and K. Sandhoff, *Biological function of the cellular lipid BMP-BMP as a key activator for cholesterol sorting and membrane digestion.* Neurochemical research, 2011. **36**(9): p. 1594-600.

15. Bouvier, J., et al., *Selective decrease of bis(monoacylglycero)phosphate content in macrophages by high supplementation with docosahexaenoic acid.* J Lipid Res, 2009. **50**(2): p. 243-55.
16. Matsuo, H., et al., *Role of LBPA and Alix in multivesicular liposome formation and endosome organization.* Science, 2004. **303**(5657): p. 531-4.
17. Frederick, T.E., et al., *Bis(monoacylglycero)phosphate forms stable small lamellar vesicle structures: insights into vesicular body formation in endosomes.* Biophys J, 2009. **96**(5): p. 1847-55.
18. Chevallier, J., et al., *Lysobisphosphatidic acid controls endosomal cholesterol levels.* J Biol Chem, 2008. **283**(41): p. 27871-80.
19. Sandhoff, K., *Metabolic and cellular bases of sphingolipidoses.* Biochemical Society transactions, 2013. **41**(6): p. 1562-8.
20. Sandhoff, K. and K. Harzer, *Gangliosides and gangliosidoses: principles of molecular and metabolic pathogenesis.* The Journal of neuroscience : the official journal of the Society for Neuroscience, 2013. **33**(25): p. 10195-208.
21. Neufeld, E.F., *Lysosomal storage diseases.* Annu Rev Biochem, 1991. **60**: p. 257-80.
22. Gravel, R.A., et al., *The GM2 gangliosidoses*, in *The Metabolic and Molecular Bases of Inherited Disease*, C.R. Scriver, et al., Editors. 1995, McGraw-Hill, Inc.: New York. p. 2839-2879.
23. Kasperzyk, J.L., et al., *N-butyldeoxygalactonojirimycin reduces neonatal brain ganglioside content in a mouse model of GM1 gangliosidosis.* J Neurochem, 2004. **89**(3): p. 645-53.
24. Hauser, E.C., et al., *Inheritance of lysosomal acid beta-galactosidase activity and gangliosides in crosses of DBA/2J and knockout mice.* Biochem Genet, 2004. **42**(7-8): p. 241-57.
25. Kasperzyk, J.L., et al., *Substrate reduction reduces gangliosides in postnatal cerebrum-brainstem and cerebellum in GM1 gangliosidosis mice.* Journal of lipid research, 2005. **46**(4): p. 744-751.
26. Hein, L.K., S. Duplock, and M. Fuller, *Selective reduction of bis(monoacylglycero)phosphate ameliorates the storage burden in a THP-1 macrophage model of Gaucher disease.* J Lipid Res, 2013. **54**(6): p. 1691-7.
27. Vanier, M.T., *Biochemical studies in Niemann-Pick disease. I. Major sphingolipids of liver and spleen.* Biochim Biophys Acta, 1983. **750**(1): p. 178-84.
28. Rouser, G., et al., *Accumulation of a glycerolphospholipid in classical niemann-pick disease.* Lipids, 1968. **3**(3): p. 287-90.
29. Asumendi, A., et al., *Implication of mitochondria-derived ROS and cardiolipin peroxidation in N-(4-hydroxyphenyl)retinamide-induced apoptosis.* Br J Cancer, 2002. **86**(12): p. 1951-6.
30. Harder, A., F. Widjaja, and H. Debuch, *Studies on lipids from liver and spleen of a child (O.L.) with Niemann-Pick's disease type C.* J Clin Chem Clin Biochem, 1984. **22**(2): p. 199-201.
31. Kahma, K., et al., *Low and moderate concentrations of lysobisphosphatidic acid in brain and liver of patients affected by some storage diseases.* Lipids, 1976. **11**(7): p. 539-44.

32. Kakela, R., P. Somerharju, and J. Tyynela, *Analysis of phospholipid molecular species in brains from patients with infantile and juvenile neuronal-ceroid lipofuscinosis using liquid chromatography-electrospray ionization mass spectrometry.* J Neurochem, 2003. **84**(5): p. 1051-65.
33. Jabs, S., et al., *Accumulation of bis(monoacylglycero)phosphate and gangliosides in mouse models of neuronal ceroid lipofuscinosis.* Journal of neurochemistry, 2008. **106**(3): p. 1415-25.
34. Hobert, J.A. and G. Dawson, *A novel role of the Batten disease gene CLN3: association with BMP synthesis.* Biochem Biophys Res Commun, 2007. **358**(1): p. 111-6.
35. Clarke, L.A., et al., *Biomarkers for the mucopolysaccharidoses: discovery and clinical utility.* Mol Genet Metab, 2012. **106**(4): p. 395-402.
36. Meikle, P.J., et al., *Effect of lysosomal storage on bis(monoacylglycero)phosphate.* The Biochemical journal, 2008. **411**(1): p. 71-8.
37. Walkley, S.U. and M.T. Vanier, *Secondary lipid accumulation in lysosomal disease.* Biochimica et biophysica acta, 2009. **1793**(4): p. 726-36.
38. Hullin-Matsuda, F., et al., *Bis(monoacylglycero)phosphate, a peculiar phospholipid to control the fate of cholesterol: Implications in pathology.* Prostaglandins Leukot Essent Fatty Acids, 2009. **81**(5-6): p. 313-24.
39. Amidon, B., et al., *Biosynthetic conversion of phosphatidylglycerol to sn-1:sn-1' bis(monoacylglycerol) phosphate in a macrophage-like cell line.* Biochemistry, 1995. **34**(16): p. 5554-60.
40. Sango, K., et al., *Mouse models of Tay-Sachs and Sandhoff diseases differ in neurologic phenotype and ganglioside metabolism.* Nat Genet, 1995. **11**(2): p. 170-6.
41. Hahn, C.N., et al., *Generalized CNS disease and massive GM1-ganglioside accumulation in mice defective in lysosomal acid beta-galactosidase.* Hum-Mol-Genet, 1997. **6**(2): p. 205-11.
42. Hauser, E.C., A. d'Azzo, and T.N. Seyfried, *Inheritance of brain beta-galactosidase activities and gangliosides in crosses of DBA/2J and knockout mice.* J. Neurochem., 2002. **81 (Suppl. 1)**: p. 11.
43. Galjaard, H., *Genetic Metabolic Disease: Diagnosis and Prenatal Analysis*. 1980, Amsterdam: Elsevier Sicence Publishers.
44. Cork, L.C., et al., *GM2 ganglioside lysosomal storage disease in cats with beta-hexosaminidase deficiency.* Science, 1977. **196**(4293): p. 1014-7.
45. Cork, L.C., J.F. Munnell, and M.D. Lorenz, *The pathology of feline GM2 gangliosidosis.* Am J Pathol, 1978. **90**(3): p. 723-34.
46. Baker, H.J., et al., *The gangliosidoses: comparative features and research applications.* Vet Pathol, 1979. **16**(6): p. 635-49.
47. Martin, D.R., et al., *An inversion of 25 base pairs causes feline GM2 gangliosidosis variant.* Experimental neurology, 2004. **187**(1): p. 30-7.
48. Martin, D.R., et al., *Molecular consequences of the pathogenic mutation in feline GM1 gangliosidosis.* Molecular genetics and metabolism, 2008. **94**(2): p. 212-21.

49. Baker, H.J., Jr., et al., *Neuronal GM1 gangliosidosis in a Siamese cat with beta-galactosidase deficiency.* Science, 1971. **174**(4011): p. 838-9.
50. Baek, R.C., et al., *Comparative analysis of brain lipids in mice, cats, and humans with Sandhoff disease.* Lipids, 2009. **44**(3): p. 197-205.
51. Baker, H.J. and J.R. Lindsey, *Animal model: feline GM1 gangliosidosis.* Am J Pathol, 1974. **74**(3): p. 649-52.
52. Muthupalani, S., et al., *GM1-gangliosidosis in American black bears: clinical, pathological, biochemical and molecular genetic characterization.* Molecular genetics and metabolism, 2014. **111**(4): p. 513-21.
53. Baek, R.C., et al., *N-butyldeoxygalactonojirimycin reduces brain ganglioside and GM2 content in neonatal Sandhoff disease mice.* Neurochem Int, 2008. **52**(6): p. 1125-33.
54. Seyfried, T.N., G.H. Glaser, and R.K. Yu, *Cerebral, cerebellar, and brain stem gangliosides in mice susceptible to audiogenic seizures.* J. Neurochem., 1978. **31**(1): p. 21-27.
55. Macala, L.J., R.K. Yu, and S. Ando, *Analysis of brain lipids by high performance thin-layer chromatography and densitometry.* J Lipid Res, 1983. **24**(9): p. 1243-50.
56. Folch, J., M. Lees, and G.H. Sloane-Stanley, *A simple method for the isolation and purification of total lipids from animal tissues.* J. Biol. Chem., 1957. **226**: p. 497-509.
57. Seyfried, T.N., E.J. Weber, and R.K. Yu, *Influence of trichloroacetic acid-phosphotungstic acid on the thin-layer chromatographic mobility of gangliosides.* Lipids, 1977. **12**: p. 979-980.
58. Gross, S., A. Summers, and R.H. McCluer, *Formation of ganglioside internal esters by treatment with trichloroacetic acid-phosphotungstic acid reagent.* J Neurochem, 1977. **28**(5): p. 1133-6.
59. Ando, S., N.C. Chang, and R.K. Yu, *High-performance thin-layer chromatography and densitometric determination of brain ganglioside compositions of several species.* Analytical biochemistry, 1978. **89**(2): p. 437-50.
60. Seyfried, T.N., R.K. Yu, and N. Miyazawa, *Differential cellular enrichment of gangliosides in the mouse cerebellum: Analysis using neurological mutants.* J. Neurochem., 1982. **38**: p. 551-559.
61. Arthur, J.R., K.A. Heinecke, and T.N. Seyfried, *Filipin recognizes both GM1 and cholesterol in GM1 gangliosidosis mouse brain.* Journal of lipid research, 2011. **52**(7): p. 1345-51.
62. Yang, K., et al., *Automated lipid identification and quantification by multidimensional mass spectrometry-based shotgun lipidomics.* Analytical chemistry, 2009. **81**(11): p. 4356-68.
63. Broekman, M.L., et al., *Complete Correction of Enzymatic Deficiency and Neurochemistry in the GM1-gangliosidosis Mouse Brain by Neonatal Adeno-associated Virus-mediated Gene Delivery.* Mol Ther, 2007. **15**(1): p. 30-37.
64. Baek, R.C., et al., *AAV-mediated gene delivery in adult GM1-gangliosidosis mice corrects lysosomal storage in CNS and improves survival.* PloS one, 2010. **5**(10): p. e13468.

65. Suzuki, Y., H. Sakuraba, and A. Oshima, *b-Galactosidase deficiency (b-galactosidosis): GM1 gangliosidosis and Morquio B disease*, in *The Metabolic and Molecular Bases of Inherited Disease*, C.R. Scriver, et al., Editors. 1995, McGraw-Hill Inc.: New York. p. 2785-2823.
66. Vanier, M.T., et al., *Prenatal diagnosis of Niemann-Pick type C disease: current strategy from an experience of 37 pregnancies at risk.* Am J Hum Genet, 1992. **51**(1): p. 111-22.
67. Besley, G.T. and M. Elleder, *Enzyme activities and phospholipid storage patterns in brain and spleen samples from Niemann-Pick disease variants: a comparison of neuropathic and non-neuropathic forms.* J Inherit Metab Dis, 1986. **9**(1): p. 59-71.
68. Phaneuf, D., et al., *Dramatically different phenotypes in mouse models of human Tay-Sachs and Sandhoff diseases.* Human molecular genetics, 1996. **5**(1): p. 1-14.
69. Futerman, A.H. and G. van Meer, *The cell biology of lysosomal storage disorders.* Nat Rev Mol Cell Biol, 2004. **5**(7): p. 554-65.
70. Kobayashi, T., et al., *Separation and characterization of late endosomal membrane domains.* J Biol Chem, 2002. **277**(35): p. 32157-64.
71. Arthur, J.R., et al., *Ethylenedioxy-PIP2 oxalate reduces ganglioside storage in juvenile Sandhoff disease mice.* Neurochemical research, 2013. **38**(4): p. 866-75.
72. Sano, R., et al., *GM1-ganglioside accumulation at the mitochondria-associated ER membranes links ER stress to Ca(2+)-dependent mitochondrial apoptosis.* Molecular cell, 2009. **36**(3): p. 500-11.
73. Kobayashi, T., et al., *A lipid associated with the antiphospholipid syndrome regulates endosome structure and function.* Nature, 1998. **392**(6672): p. 193-7.
74. Hayakawa, T., et al., *Differential membrane packing of stereoisomers of bis(monoacylglycero)phosphate.* Biochemistry, 2006. **45**(30): p. 9198-209.
75. Reaves, B.J., et al., *Loss of cation-independent mannose 6-phosphate receptor expression promotes the accumulation of lysobisphosphatidic acid in multilamellar bodies.* Journal of cell science, 2000. **113 (Pt 22)**: p. 4099-108.
76. Kolter, T. and K. Sandhoff, *Principles of lysosomal membrane digestion: stimulation of sphingolipid degradation by sphingolipid activator proteins and anionic lysosomal lipids.* Annual review of cell and developmental biology, 2005. **21**: p. 81-103.
77. Wendeler, M., et al., *Expression of the GM2-activator protein in the methylotrophic yeast Pichia pastoris, purification, isotopic labeling, and biophysical characterization.* Protein expression and purification, 2004. **34**(1): p. 147-57.
78. Kobayashi, T., et al., *Late endosomal membranes rich in lysobisphosphatidic acid regulate cholesterol transport.* Nature cell biology, 1999. **1**(2): p. 113-8.
79. Jeyakumar, M., et al., *Central nervous system inflammation is a hallmark of pathogenesis in mouse models of GM1 and GM2 gangliosidosis.* Brain, 2003. **126**(Pt 4): p. 974-87.

80. Sano, R., et al., *Chemokine-induced recruitment of genetically modified bone marrow cells into the CNS of GM1-gangliosidosis mice corrects neuronal pathology.* Blood, 2005. **106**(7): p. 2259-68.
81. Sargeant, T.J., et al., *Adeno-associated virus-mediated expression of beta-hexosaminidase prevents neuronal loss in the Sandhoff mouse brain.* Human molecular genetics, 2011. **20**(22): p. 4371-80.
82. Maguire, C.A., et al., *Directed evolution of adeno-associated virus for glioma cell transduction.* J Neurooncol, 2010. **96**(3): p. 337-47.
83. Meijer, D.H., et al., *Controlling brain tumor growth by intraventricular administration of an AAV vector encoding IFN-beta.* Cancer Gene Ther, 2009. **16**(8): p. 664-71.
84. Holbrook, P.G., et al., *Bis(monoacylglycero)phosphate from PC12 cells, a phospholipid that can comigrate with phosphatidic acid: molecular species analysis by fast atom bombardment mass spectrometry.* Biochim Biophys Acta, 1992. **1125**(3): p. 330-4.
85. Huterer, S. and J. Wherrett, *Metabolism of bis(monoacylglycero)phosphate in macrophages.* J Lipid Res, 1979. **20**(8): p. 966-73.
86. Cochran, F.R., et al., *Regulation of arachidonic acid metabolism in resident and BCG-activated alveolar macrophages: role of lyso(bis)phosphatidic acid.* J Immunol, 1987. **138**(6): p. 1877-83.
87. Nakashima, S., et al., *A mouse model for Niemann-Pick disease: phospholipid class and fatty acid composition of various tissues.* J Lipid Res, 1984. **25**(3): p. 219-27.
88. Mortuza, G.B., et al., *Characterisation of a potential biomarker of phospholipidosis from amiodarone-treated rats.* Biochim Biophys Acta, 2003. **1631**(2): p. 136-46.
89. Baronas, E.T., et al., *Biomarkers to monitor drug-induced phospholipidosis.* Toxicol Appl Pharmacol, 2007. **218**(1): p. 72-8.
90. Tjiong, H.B., J. Lepthin, and H. Debuch, *Lysosomal phospholipids from rat liver after treatment with different drugs.* Hoppe-Seyler's Zeitschrift fur physiologische Chemie, 1978. **359**(1): p. 63-9.
91. Harder, A. and H. Debuch, *Effect of chloroquine treatment on the different phospholipid species of rat liver lysosomes.* Hoppe-Seyler's Zeitschrift fur physiologische Chemie, 1982. **363**(7): p. 717-23.
92. Stremmel, W. and H. Debuch, *[Bis(monoacylglycero)phosphate--a marker lipid of secondary lysosomes? (AUTHOR'S TRANSL)].* Hoppe-Seyler's Zeitschrift fur physiologische Chemie, 1976. **357**(6): p. 803-10.
93. Appelqvist, H., et al., *The lysosome: from waste bag to potential therapeutic target.* J Mol Cell Biol, 2013. **5**(4): p. 214-26.
94. Renate, L.-R., *Lysosomes*. Medical Intelligence Unit. 2005: Springer US.
95. Huysentruyt, L.C., et al., *Metastatic cancer cells with macrophage properties: evidence from a new murine tumor model.* Int J Cancer, 2008. **123**(1): p. 73-84.
96. Seyfried, T.N., M. el-Abbadi, and M.L. Roy, *Ganglioside distribution in murine neural tumors.* Mol Chem Neuropathol, 1992. **17**(2): p. 147-67.

97. Seyfried, N.T., et al., *Up-regulation of NG2 proteoglycan and interferon-induced transmembrane proteins 1 and 3 in mouse astrocytoma: A membrane proteomics approach.* Cancer Lett, 2008. **263**(2): p. 243-52.
98. Huang, F.J., et al., *Pericyte deficiencies lead to aberrant tumor vascularizaton in the brain of the NG2 null mouse.* Dev Biol, 2010. **344**(2): p. 1035-46.
99. Binello, E., et al., *Stemness of the CT-2A Immunocompetent Mouse Brain Tumor Model: Characterization In Vitro.* Journal of Cancer, 2012. **3**: p. 166-74.
100. Yohe, H.C., D.L. Coleman, and J.L. Ryan, *Ganglioside alterations in stimulated murine macrophages.* Biochim Biophys Acta, 1985. **818**(1): p. 81-86.
101. Abdul-Hammed, M., et al., *Role of endosomal membrane lipids and NPC2 in cholesterol transfer and membrane fusion.* Journal of lipid research, 2010. **51**(7): p. 1747-60.
102. Orso, E., M. Grandl, and G. Schmitz, *Oxidized LDL-induced endolysosomal phospholipidosis and enzymatically modified LDL-induced foam cell formation determine specific lipid species modulation in human macrophages.* Chem Phys Lipids, 2011. **164**(6): p. 479-87.
103. Roth, S.L. and G.R. Whittaker, *Promotion of vesicular stomatitis virus fusion by the endosome-specific phospholipid bis(monoacylglycero)phosphate (BMP).* FEBS Lett, 2011. **585**(6): p. 865-9.
104. Chapuy-Regaud, S., et al., *Progesterone and a phospholipase inhibitor increase the endosomal bis(monoacylglycero)phosphate content and block HIV viral particle intercellular transmission.* Biochimie, 2013. **95**(9): p. 1677-88.
105. Liu, T., et al., *Calcium triggers exocytosis from two types of organelles in a single astrocyte.* J Neurosci, 2011. **31**(29): p. 10593-601.
106. Li, D., et al., *Lysosomes are the major vesicular compartment undergoing Ca2+-regulated exocytosis from cortical astrocytes.* J Neurosci, 2008. **28**(30): p. 7648-58.
107. Kiebish, M.A., et al., *Mitochondrial lipid and electron transport chain abnormalities in mouse brain tumors* J. Neurochem., 2007. **102 (Suppl. 1)**: p. 64.
108. Wen, P.Y. and S. Kesari, *Malignant gliomas in adults.* N Engl J Med, 2008. **359**(5): p. 492-507.
109. Krex, D., et al., *Long-term survival with glioblastoma multiforme.* Brain, 2007. **130**(Pt 10): p. 2596-606.
110. Seyfried, T.N., L.M. Shelton, and L.C. Huysentruyt, *The VM Mouse Model of Glioblastoma Multiforme*, in *Neuromethods*, R.a.M. Martinez-Murillo, A., Editor. 2012, Springer Science+Business Media, LLC.
111. Talacchi, A., et al., *Surgical treatment of high-grade gliomas in motor areas. The impact of different supportive technologies: a 171-patient series.* Journal of neuro-oncology, 2010. **100**(3): p. 417-26.
112. Lun, M., et al., *The natural history of extracranial metastasis from glioblastoma multiforme.* Journal of neuro-oncology, 2011. **105**(2): p. 261-73.
113. Kalokhe, G., et al., *Metastatic glioblastoma: case presentations and a review of the literature.* Journal of neuro-oncology, 2012. **107**(1): p. 21-7.

114. Liwnicz, B.H. and L.J. Rubinstein, *The pathways of extraneural spread in metastasizing gliomas: a report of three cases and critical review of the literature.* Hum Pathol, 1979. **10**(4): p. 453-67.
115. Beauchesne, P., *Extra-neural metastases of malignant gliomas: myth or reality?* Cancers, 2011. **3**(1): p. 461-77.
116. Huysentruyt, L.C. and T.N. Seyfried, *Perspectives on the mesenchymal origin of metastatic cancer.* Cancer Metastasis Rev, 2010. **29**(4): p. 695-707.
117. Seyfried, T.N. and L.C. Huysentruyt, *On the origin of cancer metastasis.* Critical reviews in oncogenesis, 2013. **18**(1-2): p. 43-73.
118. Karsy, M., et al., *Established and emerging variants of glioblastoma multiforme: review of morphological and molecular features.* Folia neuropathologica / Association of Polish Neuropathologists and Medical Research Centre, Polish Academy of Sciences, 2012. **50**(4): p. 301-21.
119. Chen, R., et al., *A hierarchy of self-renewing tumor-initiating cell types in glioblastoma.* Cancer Cell, 2010. **17**(4): p. 362-75.
120. Ohgaki, H. and P. Kleihues, *Genetic alterations and signaling pathways in the evolution of gliomas.* Cancer Sci, 2009. **100**(12): p. 2235-41.
121. Prestegarden, L., et al., *Glioma cell populations grouped by different cell type markers drive brain tumor growth.* Cancer research, 2010. **70**(11): p. 4274-9.
122. Huysentruyt, L.C., Z. Akgoc, and T.N. Seyfried, *Hypothesis: are neoplastic macrophages/microglia present in glioblastoma multiforme?* ASN neuro, 2011. **3**(4).
123. Fraser, H., *Brain tumours in mice, with particular reference to astrocytoma.* Food Chem. Toxicol., 1986. **24**(2): p. 105-11.
124. Shelton, L.M., et al., *A novel pre-clinical in vivo mouse model for malignant brain tumor growth and invasion.* J Neurooncol, 2010. **99**(2): p. 165-76.
125. Szatmari, T., et al., *Detailed characterization of the mouse glioma 261 tumor model for experimental glioblastoma therapy.* Cancer Sci, 2006. **97**(6): p. 546-53.
126. Kruse, C.A., et al., *A rat glioma model, CNS-1, with invasive characteristics similar to those of human gliomas: a comparison to 9L gliosarcoma.* J Neurooncol, 1994. **22**(3): p. 191-200.
127. Fomchenko, E.I. and E.C. Holland, *Mouse models of brain tumors and their applications in preclinical trials.* Clin Cancer Res, 2006. **12**(18): p. 5288-97.
128. Horten, B.C., G.A. Basler, and W.R. Shapiro, *Xenograft of human malignant glial tumors into brains of nude mice. A histopatholgical study.* J-Neuropathol-Exp-Neurol, 1981. **40**(5): p. 493-511.
129. Allavena, P., et al., *Pathways connecting inflammation and cancer.* Current opinion in genetics & development, 2008. **18**(1): p. 3-10.
130. Bellingan, G.J., et al., *In vivo fate of the inflammatory macrophage during the resolution of inflammation: inflammatory macrophages do not die locally, but emigrate to the draining lymph nodes.* J Immunol, 1996. **157**(6): p. 2577-85.
131. Ecsedy, J.A., et al., *Expression of mouse sialic acid on gangliosides of a human glioma grown as a xenograft in SCID mice.* J. Neurochem, 1999. **73**(1): p. 254-259.

132. Davies, B. and T. Morris, *Physiological parameters in laboratory animals and humans.* Pharmaceutical research, 1993. **10**(7): p. 1093-5.
133. Khanna, C. and K. Hunter, *Modeling metastasis in vivo.* Carcinogenesis, 2005. **26**(3): p. 513-23.
134. Seyfried, T.N., et al., *Cancer as a metabolic disease: implications for novel therapeutics.* Carcinogenesis, 2014. **35**(3): p. 515-27.
135. Steeg, P.S., *Tumor metastasis: mechanistic insights and clinical challenges.* Nat Med, 2006. **12**(8): p. 895-904.
136. Huysentruyt, L.C., L.M. Shelton, and T.N. Seyfried, *Influence of methotrexate and cisplatin on tumor progression and survival in the VM mouse model of systemic metastatic cancer.* Int J Cancer, 2010. **126**(1): p. 65-72.
137. Shaw, R.J., *Glucose metabolism and cancer.* Current opinion in cell biology, 2006. **18**(6): p. 598-608.
138. Nelson, D.L. and M.M. Cox, *Lehninger Principles of Biochemistry* Fifth ed. 2008, New York: W. H. Freeman.
139. Warburg, O., *The Metabolism of Tumours*. 1931, New York: Richard R. Smith. 327.
140. Warburg, O., *On the origin of cancer cells.* Science, 1956. **123**(3191): p. 309-14.
141. Warburg, O., *On the respiratory impairment in cancer cells.* Science, 1956. **124**: p. 269-270.
142. Seyfried, T.N., *Cancer as a Metabolic Disease: On the Origin, Management, and Prevention of Cancer*. 2012, Hoboken: John Wiley & Sons. 421.
143. Kiebish, M.A., et al., *Cardiolipin and electron transport chain abnormalities in mouse brain tumor mitochondria: lipidomic evidence supporting the Warburg theory of cancer.* J Lipid Res, 2008. **49**(12): p. 2545-56.
144. Arismendi-Morillo, G., *Electron microscopy morphology of the mitochondrial network in human cancer.* Int J Biochem Cell Biol, 2009. **41**(10): p. 2062-8.
145. Arismendi-Morillo, G., *Electron microscopy morphology of the mitochondrial network in gliomas and their vascular microenvironment.* Biochimica et biophysica acta, 2011. **1807**(6): p. 602-8.
146. Arismendi-Morillo, G.J. and A.V. Castellano-Ramirez, *Ultrastructural mitochondrial pathology in human astrocytic tumors: potentials implications pro-therapeutics strategies.* J Electron Microsc (Tokyo), 2008. **57**(1): p. 33-9.
147. Elliott, R.L., X.P. Jiang, and J.F. Head, *Mitochondria organelle transplantation: introduction of normal epithelial mitochondria into human cancer cells inhibits proliferation and increases drug sensitivity.* Breast cancer research and treatment, 2012. **136**(2): p. 347-54.
148. Pedersen, P.L., *Tumor mitochondria and the bioenergetics of cancer cells.* Prog Exp Tumor Res, 1978. **22**: p. 190-274.
149. Denko, N.C., *Hypoxia, HIF1 and glucose metabolism in the solid tumour.* Nat Rev Cancer, 2008. **8**(9): p. 705-13.
150. Dahia, P.L., et al., *A HIF1alpha regulatory loop links hypoxia and mitochondrial signals in pheochromocytomas.* PLoS Genet, 2005. **1**(1): p. 72-80.
151. Seyfried, T.N. and L.M. Shelton, *Cancer as a metabolic disease.* Nutr Metab (Lond), 2010. **7**(1): p. 7.

152. Pourova, J., et al., *Reactive oxygen and nitrogen species in normal physiological processes.* Acta Physiol (Oxf), 2010. **198**(1): p. 15-35.
153. Bergamini, C.M., et al., *Oxygen, reactive oxygen species and tissue damage.* Curr Pharm Des, 2004. **10**(14): p. 1611-26.
154. Kappus, H. and H. Sies, *Toxic drug effects associated with oxygen metabolism: redox cycling and lipid peroxidation.* Experientia, 1981. **37**(12): p. 1233-41.
155. Schumacker, P.T., *Reactive oxygen species in cancer cells: live by the sword, die by the sword.* Cancer cell, 2006. **10**(3): p. 175-6.
156. Vander Heiden, M.G., L.C. Cantley, and C.B. Thompson, *Understanding the Warburg effect: the metabolic requirements of cell proliferation.* Science, 2009. **324**(5930): p. 1029-33.
157. Cairns, R.A., I.S. Harris, and T.W. Mak, *Regulation of cancer cell metabolism.* Nature reviews. Cancer, 2011. **11**(2): p. 85-95.
158. Kim, S.Y., et al., *Combined 18F-fluorodeoxyglucose-positron emission tomography and computed tomography as a primary screening method for detecting second primary cancers and distant metastases in patients with head and neck cancer.* Ann Oncol, 2007. **18**(10): p. 1698-703.
159. Michelakis, E.D., et al., *Metabolic modulation of glioblastoma with dichloroacetate.* Sci Transl Med, 2010. **2**(31): p. 31ra34.
160. Marsh, J., P. Mukherjee, and T.N. Seyfried, *Drug/diet synergy for managing malignant astrocytoma in mice: 2-deoxy-D-glucose and the restricted ketogenic diet.* Nutr Metab (Lond), 2008. **5**: p. 33.
161. Ko, Y.H., et al., *Advanced cancers: eradication in all cases using 3-bromopyruvate therapy to deplete ATP.* Biochem Biophys Res Commun, 2004. **324**(1): p. 269-75.
162. Lin, B.Q., et al., *Dietary restriction suppresses tumor growth, reduces angiogenesis, and improves tumor microenvironment in human non-small-cell lung cancer xenografts.* Lung cancer, 2013. **79**(2): p. 111-7.
163. Bonorden, M.J., et al., *Intermittent calorie restriction delays prostate tumor detection and increases survival time in TRAMP mice.* Nutr Cancer, 2009. **61**(2): p. 265-75.
164. Koubova, J. and L. Guarente, *How does calorie restriction work?* Genes Dev, 2003. **17**(3): p. 313-21.
165. Dunn, S.E., et al., *Dietary restriction reduces insulin-like growth factor I levels, which modulates apoptosis, cell proliferation, and tumor progression in p53-deficient mice.* Cancer Res, 1997. **57**(21): p. 4667-72.
166. Mukherjee, P., et al., *Dietary restriction reduces angiogenesis and growth in an orthotopic mouse brain tumour model.* Br J Cancer, 2002. **86**(10): p. 1615-21.
167. Hursting, S.D. and F.W. Kari, *The anti-carcinogenic effects of dietary restriction: mechanisms and future directions.* Mutat Res, 1999. **443**(1-2): p. 235-49.
168. Mukherjee, P., L.E. Abate, and T.N. Seyfried, *Antiangiogenic and proapoptotic effects of dietary restriction on experimental mouse and human brain tumors.* Clin Cancer Res, 2004. **10**(16): p. 5622-9.

169. Mukherjee, P., et al., *Energy intake and prostate tumor growth, angiogenesis, and vascular endothelial growth factor expression.* J. Natl. Cancer Inst., 1999. **91**(6): p. 512-523.
170. Mukherjee, P., et al., *Differential effects of energy stress on AMPK phosphorylation and apoptosis in experimental brain tumor and normal brain.* Mol Cancer, 2008. **7**: p. 37.
171. Marsh, J., P. Mukherjee, and T.N. Seyfried, *Akt-dependent proapoptotic effects of dietary restriction on late-stage management of a phosphatase and tensin homologue/tuberous sclerosis complex 2-deficient mouse astrocytoma.* Clin Cancer Res, 2008. **14**(23): p. 7751-62.
172. Hursting, S.D., et al., *Calories and carcinogenesis: lessons learned from 30 years of calorie restriction research.* Carcinogenesis, 2010. **31**(1): p. 83-9.
173. Jelluma, N., et al., *Glucose withdrawal induces oxidative stress followed by apoptosis in glioblastoma cells but not in normal human astrocytes.* Mol Cancer Res, 2006. **4**(5): p. 319-30.
174. Spitz, D.R., et al., *Glucose deprivation-induced oxidative stress in human tumor cells. A fundamental defect in metabolism?* Ann N Y Acad Sci, 2000. **899**: p. 349-62.
175. Krebs, H.A., et al., *The role of ketone bodies in caloric homeostasis.* Adv. Enzyme Reg., 1971. **9**: p. 387-409.
176. Otto, C., et al., *Growth of human gastric cancer cells in nude mice is delayed by a ketogenic diet supplemented with omega-3 fatty acids and medium-chain triglycerides.* BMC Cancer, 2008. **8**: p. 122.
177. Mahoney, L.B., C.A. Denny, and T.N. Seyfried, *Caloric restriction in C57BL/6J mice mimics therapeutic fasting in humans.* Lipids Health Dis, 2006. **5**(1): p. 13.
178. Lennox, W.G. and S. Cobb, *Studies in epilepsy VIII. The clinical effect of fasting.* Arch. Neurol. Psychiat., 1928. **20**: p. 771-779.
179. Longo, V.D. and M.P. Mattson, *Fasting: molecular mechanisms and clinical applications.* Cell metabolism, 2014. **19**(2): p. 181-92.
180. Stafstrom, C.E. and J.M. Rho, *Epilepsy and the Ketogenic Diet*. 2004, Totowa, NJ: Humana Press. 352.
181. Sharman, M.J., et al., *A ketogenic diet favorably affects serum biomarkers for cardiovascular disease in normal-weight men.* J Nutr, 2002. **132**(7): p. 1879-85.
182. Seyfried, B.T., et al., *Targeting energy metabolism in brain cancer through calorie restriction and the ketogenic diet.* J Cancer Res Ther, 2009. **5 Suppl 1**: p. S7-15.
183. Zuccoli, G., et al., *Metabolic management of glioblastoma multiforme using standard therapy together with a restricted ketogenic diet: Case Report.* Nutr Metab (Lond), 2010. **7**(1): p. 33.
184. Zhou, W., et al., *The calorically restricted ketogenic diet, an effective alternative therapy for malignant brain cancer.* Nutr Metab (Lond), 2007. **4**: p. 5.
185. Woolf, E.C. and A.C. Scheck, *The Ketogenic Diet for the Treatment of Malignant Glioma.* Journal of lipid research, 2014.

186. Sawai, M., et al., *Growth-inhibitory effects of the ketone body, monoacetoacetin, on human gastric cancer cells with succinyl-CoA: 3-oxoacid CoA-transferase (SCOT) deficiency.* Anticancer Res, 2004. **24**(4): p. 2213-7.
187. Mavropoulos, J.C., et al., *Is there a role for a low-carbohydrate ketogenic diet in the management of prostate cancer?* Urology, 2006. **68**(1): p. 15-8.
188. Abdelwahab, M.G., et al., *The ketogenic diet is an effective adjuvant to radiation therapy for the treatment of malignant glioma.* PloS one, 2012. **7**(5): p. e36197.
189. Allen, B.G., et al., *Ketogenic diets enhance oxidative stress and radio-chemo-therapy responses in lung cancer xenografts.* Clinical cancer research : an official journal of the American Association for Cancer Research, 2013. **19**(14): p. 3905-13.
190. Veech, R.L., *The therapeutic implications of ketone bodies: the effects of ketone bodies in pathological conditions: ketosis, ketogenic diet, redox states, insulin resistance, and mitochondrial metabolism.* Prostaglandins Leukot Essent Fatty Acids, 2004. **70**(3): p. 309-19.
191. Poff, A.M., et al., *The ketogenic diet and hyperbaric oxygen therapy prolong survival in mice with systemic metastatic cancer.* PloS one, 2013. **8**(6): p. e65522.
192. Stafford, P., et al., *The ketogenic diet reverses gene expression patterns and reduces reactive oxygen species levels when used as an adjuvant therapy for glioma.* Nutr Metab (Lond), 2010. **7**: p. 74.
193. Ranes, M.K., et al., *N -butyldeoxynojirimycin reduces growth and ganglioside content of experimental mouse brain tumours.* Br J Cancer, 2001. **84**(8): p. 1107-14.
194. El-Abbadi, M., et al., *Ganglioside composition and histology of a spontaneous metastatic brain tumour in the VM mouse.* Br J Cancer, 2001. **85**(2): p. 285-92.
195. Shapiro, W.R., J.I. Ausman, and D.P. Rall, *Studies on the chemotherapy of experimental brain tumors: evaluation of 1,3-bis(2-chloroethyl)-l-nitrosourea, cyclophosphamide, mithramycin, and methotrexate.* Cancer Res, 1970. **30**(9): p. 2401-13.
196. Williamson, B. and J.G. Coniglio, *The effects of pyridoxine deficiency and of caloric restriction on lipids in the developing rat brain.* J Neurochem, 1971. **18**(2): p. 267-76.
197. Bhagavan, N.V., *Medical Biochemistry*. Fourth ed. 2002, New York: Harcourt. 1016.
198. Meidenbauer, J.J., P. Mukherjee, and T.N. Seyfried, *The glucose ketone index calculator: a simple tool to monitor therapeutic efficacy for metabolic management of brain cancer.* Nutr Metab (Lond), 2015. **12**: p. 12.
199. Spector, R., *The War on Cancer A Progress Report for Skeptics.* Skeptical Inquirer, 2010. **34.1**.
200. Seyfried, T.N., L.M. Shelton, and P. Mukherjee, *Does the existing standard of care increase glioblastoma energy metabolism?* Lancet Oncol, 2010. **11**(9): p. 811-3.

201. Seyfried, T.N., et al., *Could metabolic therapy become a viable alternative to the standard of care for managing glioblastoma?* US Neurology, 2014. **10**(1): p. 48-55.
202. Seyfried, T.N., *Cancer as a metabolic disease: Implications for novel therapeutics*, in *Education Book*. 2013, Amer. Assoc. Cancer Res. p. 31-36.
203. Freeman, J.M., E.H. Kossoff, and A.L. Hartman, *The ketogenic diet: one decade later.* Pediatrics, 2007. **119**(3): p. 535-43.
204. Klement, R.J., *Calorie or carbohydrate restriction? The ketogenic diet as another option for supportive cancer treatment.* The oncologist, 2013. **18**(9): p. 1056.
205. Nebeling, L.C. and E. Lerner, *Implementing a ketogenic diet based on medium-chain triglyceride oil in pediatric patients with cancer.* J. Am. Diet. Assoc., 1995. **95**(6): p. 693-7.
206. Nebeling, L.C., et al., *Effects of a ketogenic diet on tumor metabolism and nutritional status in pediatric oncology patients: two case reports.* J. Am. Coll. Nutr., 1995. **14**(2): p. 202-8.
207. Seyfried, T.N., et al., *Role of glucose and ketone bodies in the metabolic control of experimental brain cancer.* Br J Cancer, 2003. **89**(7): p. 1375-82.
208. Meidenbauer, J.J., N. Ta, and T.N. Seyfried, *Influence of a ketogenic diet, fish-oil, and calorie restriction on plasma metabolites and lipids in C57BL/6J mice.* Nutrition & metabolism, 2014. **11**: p. 23.
209. Shelton, L.M., L.C. Huysentruyt, and T.N. Seyfried, *Glutamine targeting inhibits systemic metastasis in the VM-M3 murine tumor model.* Inter. J. Cancer. , 2010. **127**(10): p. 2478-85.
210. Chung, H.Y., et al., *Molecular inflammation hypothesis of aging based on the anti-aging mechanism of calorie restriction.* Microsc Res Tech, 2002. **59**(4): p. 264-72.
211. Seyfried, T.N., et al., *Metabolic control of brain cancer: Role of glucose and ketones.* Proc. Amer. Assoc. Cancer Res., 2005. **46**: p. 267.
212. VanItallie, T.B. and T.H. Nufert, *Ketones: metabolism's ugly duckling.* Nutr Rev, 2003. **61**(10): p. 327-41.
213. Tisdale, M.J., *Role of acetoacetyl-CoA synthetase in acetoacetate utilization by tumor cells.* Cancer Biochem Biophys, 1984. **7**(2): p. 101-7.
214. Morris, A.A., *Cerebral ketone body metabolism.* J Inherit Metab Dis, 2005. **28**(2): p. 109-121.
215. Poff, A.M., et al., *Ketone supplementation decreases tumor cell viability and prolongs survival of mice with metastatic cancer.* International journal of cancer. Journal international du cancer, 2014. **135**(7): p. 1711-20.
216. Bonnet, S., et al., *A mitochondria-K+ channel axis is suppressed in cancer and its normalization promotes apoptosis and inhibits cancer growth.* Cancer Cell, 2007. **11**(1): p. 37-51.
217. Luquain, C., et al., *High-performance liquid chromatography determination of bis(monoacylglycerol) phosphate and other lysophospholipids.* Analytical biochemistry, 2001. **296**(1): p. 41-8.